

NON-PROPRIETARY CALCULATIONS

Book 6 of 8

**Attachments to PG&E Letter DIL-01-004
Dated December 21, 2001**

NUCLEAR POWER GENERATION
CF3.ID4
ATTACHMENT 7.2

Index No. 402 _____
Binder No. _____

TITLE: CALCULATION COVER SHEET

Unit(s): 1 & 2 File No.: 52.27
 Responsible Group: Civil Calculation No.: 52.27.100.731
 No. of Pages 3 pages + Index (4 pages) + 1 Design Calculation YES [x] NO []
Attachment (185 pages)
 System No. 42C Quality Classification Q (Safety-Related)
 Structure, System or Component: Independent Spent Fuel Storage Facility

Subject: Analysis of Bedrock Stratigraphy and Geologic Structure at the DCPD ISFSI Site
 (GEO.DCPD.01.21, Rev. 2)

Electronic calculation YES [] NO [x]

Computer Model	Computer ID	Program Location	Date of Last Change

Registered Engineer Stamp: Complete A or B

<p>A. Insert PE Stamp or Seal Below</p> <p>Expiration Date:</p>	<p>B. Insert stamp directing to the PE stamp or seal</p> <p style="text-align: center;">REGISTERED ENGINEERS' STAMPS AND EXPIRATION DATES ARE SHOWN ON DWG 063618</p>
--	---

NOTE 1: Update DCI promptly after approval.

NOTE 2: Forward electronic calculation file to CCTG for uploading to EDMS.

CF3.ID4
ATTACHMENT 7.2

TITLE: CALCULATION COVER SHEET

CALC No. 52.27.100.731, R0

RECORD OF REVISIONS

Rev No.	Status	Reason for Revision	Prepared By:	LBIE Screen	LBIE	Check Method*	LBIE Approval		Checked	Supervisor	Registered Engineer
		Remarks	Initials/ LAN ID/ Date	Yes/ No/ NA	Yes/ No/ NA		PSRC Mtg. No.	PSRC Mtg. Date	Initials/ LAN ID/ Date	Initials/ LAN ID/ Date	Signature/ LAN ID/ Date
0	F	Acceptance of Geosciences Calc. No. GEO.DCPCP.01.21, Rev. 2. Calc. supports current edition of 10CFR72 DCPP License Application to be reviewed by NRC prior to implementation. Prepared per CF3.ID17 requirements.	AFT2 12/15/01	<input type="checkbox"/> Yes <input type="checkbox"/> No <input checked="" type="checkbox"/> NA	<input type="checkbox"/> Yes <input type="checkbox"/> No <input checked="" type="checkbox"/> NA	<input type="checkbox"/> A <input type="checkbox"/> B <input checked="" type="checkbox"/> C	N/A	N/A	N/A	LJA LJS 2 12/17/01	LJA LJS 2 12/17/01
				<input type="checkbox"/> Yes <input type="checkbox"/> No <input type="checkbox"/> NA	<input type="checkbox"/> Yes <input type="checkbox"/> No <input type="checkbox"/> NA	<input type="checkbox"/> A <input type="checkbox"/> B <input type="checkbox"/> C					
				<input type="checkbox"/> Yes <input type="checkbox"/> No <input type="checkbox"/> NA	<input type="checkbox"/> Yes <input type="checkbox"/> No <input type="checkbox"/> NA	<input type="checkbox"/> A <input type="checkbox"/> B <input type="checkbox"/> C					

*Check Method: A: Detailed Check, B: Alternate Method (note added pages), C: Critical Point Check



SUBJECT Analysis of Bedrock Stratigraphy and Geologic Structure at the DCPD ISFSI Site

MADE BY A. Tafoya DATE 12/15/01 CHECKED BY N/A DATE _____

Table of Contents:

Item	Type	Title	Page Numbers
1	Index	Cross-Index (For Information Only)	1 - 4
2	Attachment A	Analysis of Bedrock Stratigraphy and Geologic Structure at the DCPD ISFSI Site	1 – 185



SUBJECT Analysis of Bedrock Stratigraphy and Geologic Structure at the DCPD ISFSI Site

MADE BY A. Tafoya DATE 12/15/01 CHECKED BY N/A DATE _____

- 1- This table cross references between Geosciences calculation numbers and DCPD (Civil Group's) calculation numbers. This section is For Information Only.

**Cross-Index
(For Information Only)**

Item No.	Geosciences Calc. No.	Title	PG&E Calc. No.	Comments
1	GEO.DCPD.01.01	Development of Young's Modulus and Poisson's Ratios for DCPD ISFSI Based on Field Data	52.27.100.711	
2	GEO.DCPD.01.02	Determination of Probabilistically Reduced Peak Bedrock Accelerations for DCPD ISFSI Transporter Analyses	52.27.100.712	
3	GEO.DCPD.01.03	Development of Allowable Bearing Capacity for DCPD ISFSI Pad and CTF Stability Analyses	52.27.100.713	
4	GEO.DCPD.01.04	Methodology for Determining Sliding Resistance Along Base of DCPD ISFSI Pads	52.27.100.714	
5	GEO.DCPD.01.05	Determination of Pseudostatic Acceleration Coefficient for Use in DCPD ISFSI Cutslope Stability Analyses	52.27.100.715	
6	GEO.DCPD.01.06	Development of Lateral Bearing Capacity for DCPD CTF Stability Analyses	52.27.100.716	
7	GEO.DCPD.01.07	Development of Coefficient of Subgrade Reaction for DCPD ISFSI Pad Stability Checks	52.27.100.717	
8	GEO.DCPD.01.08	Determination of Rock Anchor Design Parameters for DCPD ISFSI Cutslope	52.27.100.718	
9	GEO.DCPD.01.09	Determination of Applicability of Rock Elastic Stress-Strain Values to Calculated Strains Under	52.27.100.719	Calculation to be replaced by letter



SUBJECT Analysis of Bedrock Stratigraphy and Geologic Structure at the DCPD ISFSI Site

MADE BY A. Tafoya DATE 12/15/01 CHECKED BY N/A DATE _____

**Cross-Index
(For Information Only)**

Item No.	Geosciences Calc. No.	Title	PG&E Calc. No.	Comments
		DCPD ISFSI Pad		
10	GEO.DCPD.01.10	Determination of SSER 34 Long Period Spectral Values	52.27.100.720	
11	GEO.DCPD.01.11	Development of ISFSI Spectra	52.27.100.721	
12	GEO.DCPD.01.12	Development of Fling Model for Diablo Canyon ISFSI	52.27.100.722	
13	GEO.DCPD.01.13	Development of Spectrum Compatible Time Histories	52.27.100.723	
14	GEO.DCPD.01.14	Development of Time Histories with Fling	52.27.100.724	
15	GEO.DCPD.01.15	Development of Young's Modulus and Poisson's Ratio Values for DCPD ISFSI Based on Laboratory Data	52.27.100.725	
16	GEO.DCPD.01.16	Development of Strength Envelopes for Non-jointed Rock at DCPD ISFSI Based on Laboratory Data	52.27.100.726	
17	GEO.DCPD.01.17	Determination of Mean and Standard Deviation of Unconfined Compression Strengths for Hard Rock at DCPD ISFSI Based on Laboratory Tests	52.27.100.727	
18	GEO.DCPD.01.18	Determination of Basic Friction Angle Along Rock Discontinuities at DCPD ISFSI Based on Laboratory Tests	52.27.100.728	
19	GEO.DCPD.01.19	Development of Strength Envelopes for Jointed Rock Mass at DCPD ISFSI Using	52.27.100.729	



SUBJECT Analysis of Bedrock Stratigraphy and Geologic Structure at the DCPD ISFSI Site

MADE BY A. Tafoya K1 DATE 12/15/01 CHECKED BY N/A DATE _____

**Cross-Index
(For Information Only)**

Item No.	Geosciences Calc. No.	Title	PG&E Calc. No.	Comments
		Hoek-Brown Equations		
20	GEO.DCPP.01.20	Development of Strength Envelopes for Shallow Discontinuities at DCPD ISFSI Using Barton Equations	52.27.100.730	
21	GEO.DCPP.01.21	Analysis of Bedrock Stratigraphy and Geologic Structure at the DCPD ISFSI Site	52.27.100.731	
22	GEO.DCPP.01.22	Kinematic Stability Analysis for Cutslopes at DCPD ISFSI Site	52.27.100.732	
23	GEO.DCPP.01.23	Pseudostatic Wedge Analyses of DCPD ISFSI Cutslopes (SWEDGE Analysis)	52.27.100.733	
24	GEO.DCPP.01.24	Stability and Yield Acceleration Analysis of Cross-Section I-I'	52.27.100.734	
25	GEO.DCPP.01.25	Determination of Seismic Coefficient Time Histories for Potential Sliding Masses Along Cut Slope Behind ISFSI Pad	52.27.100.735	
26	GEO.DCPP.01.26	Determination of Earthquake-Induced Displacements of Potential Sliding Masses on ISFSI Slope	52.27.100.736	
27	GEO.DCPP.01.27	Cold Machine Shop Retaining Wall Stability	52.27.100.737	
28	GEO.DCPP.01.28	Stability and Yield Acceleration Analysis of Potential Sliding Masses Along DCPD ISFSI Transport Route	52.27.100.738	



SUBJECT Analysis of Bedrock Stratigraphy and Geologic Structure at the DCPD ISFSI Site

MADE BY A. Tafoya DATE 12/15/01 CHECKED BY N/A DATE

**Cross-Index
(For Information Only)**

Item No.	Geosciences Calc. No.	Title	PG&E Calc. No.	Comments
29	GEO.DCPP.01.29	Determination of Seismic Coefficient Time Histories for Potential Sliding Masses on DCPD ISFSI Transport Route	52.27.100.739	
30	GEO.DCPP.01.30	Determination of Potential Earthquake-Induced Displacements of Potential Sliding Masses Along DCPD ISFSI Transport Route	52.27.100.740	
31	GEO.DCPP.01.31	Development of Strength Envelopes for Clay Beds at DCPD ISFSI	52.27.100.741	
32	GEO.DCPP.01.32	Verification of Computer Program SPCTLR.EXE	52.27.100.742	
33	GEO.DCPP.01.33	Verification of Program UTEXAS3	52.27.100.743	
34	GEO.DCPP.01.34	Verification of Computer Code - QUAD4M	52.27.100.744	
35	GEO.DCPP.01.35	Verification of Computer Program DEFORMP	52.27.100.745	
36	GEO.DCPP.01.36	Reserved	52.27.100.746	
37	GEO.DCPP.01.37	Development of Freefield Ground Motion Storage Cask Spectra and Time Histories for the Used Fuel Storage Project	52.27.100.747	

DEC 15 2001 4:01PM P 3

FROM : Cluff - San Francisco

DEC. 15, 2001 2:30PM

PG&E GEOSCIENCES DEP

PHONE NO. : 415 564 6697

NO.089 P.1/5

AT
12/15/01

PG&E
Geosciences Department
Departmental Calculation Procedure

Page: 1 of 1

Title: Calculation Cover Sheet

PACIFIC GAS AND ELECTRIC COMPANY
GEOSCIENCES DEPARTMENT
CALCULATION DOCUMENT

Calc Number: GEO.DCFF. 01.21Revision: 2Date: December 14, 2001No. of Calc Pages: 181

Verification Method: _____

No. of Verification Pages: 2 } NOT ATTACHED
AT 12/15/01TITLE Analysis of Bedrock Stratigraphy and Geologic Structure at the DCFP ISFSI Site

PREPARED BY

William R. Lettis
William R. Lettis
Printed Name

DATE 12/14/01

William Lettis & Associates, Inc.
Organization

VERIFIED BY

Scott C. Lindvall
Scott C. Lindvall
Printed Name

DATE 12/14/01

William Lettis & Associates, Inc.
Organization

APPROVED BY

Lloyd S. Cluff
Lloyd S. Cluff
Printed Name

DATE 12/15/01

PG&E Geosciences Dept.
Organization



Exp. 12/31/02

PG&E
Geosciences Department
Departmental Calculation Procedure

Page: 1 of 1

Title: Calculation Cover Sheet

PACIFIC GAS AND ELECTRIC COMPANY
GEOSCIENCES DEPARTMENT
CALCULATION DOCUMENT

Calc Number: GEO.DCPP. 01.21

Revision: 2

Date: December 14, 2001

No. of Calc Pages: 181

Verification Method: _____

No. of Verification Pages: 2

TITLE Analysis of Bedrock Stratigraphy and Geologic Structure at the DCPP ISFSI Site

PREPARED BY

William R. Lettis
William R. Lettis
Printed Name

DATE 12/14/01

William Lettis & Associates, Inc.
Organization

VERIFIED BY

Scott C. Lindvall
Scott C. Lindvall
Printed Name

DATE 12/14/01

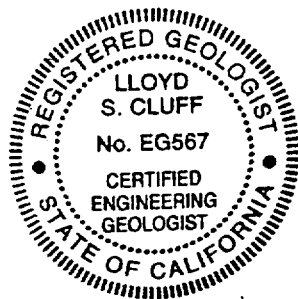
William Lettis & Associates, Inc.
Organization

APPROVED BY

Lloyd S. Cluff
Lloyd S. Cluff
Printed Name

DATE _____

PG&E Geosciences Dept.
Organization



Exp. 12/31/02

PG&E
Geosciences Department
Departmental Calculation Procedure

Page: 1 of 1

Title: Record of Revision

Calc Number: GEO.DCPP.01.21**Analysis of Bedrock Stratigraphy and Geologic Structure at the DCPD ISFSI Site**

Rev. No.	Reason for Revision	Revision Date
0	Initial Issue	10/15/01
Rev 1	Remove letter designations from Record of Revisions (pg. 2); added references to the transmittals of maps and air photos from PG&E Geosciences to WLA; edited the section on Topographic maps (formerly 2.2 and now 2.1); added information on x-ray diffraction to the stratigraphic descriptions (5.2.1 to 5.2.3); revised the geologic maps (Figs. 21-1, 21-3, and 21-4) and cross sections (Figs. 21-14 to 21-25); added cross section L-L'; added sections on rockslide mass models (5.6.3) and estimate of potential slide mass displacement (5.6.4); changed section 5.6.3 Rock Block Dimensions to section 5.6.5; general minor edits to text and figures.	11/6/01
Rev 2	Revised Introduction (Section 1); added description of geology along the transport route (5.5); added discussion of origin and non-capability of minor faults in the ISFSI study area (5.3.2.1); discussion of pre-existing landslides in Diablo Canyon near ISFSI site (5.7.1); general minor edits to text and figures in response to QA and ITR review	12/12/01

DCPP ISFSI

CALCULATION PACKAGE GEO.DCPP.01.21
Analysis of Bedrock Stratigraphy and Geologic Structure
at the DCPD ISFSI Site

DCPP ISFSI
Calculation package GEO.DCPP.01.21
Analysis of Bedrock Stratigraphy and Geologic Structure
at the DCPD ISFSI Site

Table of Contents

	<u>Page</u>
1.0 INTRODUCTION	8
1.1 Location and Site Description.....	9
1.2 Purpose.....	9
2.0 INPUTS.....	12
2.1 ISFSI Project Maps and Air Photos	12
2.2 Compilation of Topographic Base Maps	15
2.3 Geologic Input	17
3.0 ASSUMPTIONS.....	19
4.0 METHODS	22
4.1 Bedding.....	22
4.2 Clay Beds.....	24
4.3 Cross Sections.....	25
5.0 ANALYSIS (BODY OF CALCULATION)	30
5.1 Bedrock Evolution	30
5.2 Stratigraphic Analysis.....	38
5.2.1 General Stratigraphy	38
5.2.2 ISFSI Study Stratigraphy	38
5.2.2.1 Dolomite (Unit Tof _{b-1})	40
5.2.2.2 Sandstone (Unit Tof _{b-2}).....	41
5.2.2.3 Friable Bedrock.....	42
5.2.2.4 Clay Beds.....	44
5.3 Structural Analysis.....	47
5.3.1 Folds.....	48

Table of Contents (continued)

5.3.2	Faults.....	50
5.3.2.1	Fault Origin and Capability	52
5.3.3	Bedrock Discontinuities.....	54
5.4	Stratigraphy and Structure of the ISFSI Pads Foundation	57
5.5	Stratigraphy and Structure of the Transport Route	58
5.6	Comparison of Power Block and ISFSI Site.....	62
5.7	Parameters Recommended for Stability Analysis.....	64
5.7.1	Pre-existing Landslides in Diablo Canyon near the ISFSI Site ...	64
5.7.2	Clay Bed Strength.....	66
5.7.3	Geometry and Structure of Slide Mass Models	67
5.7.4	Conceptual Rockslide Mass Models.....	68
5.7.5	Estimate of Potential Slide Mass Displacement	70
5.7.6	Rock Block Dimensions	72
6.0	RESULTS	73
7.0	SOFTWARE.....	73
8.0	CONCLUSIONS.....	74
9.0	REFERENCES	75

List of Tables

Table 21-1	Interpretation of bedding in boreholes, ISFSI study area.
Table 21-2	Evaluation of clay 'seams' on low-angle fractures and bedding, ISFSI study area borings.
Table 21-3	Thickness measurements of clay beds in borings and trenches.
Table 21-4	Friable rock zones in ISFSI study area borings.
Table 21-5	Discontinuity data for minor faults.
Table 21-6	Selected fractures (joints, faults and shears) observed in borings and trenches.
Table 21-7	Comparison of seismic wave velocities in the ISFSI study area and at the DCPD power block.

List of Table of Contents (continued)

List of Figures

- Figure 21-1. Geologic map of bedrock and landslides in the plant site area.
- Figure 21-2. Aerial view of the ISFSI study area.
- Figure 21-3. Geologic map of the ISFSI study area and transport route vicinity.
- Figure 21-4. Geologic map of ISFSI and CTF sites.
- Figure 21-5. Generalized stratigraphic column at the ISFSI and power block sites.
- Figure 21-6. Index map of topographic surveys.
- Figure 21-7. Diagrammatic cross section illustrating the depositional and structural history at the ISFSI.
- Figure 21-8. Chronology of stratigraphy and geologic processes at the ISFSI study area.
- Figure 21-9. Summary logs of borings on slope above ISFSI site.
- Figure 21-10. Summary logs of borings near southwest end of ISFSI site.
- Figure 21-11. Summary logs of borings at ISFSI site.
- Figure 21-12. Summary logs of borings near east end of ISFSI site.
- Figure 21-13. Explanation for cross sections.
- Figure 21-14. Cross section A-A'.
- Figure 21-15. Cross section B-B'''.
- Figure 21-16. Cross section C-C'.
- Figure 21-17. Cross section D-D'.
- Figure 21-18. Cross section E-E'.
- Figure 21-19. Cross section F-F' through Patton Cove landslide.
- Figure 21-20. Cross section G-G'.
- Figure 21-21. Cross section H-H'.
- Figure 21-22. Cross section I-I'.
- Figure 21-23. Cross section J-J'.
- Figure 21-24. Cross section K-K'.
- Figure 21-25. Cross section L-L'.
- Figure 21-26. Measuring bedding attitude, ISFSI study area.

Table of Contents (continued)

List of Figures (continued)

- Figure 21-27. Examining core from ISFSI study area.
- Figure 21-28. Core boxes from ISFSI study area laid out in stratigraphic order.
- Figure 21-29. Clay bed in Trench T-14B.
- Figure 21-30. Clay bed at 55 feet in Boring 00BA-1.
- Figure 21-31. Clay bed at 130 feet in Boring 01-I.
- Figure 21-32. Minor fault in Trench T-1.
- Figure 21-33. Bedded dolomite on Reservoir Road.
- Figure 21-34. Minor fault in Trench T-20A.
- Figure 21-35. Sandstone outcrop in ISFSI study area.
- Figure 21-36. Clay beds and dolomite in Trench T-11C.
- Figure 21-37. Regional structure map.
- Figure 21-38. Comparison of orientations of minor faults and folds in the ISFSI study area with other structures.
- Figure 21-39. Minor faults in Diablo Creek Road.
- Figure 21-40. 1968 aerial photograph of ISFSI study area.
- Figure 21-41. Azimuth plot of faults and joints in borings and trenches.
- Figure 21-42. Geology of ISFSI and CTF SITES at proposed final grades.
- Figure 21-43. Summary log of 1977 Power Block Boring DDH-D.
- Figure 21-44. ISFSI site suspension logs and interpreted average seismic velocities.
- Figure 21-45. Comparison of seismic shear-wave velocities at the Power Block and ISFSI sites.
- Figure 21-46. Slide mass model 1.
- Figure 21-47. Slide mass model 2.
- Figure 21-48. Slide mass model 3.

Calculation Package GEO.DCPP.01.21

Title: Analysis of Bedrock Stratigraphy and Geologic Structure at the DCP
ISFSI Site

Calc Number: GEO.DCPP.01.21

Revision: Rev. 2

Author: William R. Lettis

Date: December 14, 2001

Verifier: Scott C. Lindvall

1.0 INTRODUCTION

The Diablo Canyon Power Plant (DCPP) Independent Spent Fuel Storage Facility (ISFSI) will be located on the plant site property in an area underlain by bedrock of the Tertiary Obispo Formation (Figure 21-1). The ISFSI will include the ISFSI pads, a Cask Transfer Facility (CTF), and a transport route leading from the power block to the CTF and onto the ISFSI pads. The ISFSI pads will be constructed on a bench cut into the Obispo Formation. For the purpose of discussion in this calculation package, the ISFSI pads, CTF, and cutslope and existing hillslope above the ISFSI pads are referred to as the ISFSI study area. The transport route includes the proposed route and the adjoining slopes above and below the route.

This calculation package describes the geology of the ISFSI study area and along the transport route. The stratigraphic and structural analysis was performed by William Lettis, Jeff Bachhuber, and Charles Brankman of WLA under the project direction and participation of William Page of PG&E Geosciences. The preparation of this calculation package was performed under the 2000 WLA Work Plan (Rev. 2) (William Lettis & Associates, Inc., Work Plan, 2000) using data collected under that Work Plan and a second WLA Work Plan (Rev. 1) (William Lettis & Associates, Inc., Work Plan, 2001) .

1.1 Location and Site Description

The ISFSI study area is located on a prominent ridge directly south of the Raw Water Reservoir and east of the Diablo Canyon power plant (Figures 21-1 and 21-2). The ridge area was used formerly as a borrow source to derive fill material for construction of the 230 kV and 500 kV switchyards. The borrow excavation, performed in 1971, removed up to 100 feet of material from the ISFSI site area and extended deep into bedrock. As a result, the ISFSI and CTF facilities will be founded on bedrock, and the foundation stability and seismic response will be controlled by the bedrock properties. The former borrow activity at the site stripped surficial soil and weathered rock from the hillside above the ISFSI site, leaving a bedrock slope covered with a veneer of rock rubble. The proposed cutslopes south of the ISFSI pads will be cut entirely in bedrock. Therefore, understanding the structural geometry and rock mass characteristics of bedrock are important for evaluating slope stability of both the existing slope and the proposed cutslopes.

The transport route follows existing paved roads from the power block to the CTF and onto the ISFSI pads, except for a new portion of the route from Shore Cliff Road to Reservoir Road that will be constructed to avoid a landslide at Patton Cove along the coast (Figure 21-3). The route is located on a nearly flat, graded surface along Plant View and Shore Cliff roads, and progressively climbs elevation along the new bypass road and along Reservoir Road. The bypass road will be constructed, and the lower part of Reservoir Road is constructed, on engineered fill over thick colluvium. The upper part of Reservoir Road is constructed on a cut-and-fill bench into bedrock of the Obispo Formation.

1.2 Purpose

This calculation package presents detailed analyses to characterize the stratigraphy and structure of bedrock in the ISFSI study area and along the transport route. Understanding the bedrock stratigraphy and structure is important for four purposes: (1) to evaluate

foundation properties for the ISFSI pads, the CTF facility, and the transport route; (2) to evaluate stability of the proposed cut slopes and existing hillslope above the ISFSI pads and transport route; (3) to identify and characterize bedrock faults in the study area; and (4) to compare bedrock conditions at the ISFSI site to bedrock conditions beneath the power block for ground motion characterization.

Information on the stratigraphy, structure and rock mass properties of the bedrock was used to analyze foundation properties, hillslope and cutslope stability, and ground motion site response in the ISFSI study area and along the transport route. These analyses are contained in the following calculation packages:

Calculation packages that characterize the ISFSI pads foundation properties:

GEO.DCPP.01.01 Development of Young's Modulus and Poisson's ratios for DCPD
ISFSI based on field data

GEO.DCPP.01.03 Development of allowable bearing capacity for DCPD ISFSI pad
and CTF stability analyses

GEO.DCPP.01.04 Methodology for determining sliding resistance along base of
DCPD ISFSI pads

GEO.DCPP.01.06 Development of lateral bearing capacity for DCPD CTF stability
analyses

GEO.DCPP.01.07 Development of coefficient of subgrade reaction for DCPD ISFSI
pad stability checks

GEO.DCPP.01.15 Development of Young's Modulus and Poisson's ratio values for
DCPD ISFSI based on laboratory data

Calculation packages that evaluate slope stability of the existing hillslope above the ISFSI site, the proposed ISFSI cutslopes, and the roadcuts above the transport route:

GEO.DCIPP.01.08 Determination of rock anchor design parameters for DCPP ISFSI cutslope

GEO.DCIPP.01.19 Development of strength envelopes for jointed rock mass at DCPP ISFSI using Hoek-Brown equations

GEO.DCIPP.01.20 Development of strength envelopes for shallow discontinuities at DCPP ISFSI using Barton equations

GEO.DCIPP.01.22 Kinematic stability analysis for cutslopes at DCPP ISFSI site

GEO.DCIPP.01.23 Pseudostatic wedge analysis of DCPP ISFSI cutslope (SWEDGE analysis)

GEO.DCIPP.01.24 Stability and yield acceleration analysis of cross section I-I'

GEO.DCIPP.01.25 Determination of seismic coefficient time histories for potential sliding masses along cutslope behind ISFSI pad

GEO.DCIPP.01.26 Determination of earthquake-induced displacements of potential sliding masses on DCPP ISFSI slope

GEO.DCIPP.01.28 Stability and yield acceleration analysis of potential sliding masses along DCPP ISFSI transport route

GEO.DCIPP.01.29 Determination of seismic coefficient time histories for potential sliding masses on DCPP ISFSI transport route

GEO.DCPP.01.30 Determination of earthquake-induced displacements of potential sliding masses along DCPD ISFSI transport route

Calculation packages that provide the rock conditions for evaluating ground motion site response:

GEO.DCPP.01.02 Determination of probabilistically reduced peak bedrock accelerations for DCPD ISFSI transporter analyses

GEO.DCPP.01.11 Development of ISFSI spectra

2.0 INPUTS

2.1 ISFSI Project Maps and Air Photos

Maps showing the topography of the plant site area and of the ISFSI project facility locations were received from PG&E Geosciences Department under letter of transmittal dated October 26, 2001 (PG&E Geosciences, 2001b). These maps were used to prepare the base maps for the geologic maps presented in this Calculation Package.

<u>DRAWING</u>	<u>REVISION</u>	<u>TITLE</u>
471124	1	Plot Plan
PGE-009-SK-001	0	Site Plot Plan, ISFSI Cask Storage Pad, Cask Transfer Facility
UFSP-SK-004	A	Cask Transfer Facility Structure (Schematic)
USFP-SK-005	A	Four Topographic Profile Surveys (CYN-14r.dgn)
354970	I	Site Plan Liquid Storage Warehouse
438042	18	Finished Grading Plan, Plant Area

<u>DRAWING</u>	<u>REVISION</u>	<u>TITLE</u>
445669	2	As Built Location of Overhead Power Lines and Property Access Road
445670	7	As Built Location of Compressor Building and Surrounding Buried & Overhead Utilities As Built Location of Buried Conduits, Overhead Power Line, Meteorological Facilities & Intake Structure
445675	12	As Built Location of Intake Structure Area & Breakwater Road
445708	1	Access Road to 150 ft. Meteorological Tower
445719	0	Access Road to 150 ft. Meteorological Tower
445720	0	Access Road to 150 ft. Meteorological Tower
445724	0	Access Road to 150 ft. Meteorological Tower
445725	0	Access Road to 150 ft. Meteorological Tower
445726	0	Access Road to 150 ft. Meteorological Tower
445727	0	Access Road to 150 ft. Meteorological Tower
445731	0	Access Road to 150 ft. Meteorological Tower
445732	0	Access Road to 150 ft. Meteorological Tower
472116	4	Finish Grading & Drainage Plan N.P.O. Permanent Warehouse
472117	3	Drainage Sections & Details N.P.O. Permanent Warehouse
472118	4	Vehicular Access Plan & Misc. Details N.P.O. Permanent Warehouse
472119	3	Foundation Plan and Details NPO Permanent Warehouse
472679	7	Fencing Plan and Detail for the Southern Portion of the Power Plant Yard
512292	11	Site Master Plan Master Plan Area A
515971	4	Finished Grading Plan Yard Area and Administration Building
515973	3	Concrete Outline Foundation Plan Administration Building
516969	8	Ground Floor Plan Cold Machine Shop
516992	8	Finished Grading Plan Cold Machine Shop
516994	5	Foundation, Plan and Details Cold Machine Shop

<u>DRAWING</u>	<u>REVISION</u>	<u>TITLE</u>
517998	4	Plan, Sections & Details Stormwater/Transformer Deluge Retention Drainage System
Diablo-pns-x1x	-	The Points Lists submitted by Pacific Engineering for four topographic profile lines D-D', E-E', F-F' and I-I'
CYN-r14.dwg	-	A sketch prepared by Pacific Engineering showing in plan the routes of the four field survey lines and can serve as a guide to the relative locations of the tabulated data
71498.asc	7/14/98	"Topo" of hillside
61600.asc	6/16/00	Trenches
122000.asc	12/20/00	Added trenches
42301.asc	4/23/01	Bores
9601.asc	9/6/01 & 9/7/01	Cross sections
59451	7	Plot Plan (Superseded)
478104	1	Surveys of sea floor terrain near Diablo Canyon and of breakwater configuration after wavestorm of January 28, 1981
57733	11	Equipment location Section FF Auxiliary, Fuel Handling and Turbine Buildings
438002	8	Excavation Plan Plant Site
438003	2	Excavation sections Plant Site
438023	2	May, 1968, Topography Plant Site Area
438034	7	Foundations for water tanks
438200	7	Excavation for containment, turbine-generator & auxiliary buildings
439514	9	Concrete outline section J-J Auxiliary Building – Areas H & K
443060	9	Excavation of Turbine Building
443061	2	Excavation of Auxiliary Building
455934	2	Excavation, Grading Plan & Sections Solid Radwaste Storage Building
455937	3	Finish Grading Plan & Sections Solid Radwaste Storage Building
500973	13	Equipment Location Section "C-C" Turbine, Containment & Fuel Handling Buildings

<u>DRAWING</u>	<u>REVISION</u>	<u>TITLE</u>
517120	7	Fencing and Grading Radwaste Storage and Laundry Facility Area
517746	1	Site Preparation Plan & Sections NPO Permanent Warehouse
517780	10	Finish Grading Plan and Sections Radwaste Storage Building

In addition, stereo aerial photographs of the ISFSI study area and transport route were acquired and interpreted for the study. These photos include:

<u>Date</u>	<u>Company</u>	<u>Frames</u>	<u>Scale</u>
5/22/68	Towill Corporation	Flight 2777 Frames 2808-1 to 2808-3	1:24,000 black & white
		Flight 2773 Frames 2805-3 and 2805-4	
7/4/86	PG&E	Flight PG&E 737 Frames 2-159, 2-160 and 2-114 to 2-116	1:24,000 color
1/11/87	PG&E	Flight PG&E 753 Frames 5-10 to 5-12 and 6-4 to 6-9	1:24,000 black & white
7/13/00	Golden Aerial Surveys	Flight GS4295 Frames 1-1 to 1-6 and 2-1 to 2-2	1:20,000 color

2.2 Compilation of Topographic Base Maps

Four different topographic base maps were compiled to make a complete topographic map of the ISFSI study area and transport route. This topographic map was used as the base map for preparation of geologic maps and cross sections. As shown on Figure 21-6 and discussed below, these maps cover different parts of the plant site at different scales and topographic contour intervals:

- (1) Towill Corporation's topographic map of the power plant property based on 1966 aerial photography and prepared at a scale of 1:2,400. These maps were made prior to power plant construction and site grading, and have gone through numerous revisions that primarily consist of addition of site facilities and areas of major grading. Elevation contours are 5 to 10 feet. These maps are used to depict topography outside of graded areas and facilities. The pre-construction topography from these maps was also plotted on several cross sections to illustrate the geomorphology prior to construction.
- (2) PG&E's 1986 facility layout Plot Plan map, Sheet No. 471124, prepared at a scale of 1:2,400. This plan shows as-built footprints of site facilities and graded areas (such as parking lots and the switchyard fill pads), overprinted on a modified topographic base with 100-foot elevation contours taken from the Towill topographic map.
- (3) PG&E's topographic/civil maps prepared at a scale of 1:240 (referred to as the "20-scale civil drawings") and modified at various times since the early 1970s. The 20-scale topographic/civil maps include as-built topography and facility layouts. These maps have gone through numerous revisions to incorporate new facilities or changes in graded conditions, but do not include all newer facilities and changes. Contour intervals are typically 5 feet. The topography from the 20-scale drawings is used to show current as-built elevation contours in the areas of the power plant.
- (4) 2000-2001 ISFSI Site topographic map prepared at a scale of 1:600 (referred to as "ISFSI site map"). The ISFSI site map covers the ISFSI and CTF sites, and is based on both photogramatic and land surveys. Several phases of field surveys were performed to locate exploratory borings, trenches, geologic reference points, and cross section profiles. Topographic contours

are resolved to 5-foot vertical intervals. This map is used as the base for Figure 21-4 and for cross sections in this area.

The geologic maps shown on Figures 21-1, 21-3 and 21-4 cover different parts of the power plant site area and ISFSI study area and, thus, required the use of one or more of the different topographic maps. The different base maps were merged to create a uniform topographic base registered to the California State Coordinate System that is a common grid for cross-referencing. The contours were smoothed and adjusted at the map boundaries to eliminate mismatching at map edges. Some contour lines were removed to provide consistent map-to-map contour spacing. After the base topography was merged and edited, selected major plant facilities were added for reference. In the ISFSI site area, field surveys were also made to accurately locate the ISFSI borings and trenches. In order to provide accurate topography for the cross section profiles that extended into areas of the older Towill topographic map, the profiles were surveyed in the field as shown on Figure 21-6. These survey profiles, as well as the surveyed points in the ISFSI site area, were used to cross check between the various map sets and provide additional control for geologic data.

2.3 Geologic Inputs

Bedrock in the ISFSI study area has undergone a complex history of deposition, alteration and deformation. This complex history makes it difficult to recognize and correlate distinct lithologies and to identify bedding within the bedrock. Therefore, considerable effort was made to resolve this history and to understand the current stratigraphic and structural condition of the rock. This effort included:

- detailed surface mapping (William Lettis & Associates, Inc. (2001) Diablo Canyon ISFSI Data Report A);
- continuous rock coring (William Lettis & Associates, Inc. (2001) Diablo Canyon ISFSI Data Report B) supplemented by downhole velocity measurements (William Lettis & Associates, Inc. (2001) Diablo Canyon ISFSI Data Report C) and caliper

and optical televiewer data (William Lettis & Associates, Inc. (2001) Diablo Canyon ISFSI Data Report E);

- seismic surface refraction surveys (William Lettis & Associates, Inc. (2001) Diablo Canyon ISFSI Data Report C);
- trenching (William Lettis & Associates, Inc. (2001) Diablo Canyon ISFSI Data Report D) and measuring of rock discontinuities (William Lettis & Associates, Inc. (2001) Diablo Canyon ISFSI Data Report F), in situ strength properties (William Lettis & Associates, Inc. (2001) Diablo Canyon ISFSI Data Report H), and structure (William Lettis & Associates, Inc. (2001) Diablo Canyon ISFSI Data Report A);
- laboratory analysis of rock mass properties (William Lettis & Associates, Inc. (2001) Diablo Canyon ISFSI Data Report I) and of clay bed properties (William Lettis & Associates, Inc. (2001) Diablo Canyon ISFSI Data Report G); and
- petrographic and x-ray analyses of hand and core samples (William Lettis & Associates, Inc. (2001) Diablo Canyon ISFSI Data Reports J and K, respectively).

The details of each study, including methodology, personnel involved, and sequence and results of investigation are given in each respective William Lettis & Associates, Inc. (2001) Diablo Canyon ISFSI Data Report prepared by William Lettis & Associates, Inc. (2001).

Descriptions of the regional and site geology are provided in William Lettis & Associates, Inc. (2001) Diablo Canyon ISFSI Data Report A, which presents geologic maps and field data with minimal interpretation. This calculation package integrates the geologic map information included in William Lettis & Associates, Inc. (2001) Diablo Canyon ISFSI Data Report A with the subsurface and laboratory test data in William Lettis & Associates, Inc. (2001) Diablo Canyon ISFSI Data Reports B through K to evaluate site-specific stratigraphy for the ISFSI study area. Interpretive geologic maps are shown on Figures 21-1, 21-3, and 21-4, and a site-specific stratigraphic column is shown on Figure 21-5. The stratigraphy was then used to define the structure and geometry of bedding and the distribution of bedrock lithology beneath the ISFSI and CTF sites, within the slope above the ISFSI site and along the transport route, and to help

identify and characterize the minor faults in the area. Topographic base maps used for Figures 21-1, 21-3 and 21-4 are shown on Figure 21-6.

This calculation package documents the iterative and interpretive procedures used to prepare: (1) a detailed stratigraphic column for bedrock in the study area (Figure 21-5); (2) a geologic model describing the evolution of bedrock in the study area (Figures 21-7 and 21-8); and (3) interpretive geologic maps (Figures 21-1, 21-3 and 21-4), summary boring logs (Figures 21-9 through 21-12), and cross sections (Figures 21-13 through 21-24) showing bedrock structure and distribution of lithologic units at the ISFSI and CTF sites and along the transport route. These data provide rock properties that were used to characterize slope stability, foundation response, and seismic ground motions. Particular emphasis was placed on correlating sedimentary facies, marker beds, and clay beds within the bedrock, and characterizing bedrock structure for use in evaluating the stability of cutslopes and hillslopes in the ISFSI study area and along the transport route.

3.0 ASSUMPTIONS

Several assumptions are used in the stratigraphic and structural analysis. These assumptions and supporting rationale are listed below. Evidence supporting these assumptions is provided in the Analysis section below. These assumptions are considered reasonable and are used to characterize the range of possible conditions of bedrock in the study area.

- (1) **Lateral Continuity.** Bedrock in the ISFSI study area was deposited in a moderate to deep marine environment (William Lettis & Associates, Inc. (2001) Diablo Canyon ISFSI Data Report L). Under such conditions, it is reasonable to assume that individual beds and groups of beds were deposited with lateral continuity of equal to or greater extent than the ISFSI site dimensions (on the order of hundreds of feet). Thus, any interruptions to bedding across the site will be due to post-depositional erosion, chemical alteration, diagenesis (including

compaction), deformation (tectonic or non-tectonic), hydrocarbon or hydrothermal fluid migration, and/or igneous intrusion. Under this assumption, clay beds are conservatively assumed to be laterally continuous for distances of hundreds of feet unless demonstrated otherwise. This assumption is realistically conservative because field observations of facies changes, areas of rock-to-rock contact, localized cemented bedding planes (rock bridges), and faults commonly disrupt the continuity of bedding and clay beds.

(2) **Facies Variation.** Bedrock in the ISFSI study area includes both marine turbidite deposits and marine pelagic and biogenic deposits. These deposits are interfingered and undergo lateral facies transition from one to the other. This facies transition is an irregular, but mappable lithologic contact in the ISFSI study area. Given this depositional contact and general knowledge of depositional environments, the facies transition is assumed to be time-transgressive. Locally distinct beds of one facies interfinger with the other facies. In these instances, the facies contact is assumed to closely approximate an individual bed or group of beds that can be used to establish the general dip and lateral continuity of bedding within the bedrock. This is a reasonable assumption where stratigraphic sequences are constrained by closely spaced borings and surface exposures. The overall geometry of the facies transition, however, given its interfingering pattern, will appear to cross cut bedding.

(3) **Dolomitization.** Bedrock in the ISFSI study area has been partially, and in places, entirely recrystallized to dolomite. This process of dolomitization has affected all rock types and beds to varying degrees and, in places, the degree of dolomitization may vary laterally along the same bed(s). Thus, the degree of dolomitization cannot be used as a distinct lithologic unit that defines bedding or distinct marker horizons in the site area. However, the finer-grained dolomite beds of Unit Tof_{b-1} generally exhibit a greater degree of dolomitization than the coarser-grained sandstone beds of Unit Tof_{b-2}.

- (4) **Alteration.** Bedrock in the ISFSI study area has undergone several periods of alteration, including addition of petroliferous fluids, near-surface mechanical and chemical weathering and probable hydrothermal alteration. Based on detailed mapping, the petroliferous alteration is assumed to be relatively random throughout the bedrock and cannot be used to discriminate either original bedrock lithology or bedding. In contrast, the surface weathering and/or hydrothermal alteration appears to have differentially effected distinct lithologies and beds over short distances. These zones of alteration are assumed to correlate laterally over short distances and, therefore, can be used to help evaluate the stratigraphy and structure of bedrock in the ISFSI study area.
- (5) **Diabase Intrusion.** Rocks of a diabase intrusive complex are common in the Diablo Canyon plant site area and locally were present in the ISFSI site prior to excavation of the borrow site in 1971. Because of the proximity of known diabase intrusions, bedrock at the site may have been structurally deformed by the intrusive complex and/or hydrothermally altered from fluids emanating from the intrusion. This is a reasonable assumption considering the known occurrence and former proximity of the diabase.
- (6) **Bedding Attitudes.** Bedding attitudes obtained at the surface and in boreholes are assumed to reflect the geometry of adjacent bedrock, and that this bedding attitude can be projected along dip and strike for distances up to 100 feet. This is a reasonable assumption that is supported by the greater than 100 bedrock attitudes measured in the ISFSI study area. Changes in bedding attitudes between different locations are interpolated using geologic judgement and interpretation of fold and fault geometry.
- (7) **Faulting.** Several minor faults occur in the ISFSI study area. The faults are assumed to have lateral and vertical continuity at least equal to the dimensions of the site (on the order of hundreds of feet). In addition, the faults are assumed to project along trend to small bedrock faults observed on the north wall of Diablo

Canyon that have similar geometry and orientations. These assumptions are reasonable given the inferred amounts of displacement on the faults (several hundred feet or more). In addition, slickensides are preserved on several exposed fault planes. The orientation of the slickensides are assumed to reflect the sense of last displacement along the fault, a commonly accepted interpretation of fault displacement. Where the fault plane attitude is not well constrained, we assume that the fault is vertical. This assumption is reasonable since the sense of fault displacement is primarily strike slip and the majority of measured fault dips are greater than 70 degrees. Faults with a well-constrained geometry are shown with a solid line on the cross sections; faults with a poorly constrained geometry are shown with a dashed line.

4.0 METHODS

Stratigraphic and structural analyses of bedrock in the ISFSI study area and along the transport route were performed using fundamental principals of geology (e.g., uniformitarianism, stratigraphic superposition and lateral continuity, cross-cutting relative age relationships, etc.). Geologic data were collected in the field through surface geologic mapping, seismic surveys, trenching and borings (see Inputs section above). The data were compiled and analyzed using guidelines provided in "Geology in the Field" (Compton, 1985). Geologic field data were supplemented with laboratory petrographic and X-ray diffraction analyses (see Inputs Section above).

4.1 Bedding

Bedding attitudes were measured to evaluate stratigraphic continuity and geometry of bedrock in the study area and at the site. Particular care was used in measuring bedding in the ISFSI study area because of the importance to the analysis of slope stability. Attitudes were obtained on surface outcrops using a Brunton Compass (Figure 21-26) and in borings using optical televiewer data supplemented by visual examination of the rock

core (Figure 21-27). All of the bedding attitudes obtained from surface outcrops in the ISFSI study area and most of the attitudes from the borings were cross-checked by at least two geologists as described in William Lettis & Associates, Inc. (2001) Diablo Canyon ISFSI Data Reports B, E, and L. Surface measurements of bedding attitudes were obtained from available exposures that exhibited moderate to well-defined bedding. These attitudes were used to help determine bedrock structure (William Lettis & Associates, Inc. (2001) Diablo Canyon ISFSI Data Report L, Table L-1). All bedding attitudes from surface exposures were plotted on the geologic maps and those near the cross section lines were used in the construction of these cross sections across the ISFSI study area and along the transport route.

Bedding attitudes also were measured in borings by examination of televiwer data, rock core, and boring logs. Distinct beds and/or zones of "stratified" or laminated bedrock were initially noted on the geologic logs by the field geologist upon first examination of the recovered core (William Lettis & Associates, Inc. (2001) Diablo Canyon ISFSI Data Report B). The dip of bedding was measured directly on the core with a protractor. Oriented coring techniques were not used; therefore, the strike and dip azimuth of bedding could not be determined in the field. Most of the dip measurements of bedding were checked by visual examination of the rock core by at least two other geologists (Figures 21-26 and 21-27). Borehole televiwer data were processed and interpreted by NORCAL (William Lettis & Associates, Inc. (2001) Diablo Canyon ISFSI Data Report E). NORCAL identified bedding planes and defined the orientation and dip of selected bedding planes. The NORCAL data were independently checked by at least two geologists by comparing the televiwer data with the rock core. Additional bedding planes, or alternate measurements of NORCAL bedding measurements were made by the geologists using geometric and trigonometric solutions. Most of the bedding attitudes determined from the televiwer data were compared visually with the rock core to verify the existence of bedding as noted on the televiwer logs and the magnitude of dip as calculated from the televiwer logs. Cross-checking between the televiwer data, rock core, and boring logs provided a consistent, verifiable and documented set of bedding attitudes. Bedding attitudes in the borings are tabulated in Table 21-1. Only those beds

that were verified by visual examination of the core were used in the construction of cross sections across the ISFSI study area.

4.2 Clay Beds

The identification and characterization of clay beds in the ISFSI study area is important for two reasons: (1) The clay beds form local marker horizons that help define the structure and geometry of bedding in the study area; and (2) the clay beds could form a basal shear surface for potential shallow and deep slope failures that might affect the ISFSI. Thus, a significant effort was focused on identifying clay beds and evaluating their orientation and lateral continuity.

Distinct clay beds were observed in trench exposures, boreholes, and roadcut exposures (Figures 21-28, 21-29, 21-30). Clay beds were identified and logged in Trenches T-11, T-12, T-14, T-15 and T-18 (William Lettis & Associates, Inc. (2001) Diablo Canyon ISFSI Data Report D). In each trench the thickness and attitude of the clay were recorded. Locations of clay beds observed in trenches and surface exposures are shown on Figure 21-4.

Clay beds also were identified in many of the borings (Table 21-2). The clay beds are more common and generally thicker in the dolomite bedrock (Unit Tof_{b-1}) and less common and thinner in the sandstone bedrock (Unit Tof_{b-2}) (Table 21-3). The identification of a clay bed (as opposed to a clay-filled fracture or joint) in the borings required careful analysis. The differentiation of clay beds from joint and fracture clay infills was initially noted by the geologist in the field during core logging (William Lettis & Associates, Inc. (2001) Diablo Canyon ISFSI Data Report B). This information was reviewed and verified by at least two geologists through visual inspection of the rock core. Because confirmed bedding attitudes defined by clear stratigraphic laminations typically dip in the range of about 5 to 20 degrees, only clay occurrences with a dip of less than 30 degrees and judged to be a clay bed were identified as possible clay beds for incorporation in cross sections and highlighted by bold font in Table 21-2. Clay seams

dipping steeper than 30 degrees are interpreted to be clay coatings and infillings along faults and joints rather than stratigraphic clay beds and were not tabulated in Table 21-2.

Borehole televiewer data also provide documentation of the presence of in situ clay beds. Clay beds were identified in the televiewer images as zones of borehole erosion, "softer" and blocky to massive layers, and non-jointed zones between more brittle jointed rock. This information is particularly useful in portions of the borings where the recovery of rock core was less than 100 percent. NORCAL provided the initial interpretation of the optical televiewer data and identified possible clay beds (William Lettis & Associates, Inc. (2001) Diablo Canyon ISFSI Data Report E). The NORCAL interpretation and the televiewer logs were then independently interpreted by at least two geologists to verify the existence of the clay beds. In most cases, clay beds identified on the televiewer logs were visually correlated and verified as clay beds in the rock core. Exceptions to the visual verification were some zones of possible clay that were not recovered in the core and appeared to have been "washed out" during drilling. Some other possible clay beds noted by examination of televiewer logs corresponded to clayey dolomite or sandstone zones in the core rather than clay beds. Confirmed clay beds identified on the televiewer logs were added to Table 21-2. All the interpreted clay beds were plotted and used to help evaluate bedding orientation and lateral continuity of the clay beds on the cross sections.

In addition, samples of the clay beds were collected for laboratory analysis of physical properties (William Lettis & Associates, Inc. (2001) Diablo Canyon ISFSI Data Report G) and petrographic analysis of lithologic and chemical composition (William Lettis & Associates, Inc. (2001) Diablo Canyon ISFSI Data Reports J and K).

4.3 Cross Sections

The following methodology was used to prepare the geologic cross sections in the ISFSI study area and along the transport route.

1. A topographic profile showing cultural features was drawn based on topographic maps of the ISFSI and Plant Site areas as described in Section 2.2, and shown on Figure 21-6. Several cross sections that extend into areas covered only by the Towill topographic base map were constructed using field-surveyed profiles as described in Section 2.2.
2. All lithologic contacts, structural features, and exploratory boring and trench locations intersecting the cross section alignment were plotted. Boring, and trench locations within 100 feet of the cross section line were extrapolated at a right angle onto the section line using the following guidelines: no data were projected across faults or fold axes; borings were projected and placed on the cross section at their true elevation unless otherwise noted; trenches were not projected uphill or downhill onto the cross section.
3. Surface bedding attitudes within 100 feet of the section line were projected perpendicular to the line of section and plotted as apparent dips. Bedding attitudes from the borings were taken from the table on bedding in the ISFSI borings (Table 21-1) and plotted as apparent dips. The apparent dips were obtained using the apparent dip nomograph from Figure 2-22 of Suppe (1985) and checked using the equation:

$$\tan \alpha = \tan \delta \times \sin \beta,$$

where α = apparent dip, δ = true dip, and β = angle between the strike of bed and strike of section (Rowland, 1986).

Clay bed attitudes were used to constrain the geometry of bedding with an uncertainty of ± 5 degrees.

4. Contacts between the main stratigraphic units, sandstone (Unit Tof_{b-2}) and dolomite (Unit Tof_{b-1}), as shown in the borings logs were projected into the

cross section. The location, thickness, and dip of friable zones of dolomite and sandstone (Tof_{b-1a}, Tof_{b-2a}) in the borings were taken from the table summarizing the friable dolomite and sandstone (Table 21-4). Clay beds were plotted from the table of clay beds (Table 21-2).

5. Information from previous maps and studies were added to the sections after reviewing the data for consistency and quality. This information included pre-excavation topography from the Towill map, geologic stratigraphic and structural data, and subsurface exploration data. Primary sources for this geologic information included studies by Harding Miller Lawson Associates (HML, 1968) and Harding Lawson and Associates (HLA, 1970) and the Diablo Canyon Power Plant FSAR (PG&E, 2000). This information was plotted on the cross sections, as appropriate, in a similar fashion to items 1 to 4 above.
6. Cross section intersections were checked for consistent interpretation, and to provide additional stratigraphic and structural control between cross sections. In this manner, a single internally consistent interpretation of the three-dimensional geology of bedrock was developed for the ISFSI study area and along the transport route.

All interpreted clay beds from the borings (Table 21-2) and from the trenches (William Lettis & Associates, Inc. (2001) Diablo Canyon ISFSI Data Report D) were plotted on the geologic cross sections. The variable thicknesses of the clay beds (Table 21-3) are indicated by different line weights: clay beds thinner than $\frac{1}{8}$ -inch have a thin line weight; $\frac{1}{8}$ - to $\frac{1}{4}$ -inch-thick beds have a medium line weight; beds thicker than $\frac{1}{4}$ -inch have a heavy line weight.

Similarly, the lateral continuity of clay beds is shown using the following criteria (see Section 5.2.2.4):

Clay beds $> \frac{1}{4}$ -inch thick – extended for 100 feet as a solid line and 100 feet as a dashed line from surface exposure, and to both sides of borings;

Clay beds $\frac{1}{8}$ - to $\frac{1}{4}$ -inch thick – extended for 50 feet as a solid line and 50 feet as a dashed line from surface exposures, and on both sides of borings; and,

Clay beds $< \frac{1}{8}$ -inch thick – extended for 25 feet as a solid line and 25 feet as a dashed line from surface exposures, and on both sides of borings.

Clay beds are shown with shorter lateral continuity where they are known to be absent in adjoining boreholes or are interpreted to be offset by faults.

Bedding attitudes measured in the boreholes are considered “local” or point attitudes because they are measured over only a 4-inch-wide core. As such, they may not record the true regional strike and dip, but may be a local attitude that is anomalous to the regional dip. For example, the attitude of the base of the clay bed at 55.4 feet depth in Boring 00BA-1 (Figure 21-30) is markedly different than the other attitudes in the boring or at the surface. Therefore, this measurement was not used on the cross section for controlling the dip of the strata of clay beds in that area.

Where possible, as between borings 01-F and 01-H, distinct lithologic beds were used to establish the dip of the strata. Elsewhere the dips measured in the boreholes and at the surface were compared and assessed for general continuity and the general attitude is used to project strata between borings.

Because the depositional environment for dolomite (Unit Tof_{b-1}) is interpreted to be pelagic deep marine (William Lettis & Associates, Inc. (2001) Diablo Canyon ISFSI Data Report L), the clay beds were assumed to have been deposited as laterally continuous

beds. The thickness of the clay beds varies because clays were deposited on irregular erosional surfaces and because subsequent erosion and/or diagenetic differential compaction may have removed or thinned clay in some areas. For example, during deposition on a submarine fan, turbidite pulses of sand associated with sandstone of Unit Tof_{b-2} may have locally scoured and eroded the deep marine, pelagic clay beds. In the sandstone sequence (Unit Tof_{b-2}), the less frequent clay beds probably represent finer-grained tails at the distal ends of the turbidite flows, or the upper fine-grained pelagic "D" and "E" layers in the classic Bouma sequence (Reading, 1981).

In cross sections, clay beds were extrapolated between surface exposures and boring control points by projecting lines parallel to bedding strata and, in several constrained areas, parallel to the general facies contact between dolomite (Tof_{b-1}) and sandstone (Tof_{b-2}). The spacing between projected clay beds was kept constant to reflect uniform bedding thickness in the rock sequence. In some cases where clay beds encountered in individual borings and surface exposures are at the same stratigraphic level and have similar thickness and character, the clay beds were interpreted to be continuous and were connected between control points for distances up to several hundred feet. We believe that this is a conservative, but reasonable, interpretation. In other cases, clay beds were not encountered at the projected locations in other borings or surface exposures, and therefore were terminated at some distance away from control points.

Some cross sections, such as sections B-B'', C-C' and J-J' (Figures 21-15, 21-16 and 21-23), cross one or more faults that have displaced strata both horizontally and vertically. Trench and borehole data were not projected across faults onto the cross sections to eliminate problems associated with mismatching of stratigraphy and inaccurate plotting of fault displacement locations.

Other cross sections, such as I-I' and G-G' (Figures 21-22 and 21-20) were drawn within and roughly parallel to the fault blocks so that the continuity of clay beds and other strata such as friable zones, could be interpreted without the complications of significant faulting.

Friable zones in the dolomite and sandstone (Units Tof_{b-1a} and Tof_{b-2a}, respectively) appear to have limited lateral extent in trenches and surface outcrops. Therefore, in the cross sections, the friable zones were extended for 50 to 100 feet away from trench or borehole control points as irregular lenses. The distance of projection is related to the thickness of the friable zone, with thicker zones (over about 10-feet thick) having more distant projection than thinner zones.

5.0 ANALYSIS (BODY OF CALCULATION)

Geologic information obtained during this study is shown on a series of geologic maps covering the plant site area (Figure 21-1), the ISFSI study area including the transport route (Figure 21-3), and the ISFSI site (Figure 21-4). Information shown on Figure 21-1 was compiled largely from pre-existing information contained in the FSAR (PG&E 2000), LTSP (PG&E, 1988), and Hall et al. (1979) supplemented by more recent site reconnaissance mapping during the ISFSI site investigations. Information shown on Figures 21-3 and 21-4 was developed primarily during the ISFSI site investigation.

The geology in the ISFSI study area is complex. Understanding the complexity of the geology and the various geologic processes giving rise to the current geologic conditions is important for interpreting the stratigraphy and structural geology at the site. Below, the geologic processes giving rise to the bedrock complexity are described, followed by an analysis of the stratigraphic and structural relations at the site.

5.1 Bedrock Evolution

Bedrock in the ISFSI study area has undergone a complex history of deposition, alteration and deformation. Based on analysis of surface and subsurface data, supplemented by petrographic analyses of rock lithology, mineralogy, and depositional

history, the following events produced the current lithology and stratigraphic character of bedrock at the site (Figures 21-7 and 21-8):

1. Original deposition
2. Diagenesis and dolomitization
3. Localized addition of petroliferous fluids
4. Diabase intrusion, hydrothermal alteration, and associated deformation
5. Tectonic deformation (folding and faulting)
6. Surface erosion and weathering (both chemical and mechanical)
7. Borrow excavation and stress unloading

This sequence of events is illustrated in Figure 21-7 and described below. The approximate timing of these events is shown on Figure 21-8.

(1) Original Depositional Environment

Sediments comprising the lithified bedrock in the ISFSI study area were originally deposited in a moderate to deep marine environment, probably on the outer continental shelf or continental slope during the early to middle Miocene. Petrographic analyses show the presence of benthic foraminifera, sponge spicules, and other biogenic material indicative of a moderate to deep marine, pelagic environment.

Deposits consist of a sequence of tuffaceous arkosic and lithic arenitic sandstones and siltstones grading laterally into biogenic chemical limestones and pelagic siltstones. Thin pelagic clay beds, locally containing foraminifera, occur interbedded with the limestone/siltstone sequence and to a lesser extent within the sandstone sequence. Deposition of the clay in a moderate to deep marine environment suggests that the clay beds originally blanketed the sea floor and formed laterally continuous beds.

The sandstone sequence is interpreted to be a turbidite clastic fan prograding and interfingering with the deep marine quiet water biogenic and pelagic limestone and

siltstone sequence (Figure 21-7A). The ISFSI study area straddles the gradational facies contact between these two depositional environments. The turbidite sequence represents high-energy submarine debris flows that have reworked pyroclastic tuffaceous shallow marine deposits out onto the outer continental shelf or continental slope. Turbidite sediment was derived from continental erosion and volcanism, and consisted of mixtures of older terrigenous debris and volcanic airfall tuff and ash and alluvially-transported debris. The lesser amounts of clay in the turbidite sequence probably reflects localized erosion and scour of the clay deposits by the high-energy turbidite flows.

Borehole data at the ISFSI study area clearly show an upward textural facies change from a relatively coarse sequence of sandstone to relatively fine sequence of limestone and siltstone (now dolomite). This depositional facies change is illustrated on the upper part of Figure 21-7A.

Bedding ranges from thinly bedded (less than ¼-inch thick) to massively bedded (greater than 5 feet thick). Bedding generally is better developed and/or preserved in the limestone/siltstone sequence and less well developed and/or preserved in the sandstone sequence.

(2) Diagenesis and Dolomitization

Following deposition and burial, the entire depositional sequence was subjected to diagenesis and chemical replacement and recrystallization by a process called dolomitization (illustrated in Figure 21-7B). The degree of dolomitization varies markedly over short distances and was apparently influenced by grain size and permeability differences in the original sediments. In this process, the finer-grained limestone is completely or nearly completely recrystallized to crystalline dolomite, siltstone is strongly to moderately recrystallized, and sandstone is moderately to weakly recrystallized with localized beds of strongly recrystallized dolomite and localized beds of less-dolomitized friable sandstone. All the rock types, siltstone, sandstone and limestone, maintain their original relict textures to some extent as individual grains of

plagioclase and clastic material were replaced with dolomite. The process of dolomitization locally obscures bedding and in places makes lateral correlation of individual beds between boreholes very difficult. During diagenesis many clastic and plagioclase grains were altered to clay. In some cases, the clay was partially dolomitized; in other cases the clay is not dolomitized. Dolomite replacement increased the degree of cementation in the finer-grained rocks of the dolomite (Unit Tof_{b-1}), and as a result these rocks are somewhat stronger and more brittle than the sandstone (Unit Tof_{b-2}), which typically has less cementation.

The process of dolomitization may have been influenced by, or caused by, hydrothermal activity associated with the emplacement of shallow diabase intrusions in the site area. Diabase intrusion and hydrothermal activity is described in process 4 below.

(3) Localized Addition of Petroliferous Fluids

Zones of hydrocarbon accumulations are locally preserved throughout the rock sequence at the ISFSI study area, but preferentially within the dolomite. Black, sticky hydrocarbon films also were observed on fractures and within faults in some of the exploratory trenches (e.g., Trench T-20A, William Lettis & Associates, Inc. (2001) Diablo Canyon ISFSI Data Report D). The origin or source rock of the hydrocarbons is not known. It may be that during or after the process of dolomitization, diagenesis of the bioclastic fraction of the rock at the site caused the mobilization and localized deposition of hydrocarbons. The areas of hydrocarbon accumulation occur in patches or splotches within the rock mass as well as concentrated along some faults and joints, and are not confined to individual beds, showing that at least some migration of the hydrocarbons has occurred. The patches of hydrocarbons commonly crosscut bedding, and tend to stain and obscure the stratigraphic relationship. These patches of hydrocarbons are shown diagrammatically on Figure 21-7B.

(4) Diabase Intrusion, Hydrothermal Alteration, and Associated Deformation

Locally, hypabyssal shallow intrusions of diabase invaded the dolomitic sandstone, siltstone, and dolomite of the Obispo Formation as illustrated in Figure 21-7C.

Petrographic analyses show that the diabase is primarily an altered cataclastic gabbro and diorite. Radiometric dates on similar diabase elsewhere in the Irish Hills indicate that the intrusions are middle Miocene in age (Hall et al., 1979). The diabase occurs as sills, dikes, and larger, massive intrusive bodies. The diabase is locally exposed along Diablo Canyon Creek beneath the eastern part of the Raw Water Reservoir and along the northern margin of the canyon walls. Prior to the 1971 excavation of the borrow cut area, a large diabase sill in the Obispo sandstone and dolomite was present in the raw water reservoir area (Figure 21-14) (HLA, 1968). This body of diabase was entirely removed during the borrow excavation, and no diabase was observed in the ISFSI study area or along the transport route during surface mapping and subsurface exploration. However, the feeder vent for the now-removed diabase sill has not been identified and possibly it or other intrusions may underlie the ISFSI site.

Hydrothermal solutions associated with the diabase intrusion locally altered the diabase and probably altered the surrounding wall rock. Petrographic analyses of the diabase show clear evidence of hydrothermal alteration (William Lettis & Associates, Inc. (2001) Diablo Canyon ISFSI Data Report J).

As mentioned above, the intrusion of diabase and associated hydrothermal activity also may have caused or influenced the process of dolomitization in the site area. Intrusion of the magnesium-rich diabase would have caused circulation of natural occurring magnesium-rich seawater or hydrothermal fluids rich in magnesium from the diabase in the surrounding wall rock. Partial replacement of the calcium by magnesium in the limestone, calcareous sandstone and siltstone may have produced the observed dolomite. Possible hydrothermal "dolomitization" of the bedrock is supported by the following observations:

- Hall et al. (1979) do not map or describe dolomite in the Obispo Formation in the plant site region (10 kilometer radius), thus, the dolomite appears to be localized in the vicinity of the diabase intrusion in Diablo Canyon.
- The diabase clearly was altered by late-phase hydrothermal solutions demonstrating the presence of hydrothermal activity.
- Petrographic analyses show the presence of zeolite and rare clays within the dolomitic sandstone and dolomite (William Lettis & Associates, Inc. (2001) Diablo Canyon ISFSI Data Report J) suggesting hydrothermal activity may have produced low-grade metamorphic changes in the host rock.
- The diabase is magnesium-rich and is a possible source of magnesium to replace calcium in the dolomitization process. Alternatively, the intrusion may have driven magnesium-rich seawater, the most common source of magnesium for dolomitization, through the rocks by thermal convection.

Intrusion of the diabase also may have been accompanied by magmatic stoping and/or localized uplift, warping and faulting of the bedrock. This localized deformation is diagrammatically illustrated on Figure 21-7C. Local uplift (or doming) of the bedrock may be the cause of the change in bedding attitudes observed on the lower half of the slope above the ISFSI site (described in the Analysis section below), and possibly formed or modified joints in the bedrock.

(5) Tectonic Deformation (Folding and Faulting)

Subsequent to the diabase intrusions in the middle Miocene, bedrock in the ISFSI study area was tectonically folded and faulted (Figure 21-7D) as part of the regional deformation that formed the Pismo syncline (Hall et al., 1979). The tectonic faulting and folding deformed the bedding and facies contacts within the sandstone/dolomite sequence. Folding of the facies contact, as well as the bedding, complicates the interpretation and correlation of bedrock stratigraphy at the site.

This area-wide tectonic deformation is superimposed on the earlier localized intrusive deformation from the diabase described above. In addition, the tectonic deformation may have been locally influenced by the more ductile rheology of the diabase. The ISFSI study area is situated on a northwest-trending syncline/anticline couplet (Figures 21-3, 21-4). The syncline/anticline couplet forms tight folds with steep limbs of up to 50 to 70 degrees directly south of the ISFSI site but transitions into folds with broad crests and gentle limbs of 5 to 20 degrees across the ISFSI site as the fold axes approach the former area of the diabase intrusion. This change in structure may be the result of tectonic deformation superimposed on the earlier intrusive "doming", or it may reflect the more ductile behavior of the diabase intrusion, or it may be simply a change in tectonic deformation without any influence from the diabase intrusion.

In addition to folding, a zone of northwest-trending minor faults disrupts the bedrock stratigraphy in the ISFSI study area (e.g., cross section B-B'", Figures 21-15 and 21-32). The faults are high-angle and slickensides indicate strike-slip to oblique strike-slip displacement. As shown on Figure 21-15, northeast-side down, vertical separation of at least 50 feet, occurs across the fault zone over a width of about 200 feet. Given the northwest dip of bedding, this sense of vertical separation can be produced by pure right-lateral strike slip or by a component of oblique right slip. The strike slip displacement juxtaposes stratigraphic units of different thicknesses and lithologies. The strike slip displacement also complicates the interpretation and correlation of bedrock lithology, bedding, and facies changes in the lower part of the slope and offsets the axis of the small anticline across the site.

(6) Surface Erosion and Chemical Weathering

During the past 1 million years, the ISFSI study area and transport route has been exposed to marine, fluvial and hillslope erosion. Remnants of marine deposits and hillslope colluvium are preserved locally in the ISFSI study area where they were not removed during excavation of the borrow area in 1971.

Infiltration of surface water and groundwater migration has chemically weathered and altered the bedrock. The degree of surface weathering decreases with progressive depth beneath the site and occurs preferentially and penetrates more deeply along fractures, joints and faults as shown in Figure 21-7E. The 1971 borrow excavation at the ISFSI site area removed the surficial soil and a variable thickness of bedrock from the site, with up to 100 feet of rock removal above the ISFSI pads (cross sections A-A' and B-B''; Figures 21-14 and 21-15). The original ground surface was a resistant bedrock spur ridge that had been subjected to weathering for a substantial time period, and had developed a weathered zone penetrating an unknown depth into the rock mass. As a result, the rock now exposed in the central part of the borrow excavation that was considerably below the former ground surface is less weathered than the rock along the margins of the borrow excavation where excavation was shallower. Additional minor weathering has occurred within the rock exposed after the borrow excavation was completed, but this "secondary" zone of weathering is the result of only about 30 years of exposure, as opposed to the many tens to hundreds of thousands of years of exposure for the original bedrock surface.

The surface weathering is superimposed on the pre-existing hydrothermal alteration, petroliferous alteration and dolomitization as shown on Figure 21-7E. The combination of alteration products (to varying degrees of development) significantly masks the primary depositional lithology and bedding, and complicates the interpretation of depositional origin.

(7) Borrow Excavation and Stress Unloading

Rock removal associated with the borrow excavation decreased the lithostatic stress on the bedrock currently exposed at the site (Figure 21-7F). Since then, stress unloading has caused shallow localized dilation of the rock mass, and the opening of joints, fractures and other discontinuities. This shallow dilation of the rock mass tends to mask bedding, so differentiating bedding from joints and fractures in the bedrock is difficult in surface exposures and exploratory trenches.

5.2 Stratigraphic Analysis

Bedrock in the ISFSI study area and along the transport route is differentiated into distinct, mappable lithologic units taking into account the complex depositional history and alteration of the rock mass. The following sections describe this stratigraphy.

5.2.1 General Stratigraphy

Sandstone and dolomite bedrock in the ISFSI study area and along the transport route belongs to the fine-grained member of the early to middle Miocene Obispo Formation (Tof) as mapped by Hall et al. (1979). Mapping of the DCPD plant site area differentiated three subunits (Units Tof_a, Tof_b, Tof_c) of the fine-grained member of the Obispo Formation (William Lettis & Associates, Inc. (2001) Diablo Canyon ISFSI Data Report A). As shown on Figure 21-1, Unit Tof_a occurs in the eastern part of the plant site area (entirely east of the ISFSI study area) and consists primarily of thick to massively bedded diatomaceous siltstone and tuffaceous sandstone. Unit Tof_b occurs in the central and west-central part of the DCPD plant site area, including the entire ISFSI study area, the upper part of the transport route and beneath the power block, and consists primarily of medium to thickly bedded dolomite, dolomitic siltstone, dolomitic sandstone, and sandstone. Unit Tof_c occurs in the western part of the plant site area beneath the lower part of the transport route and consists of thin to medium bedded, extensively sheared shale, claystone and siltstone. In addition, locally extensive areas of diabase intrusive rocks were mapped along the northern margin of Diablo Canyon Creek and locally below the raw water reservoir (Unit Tvr).

5.2.2 ISFSI Study Area Stratigraphy

In the ISFSI study area, Unit Tof_b is further divided into a dolomite subunit (Tof_{b-1}) and a sandstone subunit (Tof_{b-2}). For ease of discussion, these subunits are referred to as Units Tof_{b-1} and Tof_{b-2}. Figure 21-5 provides a generalized stratigraphic column illustrating the distribution of rock types within these two subunits. Unit Tof_{b-1} consists primarily of dolomite, dolomitic siltstone, fine-grained dolomitic sandstone, and limestone. Unit

Tof_{b-2} consists primarily of medium to coarse-grained dolomitic sandstone and sandstone. Figures 21-9 to 21-12 provide summary logs of all the borings drilled in the ISFSI study area during the ISFSI site investigation. These summary logs show the primary lithologic units and clay beds greater than ¼-inch thick. Additional thinner clay beds encountered in the borings are listed in Table 21-3. These data were used together with surface geologic data to construct 12 cross sections across the study area (Figures 21-13 to 21-25).

The contact between Units Tof_{b-1} and Tof_{b-2} marks a facies change from the deep marine dolomite sequence to the sandstone turbidite sequence. The contact varies from sharp to gradational and bedding from one unit locally interfingers with bedding of the other unit. For purposes of mapping, we arbitrarily place the contact at the first occurrence (proceeding down section) of medium to coarse-grained dolomitic sandstone. As shown on the cross sections, the interfingering nature of the dolomite/sandstone contact beneath the ISFSI study area can be interpreted. This relationship is shown on cross sections A-A', B-B'', C-C', and I-I' (Figures 21-14, 21-15, 21-16, and 21-22, respectively). Some of the thin interfingering beds provide direct evidence for the lateral continuity and geometry (i.e., attitude) of bedding within the hillslope (for example, between boring 01-F and 00BA-1 on section I-I').

Analysis of the cross sections shows that the facies contact between Units Tof_{b-1} and Tof_{b-2} generally extends from northwest to southeast across the ISFSI study area, with sandstone of Unit Tof_{b-2} primarily in the north and northeast part of the area and dolomite of Unit Tof_{b-1} primarily in the south and southwest part of the area. The three-dimensional distribution of the facies contact is well illustrated by comparing cross sections B-B'' and I-I' (Figures 21-15 and 21-22, respectively). This distribution of the two units indicates that the source area of sandstone turbidite sequence lay to the northeast and the moderate to deep marine basin lay to the southwest.

In addition, we recognize two different transgressions of the dolomite of Unit Tof_{b-1}, an upper transgression or tongue of dolomite and a lower transgression of dolomite. The

upper transgression of dolomite and its contact with the underlying sandstone, as described above, is well documented in the borings, trenches and surface outcrops as shown on Figures 21-4 and 21-22. The south-southwestern extent of the underlying sandstone facies is indicated by borehole 01-I (Figure 21-22), which penetrated a thick sequence of dolomite and documents the absence of sandstone above the elevation of the borehole bottom. The lower transgression or tongue of dolomite that underlies the sandstone is exposed in the roadcut along Reservoir Road in the vicinity of Parking Lot 8. Based on the occurrence of calcareous siltstone and locally abundant foraminifera in boreholes beneath the power block, the lower transgression of dolomite is inferred to extend beneath the power block as shown on cross sections B-B''' and C-C' (Figures 21-15 and 21-16, respectively).

During initial stratigraphic analysis, depositional facies within each of the two subunits were further differentiated: Unit Tof_{b-1} was divided into facies A (dolomite) and B (dolomitic siltstone); while Unit Tof_{b-2} was divided into facies C (dolomitic sandstone) and D (sandstone). These additional facies contacts were used to help evaluate the internal stratigraphy within each subunit and to understand the depositional environment of the bedrock. After thorough analysis of all the borings and surface outcrops, these additional facies (A, B, C, D) contacts could not be confidently mapped across the ISFSI study area; thus, we do not show these units on the summary boring logs or on the cross sections. However, boring logs in William Lettis & Associates, Inc. (2001) Diablo Canyon ISFSI Data Report B contain these facies designations for reference.

5.2.2.1 Dolomite (Unit Tof_{b-1})

The slope above the ISFSI site, including most of the 1971 borrow area excavation slope, is underlain by dolomite (Figure 21-4). The dolomite is exposed as scattered outcrops across the excavated slope, along the unpaved tower access road, in the upper part of most borings in the ISFSI study area (William Lettis & Associates, Inc. (2001) Diablo Canyon ISFSI Data Report B), and in most exploratory trenches (William Lettis & Associates, Inc. (2001) Diablo Canyon ISFSI Data Report D). The dolomite consists predominately of tan to yellowish-brown, competent, well-bedded dolomite, with

subordinate dolomitic siltstone to fine-grained dolomitic sandstone, and limestone (Figure 21-34). Petrographic analyses of hand and core samples from, and adjacent to, the ISFSI study area show that the rock is primarily carbonate (dolomite) with a variety of secondary components. The petrographic analyses show that the rock consists primarily of clayey dolomite, altered clayey carbonate and altered calcareous claystone, with lesser amounts of clayey fossiliferous, bioclastic and brecciated limestone, fossiliferous dolomite, and altered sandstone and siltstone (William Lettis & Associates, Inc. (2001) Diablo Canyon ISFSI Data Report J, Tables J-1 and J-2). X-ray diffraction analyses show that the dolomite has about 25% quartz, 8% feldspar, 40 to 50% dolomite (including some calcite), a few percent clays, and 15 to 20% amorphous material (William Lettis & Associates, Inc. (2001) Diablo Canyon ISFSI Data Report J, Table J-3). As described in the petrographic analysis, the carbonate component of these rocks is primarily dolomite; thus we use the general term dolomite and dolomitic sandstone to describe the rock.

The dolomite crops out on the excavated borrow area slope as flat to slightly undulating rock surfaces. The rock is moderately hard to hard and typically medium strong to brittle, with locally well-defined bedding that ranges between several inches to 10 feet thick in surface exposures and boreholes. Bedding planes are laterally continuous for several tens of feet as observed in outcrops, and may extend for hundreds of feet based on the interpreted marine depositional environment. The bedding planes are generally tight and bonded. Unbonded bedding parting surfaces are rare and generally limited to less than several tens of feet based on outcrop exposures.

5.2.2.2 Sandstone (Unit Tof_{b-2})

Strata of the sandstone Unit Tof_{b-2} generally underlies the ISFSI study area below about elevation 330 feet (Figure 21-4). Typically, the rocks in this subunit are well-cemented, hard sandstone and dolomitic sandstone and lesser dolomite beds, as encountered in the lower part of borings 98BA-1, 00BA-2 and 00BA -3, and in borings CTF-A, 01-A, 01-B, 01-C, 01-D, 01-E, 01-F, 01-G and 01-H (Figures 21-9 to 21-12).

The well-cemented sandstone encountered in the borings and trenches is tan to gray, moderately to thickly bedded, and competent (Figure 21-35). The rock is well sorted, fine to coarse-grained, and is typically moderately to well-cemented with dolomite. The rock is of low to medium hardness and medium strength. Petrographic analyses show that the sandstone is altered, and that its composition varies from arkosic to arenitic, with individual grains consisting of quartz, feldspar, and dolomite and volcanic rock fragments (William Lettis & Associates, Inc. (2001) Diablo Canyon ISFSI Data Report J). The matrix of some samples contains a significant percentage of carbonate and calcareous silt to clay matrix (probably from alteration). X-ray diffraction analyses show that the sandstone is about 20% quartz, 15 to 20% feldspar, 15% dolomite (with some calcite), and about 40% clay (10% kaolin and 30% smectite); one sample (P-21) is dominantly clastic dolomite with only 7% quartz and about 15% clays (William Lettis & Associates, Inc. (2001) Diablo Canyon ISFSI Data Report J, Table J-3). Petrographic and x-ray analyses show that the carbonate is primarily dolomite. Thus, these rocks are referred to as sandstone and dolomitic sandstone. Bedding in places is well defined, and bedding plane contacts are tight and well bonded. Similar to the dolomite beds, unbonded bedding surfaces within the sandstone are rare and generally limited to less than several tens of feet based on limited outcrop exposure.

5.2.2.3 Friable Bedrock

Distinct zones of friable bedrock are present within the generally more cemented sandstone and dolomite (Figures 21-4 and 21-32; Table 21-4). In some cases, the friable bedrock appears to reflect the original deposit without subsequent dolomitization. In other cases the friable bedrock appears to be related to subsequent chemical weathering, and/or hydrothermal alteration. All friable beds within Units Tof_{b-1} and Tof_{b-2} are designated with the subscript (a).

Unit Tof_{b-1a} consists primarily of altered-or-weathered dolomite or dolomitic siltstone that has block-in-matrix friable consistency or simply a silt and clay matrix with friable consistency. The friable rock is of low hardness and is very weak to weak. X-ray diffraction analyses show the friable dolomite to have about 20% quartz, 10% feldspar,

50% dolomite that is about half composed of a poorly crystalline phase, and 16% clay (mostly smectite) (William Lettis & Associates, Inc. (2001) Diablo Canyon ISFSI Data Report J, Table J-3). The primary differences between the dolomite and friable dolomite is the poorly crystalline phase and a higher percentage of clay, both are probably caused by weathering or alteration of the dolomite.

Unit Tof_{b-2a} consists primarily of friable sandstone, is of low hardness, and is very weak to weak. X-ray diffraction analyses show the friable sandstone has about 15% quartz, 10% feldspar, 15 to 20% dolomite (including some calcite), and 50 to 60% clay (10% kaolin, 50% smectite); one sample (P-21) is dominantly a clastic dolomite with only 7% quartz and about 15% clay (Diablo Canyon ISFSI Date Report J, Table J-3). The friable sandstone exhibits a somewhat lower feldspar content and a higher percentage of clays than the non-friable sandstone. In many cases, the friable sandstone is the original sandstone that has been chemically weathered or altered to a clayey sand (i.e., plagioclase and lithics altered to clay). In other cases, the friable sandstone simply lacks dolomite cementation and retains its original friable nature.

The friable zones in the dolomite and sandstone are known from exposures in the trenches and in the borings to be limited vertically and laterally in their extent. The vertical thickness of the friable rock encountered in borings ranges from less than 1 foot to 32 feet; the thickest friable zones were encountered in Boring 00BA-2 (Figures 21-9 through 21-12). The friable zones extend laterally for tens of feet in trench exposures, and were correlated up to about 200 feet between borings. As illustrated on the cross sections (e.g., I-I', J-J') the zones of friable rock appear more common, and possibly more laterally continuous, in the sandstone than in the dolomite. Friable beds were observed between beds of competent cemented sandstone and/or dolomite in exploratory trenches in the ISFSI pads area. Based on trench exposures and borehole correlations, friable zones are more laterally continuous in a direction along bedding than across bedding. Some thin, irregular friable zones or zones of weak rock were observed along and parallel to joints and faults. These zones do not appear to be as laterally continuous or thick as the bedding-parallel friable zones, and are not shown on cross sections.

5.2.2.4 Clay Beds

Clay beds are present within both the sandstone and dolomite subunits in the ISFSI study area (Table 21-3). The clay beds were observed in several trenches (Figure 21-36) and in many of the borings (Table 21-2; Figures 21-29, 21-30, and 21-31). Because these clay beds are potential layers of weakness in the hill slope above the ISFSI site they were investigated in detail. The clay beds generally are bedding-parallel and commonly range in thickness from thin partings (<1/16-inch thick) to beds up to 2 to 4 inches thick; the maximum thickness encountered was approximately 8½ inches in Boring 00BA1. Two-thirds of the clay beds encountered in the borings are less than ¼-inch thick; in contrast, about two-thirds of the clay beds exposed in the trenches are greater than ¼-inch thick (Table 21-3). This difference in thickness between the borings and trenches, however, probably reflects our ability to better recognize and document very thin clay beds in the rock core than in the trenches, rather than a true stratigraphic change between surface and subsurface exposures. The clay beds are yellow-brown, orange-brown, and dark brown, sandy and silty, and stiff to hard. Petrographic analyses show that the clay contains marine microfossils and small rock inclusions; the rock inclusions are angular pieces of dolomite that are matrix-supported, and have no preferred orientation or shear fabric (William Lettis & Associates, Inc. (2001) Diablo Canyon ISFSI Data Report K). In the trenches, the clay beds locally have slickensides and polished surfaces. The clay beds typically appear to be overconsolidated (because of original burial), and, where thick, have a blocky structure.

The clay beds encountered in the borings are recorded on the boring logs. In addition, in most of the borings, the clay beds were also documented in situ by a borehole televiwer. The televiwer logs show that the clay beds generally are in tight contact with the bounding rock and are bedding-parallel. The clay beds range from massive with no preferred shear fabric, to laminated with clear shear fabric. The shear fabric is interpreted to be the result of tectonic shearing during folding and flexural slip of the bedding surfaces; the shear fabric does not reflect gravitational sliding because features indicative of large-scale rock slides, such as disarticulation of the rock mass, lack of bedding

continuity or change in bedding orientation, tensional fissures and geomorphic expression of a landslide on pre-construction air photos, are not present.

Clay Beds in Dolomite. Clay beds are more frequent, thicker and more laterally continuous in the dolomite (Unit Tof_{b-1}). Examination of the continuity of clay beds within, and between, adjacent trenches, road cuts, and borings provided data on the lateral continuity (persistence) of the clay beds. Individual clay beds exposed in the trenches and road cuts appear to be persistent over distances of between tens of feet to over 160 feet, extending beyond the length of the exposures. The exposed clay beds are wavy and exhibit significant variations in thickness along the bed. Thinner clay beds (less than about ¼-inch thick) typically contain areas where asperities on the surfaces of the bounding adjacent hard rock project through or into the thin clay. The bedding surfaces also commonly are irregular and undulating with the height (amplitude) of the undulation greater than the thickness of the clay bed such that the clay beds likely have local rock-to-rock contact that increases shear strength along clay bed interfaces to a greater value than that of the clay itself. This would increase the average shear strength of the clay bed surface for analyses of potential sliding along these interfaces. For example, the clay bed exposed in Trenches T-14A and T-14B extends for about 160 feet, including the length of Trench T-14, the adjacent roadcut exposure, and correlation to the clay exposed Trench T-19. The thickness of this clay varies from about 4 inches in Trench T-14 and decreases to about ¼-inch in Trench T-19 where the clay splays into several thin clay beds. Many of the clay beds appear to correlate between outcrops and borings. For example, the clay bed in Trenches T-11 and T-12 appears to correlate over a distance of about 100 feet. Other correlations are shown on cross section I-I' (Figure 21-22). These correlations indicate that at least some clay beds extend over several hundred feet into the hillslope. However, some beds clearly do not correlate; for example, the clay beds exposed in Trenches T-14 and T-15 are not found in nearby Boring 01-I. The interpreted lateral continuity of clay beds is best illustrated on cross section I-I' (Figure 21-22).

Clay Beds in Sandstone. Clay beds are less frequent, generally thinner, and less laterally continuous in the sandstone (Unit Tof_{b-2}). As shown on Table 21-3, clay beds in the sandstone generally are less than ¼-inch thick. These thinner clay beds are difficult to correlate laterally between borings and, at least locally, are less than 50 to 100 feet in lateral extent. For example, as shown on cross sections B-B''' and I-I', (Figures 21-15 and 21-22, respectively), clay beds were not encountered in Boring 01-B but were encountered in adjacent borings 50 to 100 feet away (i.e., Borings 01-A and 01-H). Consequently, we interpret that the clay beds in the sandstone generally are thin (i.e., less than ¼-inch thick) and have lateral continuity of less than 100 feet in the ISFSI site area.

Clay Moisture Content. The clay beds encountered in the borings and trench excavations in both the dolomite and sandstone were moist. Clay beds uncovered in the trenches that dried out after exposure during the dry season, became hard and desiccated. When wetted during the rainy season, the clay in the trenches became soft and sticky; possible local perched water tables (William Lettis & Associates, Inc. (2001) Diablo Canyon ISFSI Data Report B) also may soften the upper portions of the clay beds during the rainy season in the ISFSI site area.

Clay Composition. X-ray diffraction analyses (William Lettis & Associates, Inc. (2001) Diablo Canyon ISFSI Data Report K) show that the clay-size fraction of the clay beds in Trenches T-11A, T-14A, T-14B, and T-15 consists of three primary minerals: kaolinite (a clay), ganophyllite (a zeolite), and sepiolite (a clay). The silt-size fraction of the sample consists primarily of rock and mineral fragments of quartz, dolomite/ankerite, and calcite. Petrographic examination of the clay (William Lettis & Associates, Inc. (2001) Diablo Canyon ISFSI Data Report K) shows a clay matrix with matrix-supported angular rock fragments and no shear fabric. Included rock fragments have evidence of secondary dolomitization of original calcite (limestone), and localized post-depositional contact alteration. Some samples contain microfossils (benthic foraminifera). The ganophyllite minerals appear to be expansive, as evidenced by swelling of one sample (X-1 from Trench T-14A) after thin-section mounting. Sample X-2 also had a significant

percentage of ganophyllite, and a high plasticity index (PI) of 63 (William Lettis & Associates, Inc. (2001) Diablo Canyon ISFSI Data Reports K and G, respectively).

The presence of microfossils confirms that the clay is depositional in origin and was not formed by alteration or weathering of a lithified host rock. Therefore, the clay is interpreted to reflect pelagic deposition in a marine environment.

5.3 Structural Analysis

Bedrock in the ISFSI study area has been deformed by tectonic processes and possibly by intrusion of diabase. The detailed stratigraphic framework described above provides the basis for analyzing the geologic structure in the site area.

Geologic structures in the ISFSI study area include folds, faults, and joints and fractures. Understanding the distribution and geometry of these structures is important for evaluating rock mass conditions and slope stability for two reasons: (1) folds in the bedrock produce the inclination of bedding that is important for evaluating the potential for out-of-slope bedding-plane slope failures; and (2) faults and, to a lesser extent, joints in the bedrock produce laterally continuous rock discontinuities along which potential rock failures may detach in the proposed cutslopes.

The distribution and geometry of folds and faults in the bedrock were evaluated by detailed surface geologic mapping, trenches, and borings. Data from these studies were integrated to produce geologic maps (Figures 21-1, 21-3, and 21-4) and geologic cross sections (Figures 21-13 to 21-24). Cross sections were prepared oriented both down slope and parallel to slope to evaluate the three-dimensional distribution of structures. Bedding attitudes were obtained from surface mapping (including road cut and trench exposures) and from boreholes (based on visual inspection of rock core integrated with oriented televiewer data). Bedding attitudes from surface mapping are shown on the geologic maps. Bedding attitudes from boreholes are compiled in Table 21-1. All of

these bedding attitudes were used to constrain the distribution of bedrock lithologies and geometry of bedding shown on the cross sections as described earlier.

5.3.1 Folds

As shown on the geologic maps (Figures 21-1, 21-3 and 21-4) and cross sections (Figure 21-15, 21-16, 21-17 and 21-19), bedrock in the ISFSI study area is deformed into small northwest-trending synclines and anticlines along the western limb of the larger regional Pismo syncline (Figure 21-37). On the ridge southeast of the ISFSI study area, nearly continuous outcrops of resistant beds define an anticline and two en echelon synclines (Figures 21-1 and 21-3). These folds, which are relatively tight and sharp-crested with steep limbs, plunge to the northwest.

Within the ISFSI study area, a northwest-plunging anticline appears to represent the northwestward continuation of the anticline that is exposed in the ridgetop near the Skyview Road overlook (Figure 21-1). The anticline varies from a tight chevron fold southeast of the ISFSI study area to a very broad-crested open fold across the central part of the study area. The northwestward shallowing of dips along the anticlinal trend appears to reflect a flattening of fold limbs up section. In the ISFSI study area, the broad crest of the fold is offset and disrupted by series of fold-parallel, minor faults (Figure 21-15). The minor faults offset the fold axis as well as produce local drag-folding, which tends to disrupt and complicate the fold geometry. The axis of this broad-crested anticline is approximately located on the geologic map (Figure 21-4) where it best fits the data.

The en echelon syncline found at the ridge crest along Skyview Road projects to the northwest along the southwestern margin of the ISFSI study area. In this area, the syncline transitions into an en echelon northwest-trending monocline and syncline (Figures 21-1 and 21-3). In the ISFSI study area, the syncline opens into a broad, gently northwest-plunging (generally less than 15 degrees) fold with gently sloping limbs (generally less than 20 degrees). Bedding generally dips downslope to the northwest in the upper part of the slope above the ISFSI site and parallel to the slope to the southwest

and west in the lower part of the slope. Minor undulations in the bedding reflect the transition from a tight syncline to a relatively flat monocline, or "shoulder", and then back to a broad northwest-plunging syncline. These localized interruptions to the northwest plunge of the fold may be caused by the diabase intrusion and localized doming associated with the intrusion (compare Figures 21-7c and 7d).

Understanding the location, geometry and characteristics of the syncline at the site is important for evaluating bedrock beneath the power block and establishing a correlation of bedrock between the power block and the ISFSI site. As discussed above and shown on cross sections B-B'', C-C', D-D', E-E', and F-F' (Figures 21-15 to 21-19), the western limb of the small syncline varies from steeply dipping (approximately 70 degrees northwest) across the southern part of the plant site area to gently dipping (approximately 30 degrees northwest) beneath the power block. This change in dip of the syncline across the plant site mirrors the change in dip described above across the ISFSI site area.

Based on the geometry of the syncline, bedrock beneath the power block consists of sandstone of Unit Tof_{b-2} underlain by the lower body of dolomite of Unit Tof_{b-1} (cross sections B-B'' and C-C', Figures 21-15 and 21-16, respectively). The power block is located on the same stratigraphic sequence that is exposed at the ISFSI site, but is approximately 400 feet lower in the stratigraphic section. As shown on cross section B-B'', boreholes drilled during foundation exploration for the power block encountered calcareous siltstone with abundant foraminifera. This description of the rock is very similar to the dolomite of Unit Tof_{b-1} ; thus, we interpret the lower contact between Units Tof_{b-1} and Tof_{b-2} to be present beneath the power block area.

Folding at the site occurred during growth of the northwest-trending regional Pismo syncline in the Pliocene to early Quaternary (PG&E, 1988). The smaller folds at and near the ISFSI site area are parasitic secondary folds along the southwest limb of the larger Pismo syncline. Because of their structural association to the Pismo syncline, we infer that the folding at the site also occurred during the Pliocene to early Quaternary

(Figure 21-8). Some deformation may have accompanied the earlier Miocene diabase intrusions.

5.3.2 Faults

Numerous minor, bedrock faults occur within the ISFSI study area (Figures 21-1, 21-4, 21-32, and 21-33). Based on offset lithologic and bedding contacts, most of the faults show vertical separations of a few inches to a few feet. At least five faults show vertical separation of several tens of feet. Slickensides and mullions on the fault surfaces generally show strike slip to oblique strike slip displacement (Table 21-5; Figure 21-38).

The primary faults trend northwest, subparallel to the local fold axes (Figure 21-38). They dip steeply to near-vertical, generally 70 to 90 degrees, both northeast and southwest (Table 21-5). They consist of interconnecting and anastomosing strands, in zones up to 5 feet wide. The primary faults have documented lengths of tens of feet to a few hundred feet, and are spaced from several tens of feet to hundreds of feet apart across the ISFSI site area based on trench exposures and surface geologic mapping.

Secondary faults have variable trends and inclinations. They have very small displacements, generally less than a few inches. Some secondary faults splay off of the primary faults, or form part of the primary fault zone, such as in trench T-1 and T-17. Others are far from primary faults, such as those in trenches T-11A, B, C and D, T-14B and T-15.

The fault surfaces within bedrock vary from tightly bonded or cemented rock/rock surfaces, to relatively soft slickensided clay/rock and clay film contacts. Individual faults are narrow, ranging in width from less than an inch to about 2 feet. Fault zones contain broken and slickensided rock, intermixed clay and rock, and locally soft, sheared, clayey gouge. The thickness of fault gouge and breccia is variable along the faults.

Cross section B-B''' (Figure 21-15) shows the subsurface stratigraphy and structure beneath the ISFSI pads. As shown on the map (Figure 21-4) and cross section, five

minor faults clearly juxtapose the dolomite (Tof_{b-1}) against the sandstone (Tof_{b-2}) and truncate individual friable beds. Vertical separation across individual faults ranges from about 10 feet to greater than 50 feet based on displacements of friable beds and the contact between Units Tof_{b-1} and Tof_{b-2} . Total vertical separation across the entire fault zone exceeds 50 feet. As described previously, the contact between Units Tof_{b-1} and Tof_{b-2} beneath the pads is based on the first occurrence of medium to coarse-grained sandstone, and there is no evidence of significant facies interfingering between the two units beneath the pads that would obscure the amount of offset. Therefore, the interpretation of vertical separation of bedrock along the faults is given a relatively high degree of confidence.

Subhorizontal slickensides indicate that the minor faults in the ISFSI site area have predominantly strike slip displacement (Table 21-5, Figure 21-39). Using a typical range of 10-20 degree rake on the slickensides and the vertical separation, total fault displacement is estimated to be several tens to several hundreds of feet. The faults trend subparallel to the axis of the Pismo syncline and trend approximately 35 to 55 degrees more westward than the offshore Hosgri fault zone (Figure 21-38).

The faults at the ISFSI site area may be continuous with several other minor faults exhibiting similar characteristics exposed along strike in dolomite in the Diablo Creek roadcut about 800 feet to the north (Figures 21-1, 21-3, and 21-38). Given this correlation and the presence of several hundred feet of strike slip displacement, we infer that the faults may be at least several thousand feet long. However, the correlation between faults exposed within the ISFSI site and the roadcut along Diablo Creek, assumes that the slopes northwest of Diablo Creek are in place and have not been translated or rotated down slope as the result of landsliding. Although not conclusive, some geomorphic evidence suggests the presence of an ancient landslide in this area north of Diablo Creek. If the roadcut exposure is part of a landslide mass then the faults would not correlate to the same minor faults found in the ISFSI site area. Interpretation of pre-borrow excavation aerial photography shows that the faults are not geomorphically

expressed (Figure 21-40) and there is no evidence of displaced Quaternary deposits along the fault trace.

5.3.2.1 Fault Origin and Capability

The faults most likely formed during a period of regional transtensional deformation during the Miocene. This most easily explains the observed normal oblique slip on the fault zone. A transition to transpressional deformation occurred during the late Miocene to Pliocene and is well expressed in the offshore Santa Maria Basin and along the Hosgri fault zone (PG&E, 1988). The minor bedrock faults at the ISFSI site were subsequently rotated during the growth of the Pismo Syncline, although the faults occur near the flat-lying crest of a small parasitic anticline and, thus, have not been rotated significantly. Given this origin, the faults formed during the Miocene contemporaneous with the transtensional formation of Miocene basins along the south-central coast of California prior to 5 million years ago.

Alternatively, the minor faults may be secondary faults related to growth of the regional Pismo syncline (Figure 21-37), as concluded for the small bedrock faults at the power block (PG&E, 2000, p. 2.5-49, -50). As shown on Figure 21-31, the faults trend subparallel to the axis of the Pismo syncline, and are located near the crest of a small anticline on the southwestern limb of the syncline. The apparent oblique displacements observed on the faults may be related to bending-moment normal faults and right shear along the axial plane of the small anticline that formed in the Pliocene to early Quaternary. The zone of minor faulting may have used the area of diabase intrusion as an area of crustal weakness to accommodate tensional stresses along the axial plane of the anticline. As described in the FSAR (PG&E, 2000, p. 2.5-14, -33, -34) and in the LTSP reports (PG&E, 1988, p. 2-34 to -38; PG&E, 1991, p. 2-10), growth of the Pismo syncline and related folds ceased prior to 500,000 to 1,000,000 years ago. Thus, the observed minor faults also would have ceased activity prior to 500,000 to 1,000,000 years ago.

A third alternative explanation for origin of the minor bedrock faults is that they are related to intrusion of the diabase into the Obispo Formation. Diabase is present locally in the ISFSI study area. Forceful intrusion, or magmatic stoping of the diabase may have produced faulting in response to stresses induced by the magma intrusion in the adjacent host rock. Hydrothermal alteration is extensive in the diabase. The altered sandstone and dolomite in the ISFSI site area are spatially associated with the zone of faulting (Figures 21-4, 21-14), indicating that the faults may have acted as a conduit for hydrothermal solutions. Assuming the hydrothermal fluids were associated with the diabase intrusion, the minor faults predate, or are contemporaneous with, intrusion of the diabase. Diabase intrusion into the Obispo Formation occurred in the middle Miocene (Hall, 1973; Hall and others, 1979), indicating that the faulting would have occurred prior to or contemporaneous with the diabase intrusion in the middle Miocene over 10 million years ago. The faulting may have originated by transtensional regional deformation as described above, and then subsequently modified by diabase intrusion.

In addition to their probable origin related to transtensional deformation in the Miocene, or to growth of the Pismo syncline in the Pliocene to early Quaternary, or to intrusion of the diabase in the middle Miocene, several additional lines of evidence indicate that the minor faults are not capable and do not present a surface faulting hazard at the site:

1. As described in the LTSP Final Report (PG&E, 1988, p. 37 to 39, Plates 10 and 12) the Quaternary marine terrace sequence in the plant site vicinity is not deformed, providing direct stratigraphic and geomorphic evidence demonstrating the absence of capable faulting. The minor faults observed at the ISFSI site project northwest across, but do not visibly displace the lower marine terrace platform, within a limit of resolution of ± 5 feet indicating the absence of deformation in the last 120 thousand years. Assuming that the displacement does not die out at the coast, this resolution is enough to recognize the greater than 50 of feet of vertical separation on the faults at the ISFSI site. However, no displacement of the terrace sequence is observed.

2. As described in the DCPD FSAR (PG&E, 2000, p. 2.5-35 to -50, Figures 2.5-13 to -16), similar northwest-trending minor faults were mapped in bedrock in the power block area. Detailed trenching investigations of these faults and mapping of the power block excavation provide direct stratigraphic evidence that they do not displace and, hence, are older than the late Pleistocene (120,000 years old) marine terrace deposits. By analogy, the minor faults at the ISFSI site also would be older than late Pleistocene.

3. Interpretation of aerial photographs taken before the 1971 excavation of the ISFSI site area (former borrow area) and construction of the raw water reservoir (Figure 21-32), shows that there are no geomorphic features in the ISFSI site area (tonal lineaments, drainage anomalies, scarps, etc.) indicative of displacement of the minor faults prior to grading. The landscape in the ISFSI site area is interpreted to have formed in the middle to late Quaternary (about 430,000 years ago), based on the preserved remnants of marine terraces in the surrounding site area.

Based on these lines of evidence, the minor faults observed in bedrock at the ISFSI site are not capable, hence, there is no potential for surface faulting at the ISFSI site.

5.3.3 Bedrock Discontinuities

Extensive data on bedrock discontinuities (joints and faults) were collected from the 12 borings and 15 of the trenches within the ISFSI site area to assess their orientation, intensity, and spatial variability across the ISFSI site area. These data are presented in William Lettis & Associates, Inc. (2001) Diablo Canyon ISFSI Data Report F and summarized in Table 21-6. Rose diagrams summarizing trends of faults and joints are presented in Figure 21-41. The discontinuity data were used in both the kinematic slope stability analyses (Calculation Package GEO.DCPP.01.22) and the pseudostatic wedge stability analyses (Calculation Package GEO.DCPP.01.23).

Bedrock discontinuities include joints, faults, bedding, and fractures of unknown origin. These discontinuities, in particular joints, are pervasive throughout bedrock in the ISFSI

study area and along the transport route (Figure 21-41). Steeply dipping faults and joint sets are the dominant discontinuities, giving the rock mass a subvertical fabric. Random and poorly developed low-angle joints also occur subparallel to bedding. The fault discontinuities are described in Section 5.3.2. Joint discontinuities are described below.

Joint contacts vary from tight to partially tight to slightly open; joint surfaces are slightly smooth to rough, and have thin iron oxide or manganese coatings (William Lettis & Associates, Inc. (2001) Diablo Canyon ISFSI Data Report H). Joint lengths in trenches and outcrops typically range from a few feet to about 20 feet, and typical joint spacings range from about ½-foot to 4 feet with an observed maximum spacing of about 14 feet (as summarized on Table F-6, William Lettis & Associates, Inc. (2001) Diablo Canyon ISFSI Data Report F). The intersections of various joints, faults, and bedding divide the bedrock into blocks generally 2 to 3 feet in dimension, but up to a maximum of about 14 feet. Rock blocks formed by intersecting joints larger than those described above generally are keyed into the rock mass by intact rock bridges or asperity interlocking. The largest expected “free” block in the rock mass is, therefore, estimated to be on the order of about 14 feet in maximum dimension.

Both the well cemented sandstone and the dolomite contain numerous joints. The jointing typically is confined to individual beds or group of beds, giving the bedrock a blocky appearance in outcrop. Joints are less well-developed and less frequent in the friable sandstone and friable dolomite. Linear zones of discoloration in the friable sandstone may represent former joints and small faults, but these zones are partially recemented, and not as frequent or obvious as joints in the harder rock.

The character of joints also differs between the upper, dilated zone of bedrock (generally within the upper 4 feet in the ISFSI study area, but conservatively estimated to extend to a maximum of 20 feet deep, particularly toward the edges of the old borrow cut where the amount of rock removed in 1971 is minimal) and the underlying zone of “tight” bedrock. Joints are generally tight to open in the upper zone. In the lower zone, the joints are tight and, in places, bonded and healed. This is well demonstrated in borehole optical

televiewer logs included in William Lettis & Associates, Inc. (2001) Diablo Canyon ISFSI Data Report E that show the joints are typically tight and/or partly bonded throughout the borings. Discontinuities in recovered rock core appear to be more open than observed in the optical televiewer logs, and appear to have undergone stress-relief dilation and mechanical disruption during coring and core extraction. In both zones, the joints are locally clay-filled, and commonly contain thin fillings of clay, calcite, dolomite, and locally, gypsum. Joints and fractures in the borings are very closely to widely spaced (less than 0.1-foot to 3-foot spacing), with local crushed areas between joints.

Plots of fracture orientation and density are shown on Figure 21-41. In preparing these rose diagrams (Figure 21-41), discontinuity data from trenches (William Lettis & Associates, Inc. (2001) Diablo Canyon ISFSI Data Report F) were filtered to exclude bedding and to include only joints and faults. Data for the boreholes were taken from the optical televiewer (OPTV) image logs and the discontinuities identified by NORCAL (see William Lettis & Associates, Inc. (2001) Diablo Canyon ISFSI Data Report E). Each feature identified on the logs by NORCAL was examined in detail by one or more geologists familiar with the core from the borings, to determine if the feature represents a true structural discontinuity. In many cases, the feature appeared to be alteration, discoloration of the bedrock, or a feature with a poorly constrained or undetermined orientation. Only those features that were interpreted as structural discontinuities (i.e., joints or faults), and for which accurate orientations could be determined, were included in the data set for the rose plots. The discontinuities used in the rose plots are tabulated in Table 21-6.

Examination of Figure 21-41 shows that the discontinuity data display a spatial variability across the site, even between trenches and borings located relatively close to each other. Jointing likely developed during several phases of folding, faulting, and diabase intrusion. As a result, joints exhibit variable orientations and cross-cutting, intersecting relationships. In general, the discontinuities group into two broad sets: a west- to west-northwest-striking set (e.g., Trenches T-1, T-3) and a north-northwest-striking set (e.g., Trenches T-5, T-15). In some trenches, fractures from both sets are

present (e.g., Trenches T-6, T-14, T-19, while some show a much greater scatter in orientation (e.g., Trenches T-17 and T-18). In these cases, a general northwest-southeast striking orientation is apparent. The variation in orientation of the discontinuities with strata and locality across the ISFSI site documents that the joints are limited in continuity.

The general northwest-southeast striking character of the fractures in the ISFSI site area is consistent with both the overall northwest striking regional structural grain associated with the Hosgri fault system, and with the axis of the Pismo syncline and the local fold axes in the ISFSI site area, described above (Figure 21-38). Local variations in discontinuity orientations and intensity are attributed to rheological differences between dolomite and sandstone, and their friable zones, as well as proximity to the minor faults that cut across the site area and/or former zones of diabase intrusion.

5.4 Stratigraphy and Structure of the ISFSI Pads Foundation

Figure 21-42 shows the expected bedrock conditions that will be encountered in the ISFSI pads foundation excavation at the assumed pads subgrade elevation of 302 feet. The pads will be founded primarily on dolomitic sandstone of Unit Tof_{b-2} and dolomite of Unit Tof_{b-1} . Dolomitic sandstone generally underlies most of the site, while dolomite underlies the eastern end of the site. The proposed cutslopes above the site are generally underlain by dolomitic sandstone in the western and central parts of the cut and by dolomite in the upper and eastern parts of the cut.

Locally, friable sandstone (Tof_{b-2a}) and friable dolomite (Tof_{b-1a}) underlies the ISFSI pads foundation and the proposed cutslopes as shown on Figure 21-43. Because the zones are highly variable in thickness and continuity, their actual distribution likely will vary from that shown on Figure 21-42. In particular, a large body of friable dolomite underlies the southeast portion of the proposed cut slope. Other smaller occurrences of friable sandstone and dolomite are expected to be encountered in the excavation. These friable rocks locally have “dense soil-like” properties; thus, specific analyses were performed to determine the foundation properties and slope stability of these friable rock zones

(William Lettis & Associates, Inc. (2001) Diablo Canyon ISFSI Data Report I and Calculation packages GEO.DCPP.01.03 and 04). Small zones of altered diabase may be found in the excavations. This rock has properties similar to the friable sandstone.

In two places beneath the ISFSI pads foundation, clay beds within dolomite and sandstone are expected to daylight and/or occur within 5 feet of the base of the foundation (Figure 21-42). Additional clay beds may be exposed in the pads foundation. Although, available geologic data do not document the presence of clay beds that will daylight in the ISFSI cutslope, some may be encountered when the cuts are made.

In addition, a zone of minor faults trends northwest-southeast across the central and eastern part of the ISFSI pads, and other minor faults may be present in the western part as well. These faults are shown on the geologic map (Figure 21-42) and on cross sections A-A', B-B'', G-G', H-H', and I-I' (Figures 21-14, 21-15, 21-20, 21-21 and 21-22). The faults have vertical separations of 10 to 30 feet and locally juxtapose different bedrock units.

The CTF will be founded primarily on dolomitic sandstone (Unit Tof_{b-2}) and friable sandstone (Unit Tof_{b-2a}) as shown on Figures 21-22 and 21-41.

5.5 Stratigraphy and Structure of the Transport Route

The transport route begins behind the power block, and ends at the Diablo Canyon ISFSI. The route will follow existing paved roads: Plant View, Shore Cliff, and Reservoir roads (Figure 21-3), except where routed north of the intersection of Shore Cliff and Reservoir roads to avoid an existing landslide at Patton Cove. The lower two-thirds of the route traverses thick surficial deposits, including marine terrace, debris-flow, and colluvial deposits of varying thicknesses. These surficial deposits overlie two units of the Obispo Formation bedrock: unit Tof_b sandstone and dolomite, and unit Tof_c claystone, siltstone, and shale. The upper one-third of the route is located on engineered fill placed over

dolomite and sandstone bedrock (units Tof_{b-1} and Tof_{b-2} of the Obispo Formation (Figure 21-3). Locally, the road is located on cut-and-fill bench notched into bedrock.

In the geologic description below, approximate stations are assigned to assist in defining distances between locations, starting from the power block and ending at the ISFSI (Figure 21-3). Although not surveyed, this informal stationing is in standard engineering format to represent the distance, in feet, from the start of the road to the station location (for example, 21+00 is 2,100 feet from the start of the road). The specific conditions along the route are discussed below.

Station 00+00 (south side of power block) to 20+00 (near Reservoir Road): The transport route generally follows Plant View Road and Shore Cliff Road. The route starts at the power block and crosses flat, graded topography on the lower coastal marine terrace (Q_2) (Figure 21-7). Behind the power block, the route is founded on sandstone (Tof_b) of the Obispo Formation. From there to near Reservoir Road, the transport route is founded on surficial deposits 10 to 40 feet thick and local engineered fill in trenches and other excavations made during construction of the power plant. The surficial deposits consist primarily of debris-flow and colluvial deposits that overlie the marine bedrock terrace platform (Figures 21-7 and 21-17). These deposits range in age from middle Pleistocene to Holocene, and consist of overconsolidated to normally consolidated clayey sand and gravelly clay. The deposits contain some carbonate cementation and paleosols, and typically are stiff to very stiff (medium dense to dense). Bedrock below the marine terrace platform consists of east-dipping sandstone (Tof_b) from station 00+00 to about 07+00, and steeply dipping claystone and shale (Tof_c) from about 07+00 to 20+00. Because of the thickness of the overburden, bedrock structure will have no effect on the foundation stability of the road.

Station 20+00 to 34+00 (Shore Cliff Road to Reservoir Road at Hillside Road): From station 20+00 to 26+00, the transport route will be located on a new road north of the intersection of Shore Cliff Road and Reservoir Road to avoid an existing landslide at

Patton Cove (Figures 21-2, 21-6, 21-25). A 5- to 50-foot-thick prism of engineered fill will be placed to raise the elevation of the roadbed from the lower part of the marine terrace to the upper part of the marine terrace and fans as the road makes a large switchback. The engineered fill will overlie 20- to 80-feet-thick overconsolidated to normally consolidated Pleistocene debris-flow and colluvial deposits that cover the marine terrace platform (Q_2), which in turn, overlie steeply dipping claystone and shale of Unit Tof_c below the marine bedrock platform.

Along Reservoir Road, station 26+00 to 34+00, the route follows the higher part of this terrace over the marine platforms Q_2 and Q_3 and the buried rock slope to the northeast of the platform. The surficial deposits consist of debris-flow and colluvial deposits that are up to 80 feet thick along the base of the ridge behind parking lot 8 (Figure 21-25).

Bedrock below the marine terrace is claystone and shale (Tof_c) from station 26+00 to 29+50 and sandstone (Tof_b) from station 29+50 to 34+00. Because of the thickness of the overburden, bedrock structure will have no effect on the foundation stability of the road.

Station 34+00 (Reservoir Road at Hillside Road) to 49+00 (along Reservoir Road): The route follows Reservoir Road to the raw water reservoir area. The road traverses the west flank of the ridge on an engineered cut-and-fill bench constructed over unit Tof_b dolomite and sandstone, and thin colluvium and debris-flow fan deposits. Bedding exposed in the roadcut dips 30 to 50 degrees into the hillslope, away from the road. Engineered fill on sandstone and dolomite underlies the inboard edge of the road, and a wedge of engineered fill over colluvium generally underlies the outboard edge of the road (Figures 21-3, 21-15, 21-17, and 21-25).

Bedrock joints exposed in this stretch of the route are similar to those at the ISFSI site. Joints are generally of short lateral persistence, confined to individual beds, and are tight to open. Joint-bounded blocks are typically well keyed into the slope, with the exception

of a 1- to 3-foot-thick outer dilated zone. No large unstable blocks or adverse structures prone to large-scale sliding were observed.

Station 49+00 (along Reservoir Road) to 53+50 (ISFSI pads): The route leaves the existing Reservoir Road and crosses the power plant overview parking area. The route will be placed on new engineered fill up to 5 feet thick that will overlie thin engineered fill (up to 4 feet thick) that was placed over sandstone and friable sandstone (Tof_{b-2} and Tof_{b-2a}), the same rock that underlies the ISFSI pads and CTF site.

Bedrock structures beneath this stretch of the route are inferred to be joints and small faults similar to those exposed at the ISFSI site (Figure 21-4). The faults would trend generally northwest, and dip steeply northeast and southeast, to vertical. The primary joint sets are near-vertical. This part of the road is on flat topography and bedrock structure will have no effect on the foundation stability of the road.

The transport route is located 100 feet north of the headscarp of the active Patton Cove landslide (Figure 21-3). A cross section through the landslide is shown on Figure 21-19. The landslide headscarp is defined by a series of cracks at the intersection of Shore Cliff and Reservoir Roads (Figure 21-19). Based on detailed mapping, borings, and an inclinometer, the landslide appears to be confined within unconsolidated deposits overlying a buried bedrock sea cliff and abrasion platform. The geometry of the bedrock surface and near vertical orientation of bedding would likely limit significant enlargement and headward encroachment of the landslide toward the transport route.

Where the transport route follows Reservoir Road at the base of the bedrock hillslope north from near Hillside Road, there is no evidence for bedrock landslides. Sandstone beds in the hillslope above the road dip obliquely into the slope at about 30 to 50 degrees (Figures 21-3, 21-14, and 21-17). These beds extend continuously across much of the hillside, providing direct evidence for the absence of bedrock slope failures. Small faults and joints in the rock mass do not appear to adversely affect potential slope stability, and the existing roadcut and natural slopes show no evidence of slope failures.

Kinematic analyses of the bedding and fractures along the road were performed where the road borders the bedrock slope. Two stretches of the route were analyzed: a northern stretch from approximately station 43+00 to 49+00 (Figure 21-43), and a northwesterly stretch from approximately station 35+00 to 42+00 (Figure 21-45) (the portion of the road between 34+00 and 35+00 is friable sandstone, and kinematic analysis of this material is not applicable). The rock mass is stable against significant wedge or rock block failures; however, the analysis indicates that rock topple failure from the cutslope into the road is possible. Field evaluations indicate that such failures would be localized and limited to small blocks.

Several colluvial or debris-flow swales are present above the transport route along Reservoir Road (Figure 21-3). These swales have been the source of past debris flows that primarily have built the large fans on the marine terraces over the past tens of thousands of years. Additional debris flows could develop within these swales during heavy rainfall events, similar to those described elsewhere in the Irish Hills following the 1997 storms (PG&E, 1997). Holocene debris-flow fan deposits extend to just below the road alignment, indicating that future debris flows could cross the road. However, large graded benches for an abandoned leach field system are present above a portion of the Reservoir Road, and concrete ditches and culverts are present in swale axes. These existing facilities will catch and divert much of the debris from future debris flows above the road. However, two debris-flow chutes are present above the road northwest of Hillside Road; this part of Reservoir Road is not protected from these potential debris flows. Based on the thickness of the colluvium in the swales (5 to 10 feet), and the slope profile, the maximum depth of debris on the road following a major rainstorm is estimated to be less than 3 feet, which easily could be removed after the event.

5.6 Comparison of Power Block and ISFSI Sites

Bedrock beneath the ISFSI site was compared to bedrock beneath the power block based on (1) stratigraphic position; (2) lithology; and (3) shear wave velocity. Based on these

three independent lines of evidence, we conclude that bedrock beneath the ISFSI site and the power block are part of the same stratigraphic sequence, and have similar bedrock properties and lithology.

1. **Stratigraphic Position.** Cross section B-B''' illustrates the stratigraphic correlation of bedrock between the ISFSI site and the power block (Figure 21-15). As shown on the cross section, the power block and ISFSI site are located on the same continuous, stratigraphic sequence of sandstone and dolomite of Unit Tof_b of the Obispo Formation. As described previously, the power block is located approximately 400 feet lower in the stratigraphic section.

Bedrock beneath the power block is also exposed directly along strike in roadcuts along Reservoir Road (Figure 21-2). Bedrock exposed in the roadcut consists of dolomite, dolomitic siltstone and dolomitic sandstone of Unit Tof_{b-1}.

2. **Lithology.** As described in the FSAR (PG&E, 2000, Section 2.5.1.2.5.6, p. 2.5-42, Figures 2.5-9, -10) bedrock beneath the power block consists predominantly of sandstone, with subordinate thin- to thick-bedded slightly calcareous siltstone (see boring descriptions provided on Figures 21-15 and 21-16). The rocks are described as thin-bedded to platy and massive, hard to moderately soft and "slightly punky," but firm. These lithologic descriptions are similar to, if not identical to, the rocks at the ISFSI site.

The "calcareous siltstone" described in the FSAR is probably dolomite or dolomitic siltstone comparable to Unit Tof_{b-1}. For example, based on their geologic descriptions, we interpret the "siltstone" and "sandstone" encountered in 1977 in power block boring DDH-D to be dolomite and dolomitic sandstone of Unit Tof_{b-1} at the ISFSI site.

Boring logs from the hillslope between the power block and the ISFSI site, included in the FSAR (PG&E, 2000, Figures 2.5-22 to 2.5-27; Appendix 2.5C,

plates A-1 to A-19), describe bedrock as tan and gray silty sandstone and tuffaceous sandstone (Figures 21-15 and 21-16). These rocks are moderately hard and moderately strong. The rock strata underlying this slope dip into the hillside and correlate with the sandstone and dolomite strata exposed on the west flank of the ridge (and west limb of the syncline) that are exposed in roadcuts along Reservoir Road south of the ISFSI site (Figures 21-1, 21-3 and 21-15) and in the deeper part of the borings at the ISFSI site.

3. **Shear Wave Velocity.** Shear wave velocity data from the various investigations at the power block are summarized on Table 21-7, and Figures 21-43 and 21-44. Velocity data in Figure 21-43 are from borehole surveys at the ISFSI site (William Lettis & Associates, Inc. (2001) Diablo Canyon ISFSI Data Report C) and comparative velocities at the power block in Figure 21-44 are from the FSAR. Shear-wave velocities from surface refraction and borehole geophysical surveys at the ISFSI site are within the same range as those obtained at the power block (Figure 21-45). The velocity profiles at both sites are similar to one another and are consistent with the “rock” classification for purposes of ground motion estimation (Abrahamson and Shedlock, 1997).

5.7 Parameters Recommended for Stability Analysis

An analysis of slope stability is presented in Calculation packages GEO.DCPP.01.24 to GEO.DCPP.01.26. The following physical and stratigraphic descriptions and parameters provided the basis for these analyses.

5.7.1 Pre-Existing Landslides in Diablo Canyon Near the ISFSI site

Large, deep-seated landslide complexes exhibiting geomorphically well-expressed headscarps are present on the south slopes of Diablo Canyon near the ISFSI site, and south of the 230 kV and 500 kV switchyards (Figure 21-1). The complex lies entirely east of the ISFSI site, and does not encroach, undermine, or otherwise affect the ISFSI. These landslides consist of large (exceeding 100 acres), deep-seated, coalescing slides

that have failed within colluvium, and Tof_a and Tof_b bedrock on the north limb of an anticline (Section 5.3.1). The dip of the bedrock bedding in the vicinity of the slide complex is consistently to the north and downslope at moderately steep dip angles. This condition suggests that the failure planes for these slides probably are either at the contact between bedrock and overlying weathered bedrock, or within the bedrock along bedding planes, clay beds, or locally weaker diabase beds. In contrast, bedding dip directions at the ISFSI site are variable, and, where locally dipping out-of-slope, are at more-gentle dip inclinations than in the area of the old landslide complex to the east.

Although the overall shape of the landslide complex is well-expressed geomorphically, the landslide deposits have been modified and subdued by erosion. Thin stream-terrace deposits and remnants of a 430,000-year-old marine terrace at elevation 290 ± 5 feet appear to have been cut into the toes of some of the slides. These relations suggest that the landslides are old and likely formed in a wetter climate during the middle to late Pleistocene. The older landslide masses appear to have reached a stable configuration under the present climatic and topographic setting, and are partially buttressed by the large 500 kV switchyard fill that spans the canyon. There is no geomorphic evidence of large-scale Holocene movement, and the switchyard shows evidence of no post-construction slope movement. Localized, more-recent and shallower slides have formed within the old landslide complex, and appear to involve previously-disturbed slide materials.

The slide complex is separated from the ISFSI site by a low spur ridge that is along the trend of the anticlinal axis, and which is underlain by stable bedrock that shows no evidence of past slide activity on pre-and post-borrow excavation aerial photographs. Field mapping, subsurface exploration, and aerial photograph analyses during the ISFSI site investigations confirmed the absence of deep-seated bedrock slides at the site. Additionally, no stability problems were encountered during the 1971 borrow excavation using bulldozers and scrapers, and the slope has been stable since the 1971 excavation. The Raw Water Reservoir and Reservoir Road below the ISFSI site show no evidence of post-construction slope movements.

A former small, shallow landslide in colluvium existed at the ISFSI site prior to the 1971 borrow excavation, and is shown on Figure 21-40. This slide is apparent on the pre-excavation 1968 aerial photographs, and is expressed by a subtle, arcuate headscarp, hummocky landslide, and locally thicker vegetation probably reflecting high soil moisture within the slide debris (Figure 21-40). The slide was located in a slight swale in colluvial soils and possibly weathered bedrock that mantled the slope prior to excavation. The slide mass appears to have moved northeast along the axis of the swale, and oblique to the downdip direction of bedrock bedding. This suggests that the slide was not controlled by bedrock structure. This slide was investigated by Harding -Miller-Lawson Associates (HML, 1968), and was shown to be a shallow failure within colluvium, and possibly extending into the uppermost weathered bedrock (Cross Section A-A', Figure 21-14). This shallow slide was completely removed, along with colluvium and the surficial weathered rock zone, during the 1971 borrow excavation (Figure 21-14).

5.7.2 Clay Bed Strength

The strength of the clay in the clay beds was tested in the laboratory (William Lettis & Associates, Inc. (2001) Diablo Canyon ISFSI Data Report G). However, the overall strength of the clay bed during sliding also is a function of the clay bed thickness, rock asperities along the clay surface, and the amplitude of irregularities or undulations on the clay surface relative to the clay thickness. Clay beds greater than ¼- to ½-inch thick potentially have limited or locally no rock to rock contact and the clay thickness may exceed the amplitude of bedding surface undulations. Thus, clay beds thicker than ¼-inch should be modeled in the stability analysis using the shear strength of the clay, and are differentiated on the cross sections. In addition, disruptions of the clay beds by joints and minor faults also will tend to resist sliding and increase the effective strength of the clay bed. The thinner beds likely exhibit shear strength greater than that of the clay due to partial rock-to-rock contacts and asperities projecting through the clay. The strength of clay beds less than <¼-inch can be approximated by a combination of rock-to-rock and rock-to-clay strength.

5.7.3 Geometry and Structure of Slide Mass Models

Cross section I-I' (Figure 21-22) parallels the most likely direction of potential slope failure and illustrates the geometry of bedding in the ISFSI study area for analysis of slope stability. The cross section shows apparent dips, and the facies variation and interfingering of beds between Units Tof_{b-1} and Tof_{b-2} beneath the slope. Lateral continuity of clay beds is approximated by the relative lengths and line weights as described above in Section 4.3. The clay beds are correlated based on stratigraphic position, projection of known bedding attitudes, and superposition of sandstone and dolomite beds (i.e., we do not allow clay beds to cross cut dolomite or sandstone beds, but allow them to cross the facies change). These clay beds, as drawn, are a reasonably conservative interpretation of their lateral continuity for the analysis of the global stability of the slope.

The geometry of the folds underlying the ISFSI study area influences the potential for rock slides in the slope. As illustrated on Figures 21-3 and 21-4, the small, tightly folded, en echelon syncline at the top of the ridge above the ISFSI site transitions into a monocline above Boring 01-I. This monocline transitions into a broad syncline farther down the slope near Boring 00BA-1. The approximate locations of these transitions are indicated on cross section I-I' (Figure 21-22), but the apparent dips shown in the cross sections at the transition locations do not change because the section azimuth is subparallel to the fold axes and the direction of strata flexure is into the section. The three-dimensional change in strata geometry across these transitions will tend to disrupt and limit potential rock slides because the dip directions of the clay beds change across the transitions.

In addition, the dip of the clay beds in the upper slope above Boring 00BA-1 dip out of the slope and are parallel to the downslope direction. Lower down on the slope (at the ISFSI pads and cutslope) the beds dip westerly. This change in geometry reduces the potential for large rock slides on clay beds on the lower part of the slope compared to the slope above 00BA-1.

The continuity of some of the thicker (over about ¼-inch thick) clay beds are assumed to be up to several hundred feet. Thinner clay beds are less laterally continuous. On cross section I-I' (Figure 21-22), clay beds are shown to terminate at set distances from exposures in boreholes, trenches, or outcrops according to the protocol described in Section 4.3. Because of the generally limited lateral continuity of the clay beds, potential large rock slides (on the order of several tens to hundreds of feet in maximum dimensions) would likely require sliding on several clay beds, and stepping between beds on joints and in places through rock in a "staircase" profile. Stepping between basal clay failure surfaces would probably be localized where the individual clay beds are close together stratigraphically and thin and pinched-out. Other likely locations for stair-stepping failure or structural boundaries for possible rock slide margins are at the fold transitions as discussed previously and along the lateral margins of the slide and along steeply dipping discontinuities such as faults and friable or weak rock zones. Faults at the site are subparallel to the potential down slope motion and impart a strong near-vertical fabric in the rock mass. It is likely that lateral margins for potential larger rock slides would develop along these faults.

5.7.4 Conceptual Rockslide Mass Models

Conceptual rockslide mass models were developed for slope stability analyses of cross section I-I' (Figure 21-22) on the basis of engineering geologic evaluation of the cross section. The following assumptions were used to develop the conceptual models:

1. Basal slide surfaces generally follow low-strength clay beds encountered in ISFSI area borings and test trenches, as shown on the cross section.
2. Failure planes break up to the surface, or between clay beds, through jointed rock with steep shear/tension failure planes (70°) that follow the dominant steep joint/fault fabric in the rock mass.
3. Locations of headscarp or tensional break-up zones are controlled or strongly influenced by locations of significant change in bedding strike and direction (structural control) or termination locations of clay beds where the beds thin and rock-to-rock contact becomes dominant.

Three slide mass models were developed:

1. A shallow slide mass model (Figure 21-46) involving sliding rock masses along shallow beds encountered in test trench T-14A and Boring 01-I;
2. A medium-depth slide mass model (Figure 21-47) involving sliding rock masses along clay beds encountered at depths of between about 25' and 175' in borings 01-F, 00BA-1, and 01-I and Trench T-11D; and
3. A deep slide mass model (Figure 21-48) that involves sliding along deep clay beds behind, or below the proposed ISFSI cut slope and pad and that were encountered in borings 01-H, 01-F, 00BA-1, and 01-I at depths of between about 50 and 200 feet.

Model 1 is segmented into 2 possible geometries labeled 1a and 1b on Figure 21-46. These two modeled slide blocks daylight at a clay bed encountered in Trench T-14A (model 1a), or along projected dip of a clay bed encountered in boring 01-I. The failure headscarp/tension break-up zone extends upward from the inferred maximum upslope extent of the claybed in trenches T-14A (model 1a), or from the inferred likely extent of the uphill extent of a clay bed encountered in boring 01-I.

Model 2 is segmented into three sub-blocks: 2a, 2b, and 2c (Figure 21-47). The three blocks daylight along a clay bed encountered in trench T-11D (2a and 2b), or along the dip projection of a clay bed encountered in boring 00BA-1 (2b). Model 2a breaks up at the location of a significant change in bedding strike (dip direction) that occurs near trench T-14A, and would be a major structural discontinuity for potential slide blocks. Models 2b and 2c break up from the basal failure planes in a "stair-stepping" manner between clay beds, and have a common headscarp daylight about 50 feet above the brow of the 1971 borrow cut excavation. The geometry of the headscarp/tension break-up zone is inferred to be controlled by the uphill limit of clay beds encountered in the borings, and dominant steep joint fabric in the rock mass.

Model 3 is segmented into three sub-blocks: 3a, 3b, and 3c. The three blocks daylight in the proposed ISFSI pad cutslope, or at the junction between the ISFSI pad and base of the cutslope (Figure 21-48). All three modeled blocks have basal slide surfaces along clay beds encountered in borings 01-F, and /or 00BA-1 and 01-I. Models 3a and 3b have headscarp/tension break-up zones at the structural change in bedding strike (dip direction) described previously for model 2a (3a and 3b), or about 75 feet above the top of the borrow cut (3c) at an inferred maximum uphill extent of clay beds encountered in borings 01-I.

The toe daylight geometry reflects the propensity for failure planes to break out along bedding planes and along the projection of clay beds. The rock mass is inferred to exhibit anisotropic strength, with a lower shear strength along and parallel to bedding planes, than across bedding planes for toe shear failure. In contrast, the geometry of the headscarp-tension failure is inferred to be controlled by the dominant steep (greater than 70 degrees) joint/fault fabric in the rock mass that should control tensional failure/separation.

5.7.5 Estimate of Potential Slide Mass Displacement

Potential slide mass displacement can be constrained, in part, by past performance of the hillslope above the ISFSI site. As described below, the topographic ridge upon which the ISFSI site is located has been stable for the past 430,000 years or more. A back analysis of slope stability, therefore, provides constraints on the minimum shear strength and/or lateral continuity of the clay beds used in the analysis and a check on the conservatism of the assumptions used to analyze the stability of the proposed ISFSI site cutslopes and hillslope above the site.

Geomorphic and geologic data from mapping and trenching in the ISFSI Site Area provide evidence documenting the absence of past movements of large rock masses on the slope above the ISFSI. Analysis of pre-construction air photos shows no features indicative of such landslides: no arcuate scarps, no vegetation lineaments indicative of filled fissures, and no textural differences in the rock exposures or slopes indicative of a

broken rock mass in the ISFSI study area (Figure 21-41) (William Lettis & Associates, Inc. (2001) Diablo Canyon ISFSI Data Report A). Similarly, the many trenches and exploratory borings on the slope, the tower access road cuts, and the extensive outcrops exposed by the 1971 borrow cut did not expose tension cracks or fissure fills on the hillslope (William Lettis & Associates, Inc. (2001) Diablo Canyon ISFSI Data Reports A, B and D). Open cracks or soil-filled fissures greater than 1 to 2 feet in width should be easily recognized across the slope given the extensive rock exposure provided by the borrow cut. Therefore, we conservatively assume that any cumulative displacement in the slope greater than 3 feet would have produced features that would be evident in rock slope. The absence of this evidence places a maximum threshold of 3 feet on the amount of cumulative slope displacement that may have occurred in the geologic past.

The hillslope at the ISFSI site is older than at least 430,000 years because remnants of the Q-5 (430,000 yrs) marine terrace are cut into the slope west of the ISFSI site (Figure 21-3). Preservation of the terrace documents that the slope has had minimal erosion since that time. Moreover, gradual reduction of the ridge by erosion at the ISFSI site would not destroy deep tension cracks or deep disruption of the rock mass; these features would be preserved as filled fractures and fissures even as the slope is lowered.

The topographic ridge upon which the ISFSI site is located is presumed to have experienced strong ground shaking from numerous earthquakes on the Hosgri fault zone during the past 430,000 years. PG&E (1988, p. 3-39) provides a recurrence interval of 11,350 years for an M_w 7.2 earthquake on the Hosgri fault. Therefore, approximately 35 to 40 large earthquakes have occurred during the past 430,000 years without causing ground motions large enough to produce significant (i.e., greater than 3 feet) cumulative slope displacement. Based on the absence of cumulative slope displacement within a limit of resolution of 3 feet, the amount of possible slope displacement during the Hosgri design earthquake is a maximum of 3 feet if produced by one earthquake with very large ground motions, or, more likely about 3 to 6 inches per event if produced by multiple earthquakes with large ground motions for a cumulative displacement of up to 3 feet. Slope displacement of 3 to 6 inches, therefore, can be used as a constraint in a "back

calculation" to assess overall rock mass strength and from that to estimate the strength of clay beds under natural slope conditions (i.e., conditions prior to the 1971 excavation of the borrow area). This back calculated strength can then be used to model potential displacements of rock slide masses in the current borrow-cut condition. This is described in Calculation Package GEO.DCPP.01.24.

5.7.6 Rock Block Dimensions

The size of potential wedge block failures in the ISFSI cutslope will be controlled, in part, by the spacing, continuity and shear strength of discontinuities in the rock mass. Both the dolomite (Unit Tof_{b-1}) and sandstone (Unit Tof_{b-2}) bedrock at the site are jointed and faulted. Joints and faults in friable dolomite and friable sandstone are less well-developed and do not control the mechanical behavior of the soil-like rock. Rather, the rock strength appears to be controlled primarily by the cementation properties of the rock.

Field data on the discontinuities (William Lettis & Associates, Inc. (2001) Diablo Canyon ISFSI Data Report F) show that two primary joint sets are present as discussed above. The orientation of these joint sets varies somewhat across the site (Figure 21-41), but generally group into a west- to west-northwest-striking set and a north-northwest- to north-striking set. The joints are continuous for a few feet to about 20 feet, and commonly die out or terminate at subhorizontal bedding contacts. Field observations from surface exposures and trenches show that the joints commonly are slightly open or dilated in the upper 4 feet, probably due the stress unloading from the 1971 borrow excavation and/or surface weathering. Dilation of the joints reduces the shear strength of the discontinuity. To be conservative, we assume that the zone of near-surface dilation extends to a depth of 20 feet on the ISFSI cutslope. The Barton method is used to estimate the reduced shear strength on these discontinuities as described in Calculation Package GEO.DCPP.01.20.

Joints in the dolomite typically are spaced about ½-foot to 4 feet apart and divide the rock mass into blocks with average dimension of 2 to 3 feet with typical maximum dimensions of about 14 feet (William Lettis & Associates, Inc. (2001) Diablo Canyon ISFSI Data

Report F, Table F-6). We anticipate that the maximum block size will be less than 14 feet in dimension, and conservatively assume a maximum block size of 20 feet in the wedge block stability analysis (Calculation Package GEO.DCPP.01.23). This larger dimension conservatively allows for multiple-block wedges to form in the cutslope.

6.0 RESULTS

The results of the stratigraphic and structural analysis are presented on the geologic maps (Figures 21-1, 21-3, 21-4), a stratigraphic column (Figure 21-5), twelve cross sections (Figures 21-13 to 21-24), and a map of geologic conditions at the ISFSI and CTF foundation grade (Figure 21-42). This information was used to interpret the depositional and structural history of bedrock in the ISFSI study area and along the transport route (Figure 21-7). The results of this calculation package also provide important information used to evaluate the stability of cutslopes at the ISFSI site, the hillslope above the ISFSI site, and slopes above the transport route (Calculation packages GEO.DCPP.01.08, .22, .23, .24 and .28), and to characterize the foundation conditions at the ISFSI pads and cutslope (Calculation packages GEO.DCPP.01.03, .04 and .06).

7.0 SOFTWARE

The software program "DIPS" (Rocscience, 1999) was used to compile and analyze the structural continuity data presented on Figures 21-38 and 21-40. The DIPS program is documented and verified in Calculation package GEO.DCPP.01.22 "Kinematic stability analyses for cutslope at DCPD ISFSI site".

No other software programs were used in this calculation package.

8.0 CONCLUSIONS

This calculation package provides an analysis of the stratigraphic and structural geology of the plant site area (Figure 21-1), transport route (Figure 21-3), and the ISFSI study area (Figure 21-4). Interpreted cross sections and structural maps developed as a result of these analyses are used to characterize the ISFSI pads foundation properties, to evaluate slope stability of the existing hillside and proposed cutslopes above the ISFSI pads and along the transport route, and to understand subsurface bedrock conditions for use in evaluating ground motion site response.

Figure 21-42 shows the bedrock conditions expected at the ISFSI pads and CTF foundation grade levels. The ISFSI pads will be founded primarily on dolomitic sandstone of Unit Tof_{b-2} with dolomite of Unit Tof_{b-1} in the easternmost part of the site. Locally, friable sandstone and friable dolomite will be encountered beneath the ISFSI pads foundation. The proposed cutslopes above the site will be underlain by sandstone and dolomite, and by a large body of friable dolomite in the eastern part of the cutslope. At least two clay beds will daylight within the ISFSI pads foundation. Other clay beds may be encountered in the foundation excavation and in the cutslopes. The CTF will be founded on dolomitic sandstone of Unit Tof_{b-2} and friable sandstone of Unit Tof_{b-2a} .

Bedrock beneath the ISFSI and CTF sites is part of the same stratigraphic sequence that underlies the DCPD power block. Cross section B-B''' (Figure 21-15) illustrates the location of the ISFSI site and power block relative to the stratigraphic sequence. Bedrock encountered in boreholes at the ISFSI site and during site investigations for the power block (PG&E, 2000, Section 2.5.1.2.5.6) have similar lithology and shear wave velocities (Figure 21-45). The bedrock characteristics and velocity profiles at both sites are consistent with the "rock" classification of Abrahamson and Shedlock (1997).

Stratigraphic and structural information developed in this calculation package provide basic geologic information for the analysis of slope stability for the ISFSI pads cutslopes,

the hillslope above the IFSI site, and the slope above the transport route. In particular, cross section I-I' (Figure 21-22) should be used as the basis for analyzing global slope failure at the site assuming the geometry of bedding and lateral continuity of clay beds as shown on the cross section. The structural transitions between the monocline and the small synclinal folds are considered to be structural discontinuity boundaries that would limit the size of potential large scale rock slides in the slope.

The analyses and results presented in this calculation package are based on geologic interpretation of available surface and subsurface data using generally accepted techniques and methods. Geologic judgement, experience and knowledge of the site conditions by the geologists working on the project were used to integrate the available geologic, geophysical and geotechnical data to formulate the interpretations and conclusions presented in this calculation package. Actual subsurface conditions may vary from that shown on the geologic maps and cross sections, but those variations are not expected to significantly change or alter the primary conclusions reached in this analysis.

9.0 REFERENCES

- Abrahamson, N. A. and Shedlock, K., 1997, Overview [of Special Issue of SRL on Attenuation Relations], *Seismological Research Letters*, v. 68, no. 1, p. 9-23.
- Compton, R. R., 1985, *Geology in the Field*. New York: John Wiley & Sons, 398 p.
- Deere and Miller, 1963, Engineering classification and index properties of intact rock: Technical Report No. AFWL-TR-65-116. Air Force Weapons Laboratory, Kirkland Air Force Base, New Mexico, in Hoek, E., 2000, *Rock Engineering Course Notes*, on-line document, Chapter 3, pgs. 42 – 44.
- Hall, C.A., 1973, *Geologic map of the Morro Bay south and Port San Luis Quadrangles, San Luis Obispo County, California, U.S. Geological Survey Field Studies Map MF511*.

- Hall, C. A., Jr., Ernst, W. G., Prior, S. W., and Siese, J. W., 1979, Geologic map of the San Luis Obispo-San Simeon region: U.S. Geological Survey Miscellaneous Investigation I-1097.
- Harding-Miller-Lawson Associates, 1968, Report, soil investigation, intake and discharge lines, borrow area, and switchyards for Unit 1, Diablo Canyon site, San Luis Obispo County, California, consultant's report, 14 p.
- Harding-Lawson Associates, 1970, Landslide investigation, Diablo Canyon site, San Luis Obispo County, California, consultant's report.
- John A. Blume & Associates, 1968, Recommended Earthquake Design Criteria for Nuclear Power Plant – Unit No. 2, Diablo Canyon Site: Diablo Canyon Unit 2 PSAR, Docket No. 50-323, June 24, 1968.
- PG&E, 1988, Final Report of the Diablo Canyon Long Term Seismic Program (LTSP), 8 chapters.
- PG&E, 1989, Response to NRC Question 19, dated December 13, 1988, Docket Nos. 50-275 and 50-323.
- PG&E, 1991, Addendum to the 1988 Final Report of the Diablo Canyon Long Term Seismic Program (LTSP), 8 chapters.
- PG&E, 1997, Assessment of Slope Stability near the Diablo Canyon Power Plant, Response to NRC Request of January 31, 1997, 86 p.
- PG&E, 2000, Units 1 and 2 Diablo Canyon Power Plant, Final Safety Analysis Report Update, Revision 13.
- Reading, H.G., 1981, Sedimentary Environments and Facies: Elsevier, New York, pp. 392-386.
- Rocscience, 1999, DIPS: plotting analysis and presentation of structural data using spherical projection techniques, version 5.041, Toronto
- Rowland, S. M., 1986, Structural analysis and synthesis: a laboratory course in structural geology. Blackwell Scientific Publications, Boston, 208p.
- Suppe, J., 1985, Principals of structural geology, Prentice Hall, New Jersey, 537 p.
- William Lettis & Associates, Inc., 2001, Diablo Canyon ISFSI Data Report B, Rev. 1, Borings in ISFSI Site Area.

- William Lettis & Associates, Inc., 2001, Diablo Canyon ISFSI Data Report C, Rev. 1,
1998 Geophysical Investigations at the ISFSI Site Area, (by Agabian Associates
and GeoVision).
- William Lettis & Associates, Inc., 2001, Diablo Canyon ISFSI Data Report D, Rev. 1,
Trenches in the ISFSI Site Area.
- William Lettis & Associates, Inc., 2001, Diablo Canyon ISFSI Data Report E, Rev. 1,
Borehole Geophysical Data (by NORCAL Geophysical Consultants, Inc.).
- William Lettis & Associates, Inc., 2001, Diablo Canyon ISFSI Data Report F, Rev. 1,
Field Discontinuity Measurements.
- William Lettis & Associates, Inc., 2001, Diablo Canyon ISFSI Data Report G, Rev. 1,
Soil Laboratory Test Data – Cooper Testing Laboratory.
- William Lettis & Associates, Inc., 2001, Diablo Canyon ISFSI Data Report H, Rev. 1,
Rock Strength Data and GSI Sheets.
- William Lettis & Associates, Inc., 2001, Diablo Canyon ISFSI Data Report I, Rev. 1,
Rock Engineering Laboratory Testing - GeoTest Unlimited.
- William Lettis & Associates, Inc., 2001, Diablo Canyon ISFSI Data Report J, Rev. 1,
Petrographic Analysis (Spectrum Petrographics, Inc.).
- William Lettis & Associates, Inc., 2001, Diablo Canyon ISFSI Data Report K, Rev. 1,
Petrographic and X-Ray Diffraction Analyses of Clay Beds (by
Schwein/Christensen Laboratories, Inc.).
- William Lettis & Associates, Inc., 2001, Diablo Canyon ISFSI Data Report L, Rev. 1,
Geologic Mapping in the Plant Site and ISFSI Site Areas.
- William Lettis & Associates, Inc., Work Plan, 2000, Additional Geologic Mapping,
Exploratory Drilling, and Completion of Kinematic Analyses for the Diablo
Canyon Power Plant, Independent Spent Fuel Storage Installation Site, Rev. 2,
November 28, 2000.
- William Lettis & Associates, Inc., Work Plan 2001, Additional Exploratory Drilling and
Geologic Mapping for the DCPD ISFSI Site, Rev. 1, September 29, 2001.

Geosciences Calculation packages

GEO.DCPP.01.01 Development of Young's Modulus and Poisson's ratios for DCPD
ISFSI based on field data

- GEO.DCPP.01.02 Determination of probabilistically reduced peak bedrock accelerations for DCPD ISFSI transporter stability analyses
- GEO.DCPP.01.03 Development of allowable bearing capacity for DCPD ISFSI pad and CTF stability analyses
- GEO.DCPP.01.04 Methodology for determining sliding resistance along base of DCPD ISFSI pad
- GEO.DCPP.01.06 Development of lateral bearing capacity for DCPD CTF stability analyses
- GEO.DCPP.01.07 Development of coefficient of subgrade reaction for DCPD ISFSI pad stability checks
- GEO.DCPP.01.08 Determination of rock anchor design parameters for DCPD ISFSI cutslope and CTF guy lines
- GEO.DCPP.01.11 Development of DCPD ISFSI horizontal and vertical spectra
- GEO.DCPP.01.15 Development of Young's Modulus and Poisson's ratio values for DCPD ISFSI based on laboratory data
- GEO.DCPP.01.19 Development of Strength Envelopes for jointed rock mass at DCPD ISFSI using Hoek-Brown equation
- GEO.DCPP.01.20 Development of strength envelopes for shallow discontinuities at DCPD ISFSI using Barton equations
- GEO.DCPP.01.22 Kinematic stability analysis for cut slopes at DCPD ISFSI site
- GEO.DCPP.01.23 Pseudostatic wedge analysis of DCPD ISFSI cutslope (SWEDGE analysis)
- GEO.DCPP.01.24 Stability and yield acceleration analysis of cross section I-I'
- GEO.DCPP.01.25 Determination of seismic coefficient time histories for potential sliding masses along cut slope behind ISFSI pad
- GEO.DCPP.01.26 Determination of earthquake-induced displacements of potential sliding masses on DCPD ISFSI slope
- GEO.DCPP.01.28 Stability and yield acceleration analysis of potential sliding masses along DCPD ISFSI transport route
- GEO.DCPP.01.29 Determination of seismic coefficient time histories for potential sliding masses on DCPD ISFSI transport route

**Table 21-1 Interpretation of Bedding in Boreholes,
ISFSI Study Area**

Boring 00BA-1

Original Description from Log of Rock Boring including dip angle ⁽¹⁾ (DCPP ISFSI Data Report B)		WLA Descriptions from NORCAL Televiewer Image including dip azimuth and dip angle ⁽²⁾ (DCPP ISFSI Data Report E)		Review of Core ⁽³⁾	Interpreted Bedding Attitude ⁽⁴⁾ (strike, dip)
Depth (feet)	Description	Depth (feet)	Description		
23.0- 23.2	Four joints with thin clay coatings (altered zone)	23.1	Moderately steep joint and thin clay (?) bed, 295°, 9° (fair)	Not checked	N25°E 9°NW
34.0- 38.0	Dolomite to dolomitic sandstone, laminated bedding, dips 0°	34.0- 38.0	Massive rock with laminations, slightly etched surface at 36.9, 225°, 14° (good)	Clear bedding laminations, dips 11°, azimuth 224 measured from dip direction in televiewer	N45°W, 14°SW
39.0	Dolomite to dolomitic sandstone, laminated bedding, 0° dip	38.1	Slightly etched surface in massive rock with laminations 220°, 10° (good)	Excellent bedding, 10°	N50°W, 10°SW
45.0- 48.5	Dolomitic sandstone, laminated bedding, dips 0-7°	45.2	Color lamination in massive rock, 185°, 15° (fair)	Well defined parting surface at 48.8 feet along bedding, with fossils on bedding up to 0.2 inches, dips 10°	N85°W, 10°S
55.6- 56.3	Clay seam (0.7 foot) with planar rock contacts, bedding top dips 5°, bottom dips 5°	54.9- 56.2	Clay bed with sharp, tight rock contacts, etched, 188°, 20° (N) Remeasured dips: (good) top 11°, bottom 16° (good)	Core not available; removed for testing	N82°W, 11-16°S
59.0- 61.0	Dolomitic sandstone, bedding (?) at 59.7 dips 10°	57.0- 60.5	Hard rock with steep to moderately steep fractures, vague laminations	Good bedding at 59.7 feet, dips 16-18°, azimuth of 228° measured from fracture orientation (good)	N42°W, 16°SW
79.5	Stiff, silty clay seam (1/8-inch) on joint, dips 10°	79.2	Possible thin clay along bedding or joint, etched below 331°, 12° (N) Checked dip: 11° (fair)	2-4 mm clay bed dips 16°	N61°E, 11-16°NW
105.4	Clay seam (1/4 inch) along fracture, dips 15°	105.0- 105.3	Clay seam, etched, sharp irregular top, smooth bottom contact, 257°, 12° (N) (good)	No clay found in core; appears that clay washed out during drilling	N13°W, 12°SW
106.5	Silty clay (1/8-1/4 inch), joint, dips 10°	106.4	Tight bedding with discoloration 248-253° (N), 17-18° (N) (fair)	Not checked	N20°W, 18°SW (?)
140.0- 141.0	Sandstone, changes to laminations @ 140.9	140.4	Thin clay (?) bed, partly etched, 260°, 4° (fair)	Thin clay bed between runs, dips ~9°; not accurate	N10°W, 4°SW

**Table 21-1. Interpretation of Bedding in Boreholes,
ISFSI Study Area (continued)****Boring 00BA-2**

Original Description from Log of Rock Boring including dip angle ⁽¹⁾ (DCPP ISFSI Data Report B)		WLA Descriptions from NORCAL Televue Image including dip azimuth and dip angle ⁽²⁾ (DCPP ISFSI Data Report E)		Review of Core ⁽³⁾	Interpreted Bedding Attitude ⁽⁴⁾ (strike, dip)
Depth (feet)	Description	Depth (feet)	Description		
00.0 – 55.0	No bedding recognized		No bedding recognized	No bedding recognized	

Boring 01CTF-A

Original Description from Log of Rock Boring including dip angle ⁽¹⁾ (DCPP ISFSI Data Report B)		WLA Descriptions from NORCAL Televue Image including dip azimuth and dip angle ⁽²⁾ (DCPP ISFSI Data Report E)		Review of Core ⁽³⁾	Interpreted Bedding Attitude ⁽⁴⁾ (strike, dip)
Depth (feet)	Description	Depth (feet)	Description		
8.0- 9.4	Coarse to fine grained sandstone	8.8-8.9	Two subhorizontal, slightly open to etched partings on bedding (?), lower parting 217°, 6° (N) (poor to fair)	Core not available; removed for testing	N53°W, 6°SW (?)
12.4	Fine grained to coarse grained sandstone	12.4- 12.6	Two subhorizontal, slightly open to etched partings on bedding (?), upper parting 178°, 7° (N) (poor to fair)	Broken sandstone	N88°E, 7°S (?)
32.4- 32.6	Soft clayey sand, bedding (?), dips 30°?	32.7- 33.5	Soft clayey (?) zone, etched, irregular contacts, attitude not evident on image.	Core not available; removed for testing	??

**Table 21-1. Interpretation of Bedding in Boreholes,
ISFSI Study Area (continued)**

Boring 01-A

Original Description from Log of Rock Boring including dip angle ⁽¹⁾ (DCPP ISFSI Data Report B)		WLA Descriptions from NORCAL Televiwer Image including dip azimuth and dip angle ⁽²⁾ (DCPP ISFSI Data Report E)		Review of Core ⁽³⁾	Interpreted Bedding Attitude ⁽⁴⁾ (strike, dip)
Depth (feet)	Description	Depth (feet)	Description		
37.7- 37.8	Two clay (1 mm) coatings on joints, dips 20-30°	36.7	Low to moderate dipping joint or bedding (?), etched 224, 27, (N) remeasured orientation 230°, 20° (fair to good)	Not checked	N40°W, 20°SW
42.1	Sandstone, no recovery	41.0- 41.1	Textural change, etched, bedding (?) with clay (?) 251°, 23° (good)	Not checked	N19°W, 23°W
54.9	Silty clay with sand and gravel (1 inch), bedding (?) dips 20°	54.1- 54.3	Low-angle bedding with textural change, etched and eroded, 1/2- to 1-inch clay bed (?) 021°, 7° (N)	Could not confirm orientation, but modified pick appears reasonable	N69°E, 7°NE
55.8	Faults with thin clay coatings, slickensides, dips 8-20°	55.3	Bedding (?), etched, with thin clay (?) bed 226, 27°, (N) remeasured dip 20°, 27° (fair)	Not checked	N44W, 23°SW
58.8	1 cm clay layer, dips 20°	58.5	Subhorizontal clay layer, eroded and etched, irregular, 1/4- 1/2 inch thick, bottom 259°, 22° (N) (fair)	Not checked	N11°W, 22°W
63.0- 66.0	Fine grained dolomitic sandstone	64.7	Slightly etched bedding (?) in massive rock with broad color laminations 256°, 12° (N) (good)	Bedding surface in core dips at 11°	N14°W, 11° W

**Table 21-1. Interpretation of Bedding in Boreholes,
ISFSI Study Area (continued)****Boring 01-B**

Original Description from Log of Rock Boring including dip angle ⁽¹⁾ (DCPP ISFSI Data Report B)		WLA Descriptions from NORCAL Televue Image including dip azimuth and dip angle ⁽²⁾ (DCPP ISFSI Data Report E)		Review of Core ⁽³⁾	Interpreted Bedding Attitude ⁽⁴⁾ (strike, dip)
Depth (feet)	Description	Depth (feet)	Description		
25.0- 27.0	Medium grained sandstone, joint at 26.2 dips 0°	26.1	Tight bedding plane (?), slightly etched, in zone of vague color laminations 325°, 9° (N) (fair)	Not checked	N55°E, 9°NW
32.5	Medium grained dolomitic sandstone	32.0- 32.2	Possible bedding, etched to partly open, 258°, 22° (N) remeasured 260°, 5° (N) (fair)	Two good laminations within coarser rock, azimuth, ~N50°W, dip 10-15°	N10°W, 10°SW
37.7	Gradational contact between medium to coarse grained sandstone, dip not indicated	37.0	Sharp textural change from hard fractured rock to massive etched rock, bedding, 276°, 7° (N) (good)	Not checked	N6E, 7°W

Boring 01-C

Original Description from Log of Rock Boring including dip angle ⁽¹⁾ (DCPP ISFSI Data Report B)		WLA Descriptions from NORCAL Televue Image including dip azimuth and dip angle ⁽²⁾ (DCPP ISFSI Data Report E)		Review of Core ⁽³⁾	Interpreted Bedding Attitude ⁽⁴⁾ (strike, dip)
Depth (feet)	Description	Depth (feet)	Description		
13.0- 14.0	Sandstone, medium to fine grained	13.8	Bedding, etched, 221°, 13° (N) (fair)	Not checked	N49°W, 13°SW
16.3	Clay film on joint, dips 15°	15.9 (?)	Low-angle bedding, etched, with clay (?) (~1/8 inch) 197°, 15° (N) (good)	Surface in core not confirmed as bedding, dips 16-17°	N73°W, 15°S
23.8	Joint, dips 5°	23.7- 23.8	Bedding, etched, with clay (?) (~1/4 inch) 228°, 10° (N) Remeasured orientation: ~204°, 15° (fair to good)	Core not available; removed for testing	N66°W, 15° SW

**Table 21-1. Interpretation of Bedding in Boreholes,
ISFSI Study Area (continued)****Boring 01-D**

Original Description from Log of Rock Boring including dip angle ⁽¹⁾ (DCPP ISFSI Data Report B)		WLA Descriptions from NORCAL Televiwer Image including dip azimuth and dip angle ⁽²⁾ (DCPP ISFSI Data Report E)		Review of Core ⁽³⁾	Interpreted Bedding Attitude ⁽⁴⁾ (strike, dip)
Depth (feet)	Description	Depth (feet)	Description		
36.0- 39.0	Fine to medium grained sandstone with crushed zones, joints dip 0° and steeply	36.9- 37.1	Two subhorizontal fractures, open and in part tight, bedding (?), bottom 290°, 5° (N) (fair)	Not checked	N20°E 5°NW
55.0- 55.5	Crushed zone with clay, joint at 55.2	53.4- 54.9	Eroded and etched zone (clayey?), rough bedding (?) at base 057°, 11° (N) (good)	Sandstone layers and contact with dolomite dip 10°	N33°W, 11°NE

Boring 01-E

Original Description from Log of Rock Boring including dip angle ⁽¹⁾ (DCPP ISFSI Data Report B)		WLA Descriptions from NORCAL Televiwer Image including dip azimuth and dip angle ⁽²⁾ (DCPP ISFSI Data Report E)		Review of Core ⁽³⁾	Interpreted Bedding Attitude ⁽⁴⁾ (strike, dip)
Depth (feet)	Description	Depth (feet)	Description		
46.5- 48.0	Sandy dolomite to dolomitic sandstone; horizontal to subhorizontal laminar banding	46.5- 48.0	Unfractured, hard rock, weak laminations	Irregular bedding laminations at 47.5 feet, 090°, dip 8° measured from fracture orientation on televiwer (good)	NS, 8°E
48.0	(same as above)	48.0	Top of thin (0.1 feet) dark bed (clay?), 332°, 17 (N) remeasured ~330°, 10° (fair)	Core not available; removed for testing	N60°E, 10°NW(?)
48.8	(same as above)	48.8	Bottom of moderately dark bed (0.7 feet), parallels the base of the dark bed at 48.1 feet 360°, 4° (fair to good)	Core not available; removed for testing. But @ 50.5 feet bedding laminations in core dip 3°	EW, 3°N

**Table 21-1. Interpretation of Bedding in Boreholes,
ISFSI Study Area (continued)****Boring 01-F**

Original Description from Log of Rock Boring including dip angle ⁽¹⁾ (DCPP ISFSI Data Report B)		WLA Descriptions from NORCAL Televue Image including dip azimuth and dip angle ⁽²⁾ (DCPP ISFSI Data Report E)		Review of Core ⁽³⁾	Interpreted Bedding Attitude ⁽⁴⁾ (strike, dip)
Depth (feet)	Description	Depth (feet)	Description		
6.8	Clay film (<1/16 inch), joint, dips 20°	6.6	Partly open joint with thin clay (?), shallow bedding (?) 200°, 9° (fair)	Not checked	N70°W, 9°SW
94.3- 94.4	Clayey, silty crushed rock with clay bed (0.5-1 cm thick (¼-½ in)) dips 0-10°	93.2	Subhorizontal joint along bedding with 1/4 inch clay (?), etched 180°, 15° (N) (good)	Thick clay (1/4- 1/2 inch) over 1/4-inch- thick, white, moderately- soft calcite vein at 94.8 feet, dips 14°	EW, 14°S
117.0	Clay layer (1 cm), bedding (?) dips 8-12°	116.4	Subhorizontal bedding, etched, possible thin clay (~1/8 inch) 200°, 5° (N) Remeasured dip: 6° (good)	Core not available; removed for testing	N70°W, 6-12°SW

Boring 01-G

Original Description from Log of Rock Boring including dip angle ⁽¹⁾ (DCPP ISFSI Data Report B)		WLA Descriptions from NORCAL Televue Image including dip azimuth and dip angle ⁽²⁾ (DCPP ISFSI Data Report E)		Review of Core ⁽³⁾	Interpreted Bedding Attitude ⁽⁴⁾ (strike, dip)
Depth (feet)	Description	Depth (feet)	Description		
18.7	Clay seam (1/2-3/4 inch) above broken rock zone on bedding (?), top horizontal, bottom dips 0-5°	18.5	Subhorizontal, tight bedding laminations possible thin (<1/4 inch) clay (?), 245-251°, 11-14° (N) average 248°, 13° (N) (fair to good)	Core not available; removed for testing	N22°W, 13°SW
25.4	Joint with clay coatings (<0.5 inch), dips 0-15°	25.0	subhorizontal bedding, tight with thin clay (?) (<1/8 inch), 192, 15 (N) (fair)	Not checked	N78°W, 15°S
29.1	Joint with very thin film, dips 0°	28.8	Bedding (?), partly broken out in zone of massive rock ~210, 12° (fair)	Not checked	N60°W, 12°SW
56.3	Clayey fracture zone parallel to laminations, laminations dip 0-10°	55.8- 57.5	Steep joints and broken rock, localized clay (up to ~1/2 inch) on joint	Red brown laminations dip 5-8°	Unknown strike, dips 5-8°

**Table 21-1. Interpretation of Bedding in Boreholes,
ISFSI Study Area (continued)**

Boring 01-H

Original Description from Log of Rock Boring including dip angle ⁽¹⁾ (DCPP ISFSI Data Report B)		WLA Descriptions from NORCAL Televiewer Image including dip azimuth and dip angle ⁽²⁾ (DCPP ISFSI Data Report E)		Review of Core ⁽³⁾	Interpreted Bedding Attitude ⁽⁴⁾ (strike, dip)
Depth (feet)	Description	Depth (feet)	Description		
39.4	Two very thin clay layers between fracture blocks dip 30°	39.4- 41.2	Subhorizontal bedding, slightly etched, with thin clay (?), 253-284, 2-4° (N) Remeasured orientation on clay bed at 41.2 feet: ~240°, 5° (fair)	Three thin clay beds, dip 15°	N30°W, 15°SW
58.7	Fine to medium grained dolomitic sandstone, @ 58.9 feet clay layer, 0.01 feet thick on 'joint' dips 10°	58.7	Thin bed 211, 13° (N) (fair)	Not evident in core.	N59°W, 13°SW
82.3	Clay seam (0.05 feet thick) on joint, dips 0°	81.4	Subhorizontal bedding laminations, tight, no clay evident, 225, 12° (N) (fair)	Not checked	N45°W, 12°SW
89.6	Sandstone	88.8	Bedding, textural change 203, 1-1° (N) (fair to good)	2 mm clay bed twisted by drilling	N67°W, 11°SW
94.5	Dark gray clay layer (0.2 inch), dips 10-30°	93.6	Subhorizontal bedding, eroded with clay (?) 202, 2° (N) Remeasured: 232°, 21° (good)	Highly fractured, clay layer not found	N38°W, 21°SW

**Table 21-1. Interpretation of Bedding in Boreholes,
ISFSI Study Area (continued)****Boring 01-I**

Original Description from Log of Rock Boring including dip angle ⁽¹⁾ (DCPP ISFSI Data Report B)		WLA Descriptions from NORCAL Televiwer Image including dip azimuth and dip angle ⁽²⁾ (DCPP ISFSI Data Report E)		Review of Core ⁽³⁾	Interpreted Bedding Attitude ⁽⁴⁾ (strike, dip)
Depth (feet)	Description	Depth (feet)	Description		
33.9	Clay film (1/16 inch) on bedding, joint (?), dips 10°	34.9	Subhorizontal lamination, tight to partly eroded bedding, 309°, 6° (N) (good)	Not checked	N39°E, 6°NW
43.1	Clay on joint (1/4 inch), dips 20°	43.4- 43.6	Thin clay, eroded and etched along bedding(?), 325°, 18° (N) (good)	Not checked	N55°E, 18°NW
45.6	Clay bed (2 cm), dips 10-15°	46.2	Well imaged thin clay, etched, bedding parallel, 324°, 14° (N) (good)	Not checked	N54°E, 14°NW
48.1	Clay seam (1 cm) on joint associated with CaCO ₃ vein, dips 10- 20°	48.8	Subhorizontal joint/clay seam (1/4-1/2 inch), etched, 320°, 13° (N) (good)	Not checked	N50°E, 13°NW
57.2	Sandy crushed zone	57.6- 57.9	Subhorizontal, planar opening along eroded soft rock zone (1/2 to 1 inch); thin clay (?) along base, bedding, near bottom of clay bed 295°, 8° (N) (fair to good)	Crushed zone, remnant bedding dips 15°	N25°E, 8-15°NW
86.0- 87.0	Dolomitic sandstone, laminations dip 12-20°	86.8- 88.5	Clear laminations in hard rock, near vertical fracture	Bedding laminations dip 15°, azimuth of 285° measured using fracture orientation (good)	N15°E, 15°W
89.5- 89.8	Dolomitic sandstone	89.2- 90.7	Clear lithologic banding in unjointed, hard rock 276, 18° (N) 285, 20° (N) (fair)	Bedding laminations dip 13-14°	N15°E, 14°W

**Table 21-1. Interpretation of Bedding in Boreholes,
ISFSI Study Area (continued)****Boring 01-I (continued)**

Original Description from Log of Rock Boring including dip angle ⁽¹⁾ (DCPP ISFSI Data Report B)		WLA Descriptions from NORCAL Televewer Image including dip azimuth and dip angle ⁽²⁾ (DCPP ISFSI Data Report E)		Review of Core ⁽³⁾	Interpreted Bedding Attitude ⁽⁴⁾ (strike, dip)
Depth (feet)	Description	Depth (feet)	Description		
102.0- 105.0	Very fine grained to fine grained dolomitic sandstone, well defined laminations	102.0- 105.0	Hard rock with laminations and two near vertical fractures, at 103.7 315°, 11°	Laminations dip 13° (fair to good)	N45°E, 13°NW
106.6	Clayey/silty/sand seam (2 cm), bedding, dips 10-12°	106.4	Subhorizontal clayey seam (1 to 2 inches thick), eroded and etched along bedding top 266°, 16° (N) bottom 251°, 17° (N) (good)	Clay bed not found in core, but bedding laminations one foot above and below dip 12- 14°	N19°W, 12-14°W
123.8- 124.0	Clayey sandstone bed above coarse, 0.1-foot- thick sandstone bed, dips 10-20°	124.1	Irregular bedding contact between broken rock and soft, granular rock, eroded, 044°, 16° (N) (fair)	Not checked	N46°W, 16°NE
130.3	Stiff clay seam (1/2-1 cm) along bedding, dips 10°	130.8	Bedding with clay (?) slightly etched, 102°, 3° (N) (fair)	Not checked	N12°E, 3E
131.0	Joint with clay, dips 20°	131.6	Bedding with thin clay, subhorizontal, 171°, 8° (N) (good)	Not checked	N81°E, 8°S
156.1	Shaley seam (1/4 inch) with slickensides along bedding contact, dips 15-18	156.5- 156.8	Softer rock zone, eroded and etched, subhorizontal, possible clay at base of zone, bedding, 335°, 12° (N) (good)	Bottom of clay bed washed out during drilling.	N65°E, 12-18°NW
171.0- 171.2	Crushed zone with silty clay in joint (1/8 inch), possible slough at bottom, dips 10°	170.0- 173.0	Clear laminations and steep, partly open joints with clay (?), 285°, 12° (N) (good)	Bedding dips 12°, at 170.5 feet azimuth of ~294° measured using fracture orientation	N20°E, 12°NW
172.5- 173.1	Dolomitic sandstone, laminations dip 10-12°	171.0- 173.5	Clear lithologic banding and near vertical joint 272-285° (N), 11-12°(N)	Bedding on two beds, dips 11°, 15° (azimuth measured using fracture orientation confirms strike in televewer)	N15°E, 11°W

**Table 21-1. Interpretation of Bedding in Boreholes,
ISFSI Study Area (continued)**

Boring 01-I (continued)

Original Description from Log of Rock Boring including dip angle ⁽¹⁾ (DCPP ISFSI Data Report B)		WLA Descriptions from NORCAL Televewer Image including dip azimuth and dip angle ⁽²⁾ (DCPP ISFSI Data Report E)		Review of Core ⁽³⁾	Interpreted Bedding Attitude ⁽⁴⁾ (strike, dip)
Depth (feet)	Description	Depth (feet)	Description		
173.8- 175.0	Dolomitic sandstone, thick laminations dip ~10°	173.5- 176.6	Clear fine lithologic banding, typical: 296°, 15° (N) 285°, 14° (N) 292°, 13° (N) 309°, 10° (N) 316°, 13° (N) average 300°, 13° good)	Core has good laminations, bedding dips 10-13°	N30°E, 10-13°NW
185.0- 185.3	Two clay beds (2 cm; 1 cm) with crushed zone between, dips 10- 20°	185.7- 186.1	Subhorizontal clay bed (0.4 feet thick), etched, Bottom 317°, 18° (N) (good)	Dip on bottom of clay bed is 12-14°	N47°E, 12-14°NW
188.5	Clay film (1/16 inch) on joint, dips 10°	188.0- 189.0	Solid rock with color laminations, slightly etched, 267°, 7° (N) (good)	Not checked	N3°W, 7°E
198.4- 199.8	Dolomitic sandstone, laminations dip 5-12°	196.0- 201.0	Massive rock with color laminations, slight etching at 197.1 Following are typical: 295°, 9° (N) 291°, 10° (N) 289°, 9° (N) average 290°, 9° (good)	Well defined laminations, dip 14°, 11°	N20°E, 12°NW
215.8- 216.0	Crushed zone with clay seam, slickensides	215.9- 216.4	Irregular, subhorizontal bedding with brown clay (1 inch), eroded and etched, bottom contact 274°, 29° (N) (good)	Not checked	N4°E, 29°W
236.3	Stiff clay seam (1 cm) on bedding, dips 15°	236.8	Subhorizontal clay (1/4-1/2 inch) along laminations, etched and squeezing into hole 253°, 13° (N) (good)	Bedding in core dips 12- 13°, azimuth measured using fracture orientation confirms strike from televewer	N17°W, 13°SW

**Table 21-1. Interpretation of Bedding in Boreholes,
ISFSI Study Area (continued)**

Boring 01-I (continued)

Original Description from Log of Rock Boring including dip angle ⁽¹⁾ (DCPP ISFSI Data Report B)		WLA Descriptions from NORCAL Televue Image including dip azimuth and dip angle ⁽²⁾ (DCPP ISFSI Data Report E)		Review of Core ⁽³⁾	Interpreted Bedding Attitude ⁽⁴⁾ (strike, dip)
Depth (feet)	Description	Depth (feet)	Description		
252.4- 252.7	Bed of medium to coarse grained sandstone, contact dips 10-11°, bedding laminations dip 10°	252.9- 253.2	Washed out zone, friable sand (clay ?), bottom bedding 184°, 4° (N) remeasured 225°, 7° (fair to good)	Undulating laminations, dip 10-13°	N45°W, 10-13°W
259.2- 259.6	Very fine grained dolomitic sandstone, subhorizontal bedding laminations dip ~10°	259.1- 259.5	Lithologic banding; Following are typical: 254°, 12° (N) 262°, 13° (N) (good)	Irregular laminations at 259.0 dip ~18°, parting surfaces at 259.9 feet dip ~14-16°	N12°W, 12°W
283.6- 286.3	Very fine-grained sandstone, laminations, bedding dip 0°	286.3- 286.7	Laminations 299-315°, 13-17° (N) (fair)	Good laminations dip 11°; azimuth of 303° measured using fracture orientation	N33°E, 11°NW
289.9- 290.0	Clay seam/bed (1/2-1 cm), dips 10-15°	290.4	Subhorizontal clay bed (1/4-1/2 inch) along laminations, etched to partly open, irregular 322°, 18° (N) (fair)	Not checked	N62E, 18°NW
316.0- 316.6	Very fine grained sandstone, laminations	316.0- 317.0 °	Laminations 273°, 15 (N) 279°, 12° (N) (good)	Laminations dip 10-13°, with few irregular laminations up to 18°	N9°E, 12°W

**Table 21-1. Interpretation of Bedding in Boreholes,
ISFSI Study Area (continued)**

Notes:

- (1) Description and depth (in feet) of feature described on log of rock boring by field geologist. Dip angle measured from core with protractor by field geologist. In some cases, no field measurement was taken. Note that some features such as joints have been reinterpreted as bedding from subsequent review of core and/or interpretation of televiewer image.
- (2) WLA description and depth (in feet) of feature observed in NORCAL Televiewer image of boring. Dip azimuth and dip angle measurements taken from NORCAL interpretation are designated with (N). NORCAL measurements are described in DCPD ISFSI SAR Section 2.6 Topical Report DCPD ISFSI Data Report E. All other dip azimuth and dip angle measurements were obtained by WLA from televiewer image and represent either bedding not picked by NORCAL or remeasured by WLA where noted. WLA physically measured dip and dip azimuth on televiewer image hard copy in the following manner: Bedding occurs as sinusoidal form on unfolded borehole image. The dip direction is taken as the lowest point on the sinusoidal curve. The dip angle is calculated using the parameters of (1) measured amplitude of the sinusoidal curve (h) and (2) the boring diameter (d) in the equation $\tan(\text{dip angle}) = h/d$. A good, fair, or poor rating was assigned to the bedding attitude to convey the quality of measurement and confidence that the feature in the televiewer image represents bedding.
- (3) Comments from reinspection of core samples including dip measurements where noted. Dip azimuths are measured and noted where core could be oriented using attitudes of prominent fractures or joints obtained from televiewer images. "Not checked" refers to bedding attitudes that were interpreted from televiewer images following the last reinspection of the core.
- (4) Strike and dip of interpreted bedding. The interpreted bedding represents the best information obtained from field logs, NORCAL televiewer images, and reinspection of core samples. For example, the interpreted strike of bedding may be obtained from the televiewer images, but the corresponding dip may be taken from original field measurements of core samples, televiewer images, or measurements of core during reinspection, whichever is considered highest quality/confidence.

**Table 21-2 Evaluation of Clay 'Seams' on Low-Angle Fractures and Bedding,
ISFSI Study Area Borings**

Boring 98BA-1

Log of Rock Boring (DCPP ISFSI Data Report B)			NORCAL Televiewer Image† (DCPP ISFSI Data Report E)		Interpretation*		
Depth (feet)	Description	Dip (deg.)	Depth (feet)	Description	Clayey rock zone	Joint/ Fault	Clay Bed
11.0- 11.4	"Clay stringers"	--		No televiewer image	✓		?
26.6	Thin clay film (not clay bed)	0-5				✓?	?
65.0- 66.0	Clayey joint coatings	5-30				✓	
66.6- 67.0	Very soft clayey zone (not clay bed)	--			✓		
69.4- 70.0	Clayey rock, 1/8 inch seams; slickensides, disturbed	?				✓?	?
87.0	Silty clay in shoe	--				✓	?
90.4	Clay with slickensides, joint	25				✓	
91.5	Clay coatings with slickensides, joint	30				✓	
93.7	Clay films, polished, joint	0				✓	✓?
97.6	Clay seam on joint with slickensides	25				✓	
99.1	Clay on joint with slickensides	25				✓	
142.8	Joint, 1/16 inch clay, polished	10				✓?	✓?
145.1- 145.4	Clayey zone (not beds)	--			✓		
162.0- 162.2	Soft clayey rock zone	Low angle			✓		
165.3	Joint with clay, polished	5				✓	✓?
170.7	Joint with clay films and slickensides	0				✓	✓?
175.8	1.2 inches clay zone	15					✓?
192.4- 192.6	Clay films with slickensides (shear zone)	20				✓	
194.2	Joint with clay films, slickensides	0				✓	✓?
203.3	Bedding with clay seams (films) in 0.7 inch-wide breccia	5-10				✓?	✓?

**Table 21-2 Evaluation of Clay 'Seams' on Low-Angle Fractures and Bedding,
ISFSI Study Area Borings (continued)****Boring 98BA-2**

Log of Rock Boring (DCPP ISFSI Data Report B)			NORCAL Televiewer Image† (DCPP ISFSI Data Report E)		Interpretation*		
Depth (feet)	Description	Dip (deg.)	Depth (feet)	Description	Clayey rock zone	Joint/ Fault	Clay Bed
5.9	Joint with clay seam	10		No televiewer image		✓?	✓?
11.3	Joint with clay seam	30				✓	
13.3	Joint with clay film	30				✓	
36.5	Joint with clay film	15				✓	
38.9	Joint with clay film	15				✓	
53.4	Joint with thin clay	5				✓	✓?
58.2	Joint with thin clay, slickensides	30				✓	
59.6	Joint with thin clay	5				✓	✓?
63.6	Joint with thin clay, slickensides	10				✓	✓?
67.3	Joint with clay seams with shears	10				✓	✓?
128.5	Joint with clay films and slickensides	0				✓	✓?

Boring 98BA-3

Log of Rock Boring (DCPP ISFSI Data Report B)			NORCAL Televiewer Image† (DCPP ISFSI Data Report E)		Interpretation*		
Depth (feet)	Description	Dip (deg.)	Depth (feet)	Description	Clayey rock zone	Joint/ Fault	Clay Bed
	No clay beds described			No televiewer image			

**Table 21-2 Evaluation of Clay 'Seams' on Low-Angle Fractures and Bedding,
ISFSI Study Area Borings (continued)**

Boring 00BA-1

Log of Rock Boring (DCPP ISFSI Data Report B)			NORCAL Televiewer Image† (DCPP ISFSI Data Report E)		Interpretation*		
Depth (feet)	Description	Dip (deg.)	Depth (feet)	Description	Clayey rock zone	Joint/ Fault	Clay Bed
23.0- 23.2	Four joints with thin clay coatings (altered zone)	0	23.1	Thin clay (?) bed, N25°E, 9°NW and moderately steep joint			✓?
30.2	Clay seam (1/8 inch), bedding?	0?	29.4- 30.2	Moderately steep joint, etched, irregular with clay(?)		✓	
51.2	Crushed clayey rock	-	51.0- 51.6	Irregular joint, tight		✓	
54.5	Stiff clay (1/8 inch)	~0	53.5- 54.5	Steep filled joint, irregular tight with clay		✓	
55.6- 56.3	Clay seam (8.4 inches) with planar rock contacts, bedding	~5	54.9- 56.2	Clay bed with sharp, tight rock contacts, etched, N82°W, 11°-16°S			✓
69.2- 69.6	Crushed zone with silt, some clay	--	69.2- 69.8	Steep fracture, eroded, clay (?)		✓	
79.5	Stiff, silty clay seam (1/8 inch) on joint	10	79.2	Possible thin clay along bedding or joint, etched below N61° E, 11°-16° NW			✓
105.4	Clay seam (1/4 inch) along fracture	15	105.0- 105.3	Clay seam, etched, irregular top, sharp, smooth bottom contact, N13°W, 12°SW			✓
106.5	Silty clay (1/8-1/4 inch), joint	30	106.4	Tight bedding with discoloration N20°W, 18°SW			✓?
109.5	Clay lined joint	10	108.9- 109.0	Tight joint		✓	
140.0- 141.0	Sandstone, changes to laminations @ 140.9	--	140.4	Thin clay (?) bed, partly etched N10°E, 4°SW			✓
145.3- 145.7	Crushed, broken zone with clay coatings (1/4 inch)	--	144.3- 145.7	Steep joints, tight with clay (1/4-1/2 inch)		✓	

Table 21-2 Evaluation of Clay 'Seams' on Low-Angle Fractures and Bedding, ISFSI Study Area Borings (continued)**Boring 00BA-2**

Log of Rock Boring (DCPP ISFSI Data Report B)			NORCAL Televiwer Image† (DCPP ISFSI Data Report E)		Interpretation*		
Depth (feet)	Description	Dip (deg.)	Depth (feet)	Description	Clayey rock zone	Joint/ Fault	Clay Bed
29.8- 30.0	Crushed zone	--	29.8- 30.2	Subhorizontal soft clay (?) zone, etched, irregular contact	✓		✓?
40.4	Crushed zone	--	40.4- 40.8	Moderately steep, joint, partly open and etched, with thin clay (?)		✓	
52.4	Clay (1/16 inch) on joint, minor striations	0	52.4- 52.6	Tight, moderately steep joint		✓	

Boring 00BA-3

Log of Rock Boring (DCPP ISFSI Data Report B)			NORCAL Televiwer Image† (DCPP ISFSI Data Report E)		Interpretation*		
Depth (feet)	Description	Dip (deg.)	Depth (feet)	Description	Clayey rock zone	Joint/ Fault	Clay Bed
11.8- 12.8	Clayey sandstone (not a clay bed)	--		No televiwer image	✓		
22	Clay film on joint, polished	30				✓	
26.5	Clay (1/16 inch) with slickensides, joint	0				✓	✓?

Boring 01CTF-A

Log of Rock Boring (DCPP ISFSI Data Report B)			NORCAL Televiwer Image† (DCPP ISFSI Data Report E)		Interpretation*		
Depth (feet)	Description	Dip (deg.)	Depth (feet)	Description	Clayey rock zone	Joint/ Fault	Clay Bed
22.9	Clay film on joint, polished	30	22.6- 23.0	Moderately dipping joint, tight, thin clay (?)		✓	
32.4- 32.6	Soft clayey sand, bedding (?)	30	32.7- 33.5	Soft clayey (?) zone, etched, irregular contacts	✓		
37.7	Clay (1/16 inch) on joint, polished, slickensides	30	38.3- 40.7	Tight, steep joints		✓	
38.2	Clay film on joint, end of core run	~5	38.3- 40.7	Tight, steep joints		✓	
50.5- 50.6	Clayey rock zone, not bedding clay	10	51.1- 51.3	Low-angle band (murky water)	✓		

**Table 21-2 Evaluation of Clay 'Seams' on Low-Angle Fractures and Bedding,
ISFSI Study Area Borings (continued)**

Boring 01-A

Log of Rock Boring (DCPP ISFSI Data Report B)			NORCAL Televiwer Image† (DCPP ISFSI Data Report E)		Interpretation*		
Depth (feet)	Description	Dip (deg.)	Depth (feet)	Description	Clayey rock zone	Joint/ Fault	Clay Bed
15.2- 15.4	Clay (0.4 inch) in fracture	25-30	15.2- 15.4	Moderately dipping joint, eroded, with clay (?)		✓	
29.9	Clay layer (0.6 inch), joint	30	29.6- 29.9	Moderately dipping joint, etched to eroded, thin clay (?) (image distorted)		✓	
37.7- 37.8	Two clay coatings (1/16 inch) on joints	20-30	36.7	Low to moderate dipping joint or bedding (?), etched N40°W, 20°SW		?	✓?
42.1	Sandstone, no recovery	--	41.0- 41.1 42.2- 42.3	Textural change, etched, bedding (?) with clay (?) Moderately dipping joint below broken, eroded zone with thin clay (?) N19°W, 23°W		✓?	✓?
46.0	Faults with clay coatings, slickensides	18-25	44.2- 49.2	Eroded and etched zone irregular, near vertical joint		✓	
48.2	Clay layer (1 inch) in broken zone	0	44.2- 49.2	Eroded and etched zone irregular, near vertical joint	✓?		?
52.0- 53.9	Sandstone with joints	0	53.3	Low-angle joint, eroded with thin clay		✓	
54.9	Silty clay with sand and gravel (1 inch), bedding?	20	54.1- 54.3	Low-angle bedding with textural difference, etched and eroded, 1/2-to 1 inch clay bed (?) N69°E, 7°NE			✓
55.8	Faults with thin clay coatings, slickensides	8-20	55.3	Bedding (?), etched, with thin clay (?) bed N11°W, 22°W			✓?
58.8	0.4 inch clay layer	20	58.5	Subhorizontal clay layer, eroded and etched, irregular, 1/4-1/2 inch thick, bottom N11°W, 22°W			✓?

**Table 21-2 Evaluation of Clay 'Seams' on Low-Angle Fractures and Bedding,
ISFSI Study Area Borings (continued)****Boring 01-B**

Log of Rock Boring (DCPP ISFSI Data Report B)			NORCAL Televiewer Image† (DCPP ISFSI Data Report E)		Interpretation*		
Depth (feet)	Description	Dip (deg.)	Depth (feet)	Description	Clayey rock zone	Joint/ Fault	Clay Bed
43.3	Trace clay on two joints	0	43.3	Broken rock zone		✓	
48.7	Trace clay on joint	30	48.7	Broken rock zone		✓	

Boring 01-C

Log of Rock Boring (DCPP ISFSI Data Report B)			NORCAL Televiewer Image† (DCPP ISFSI Data Report E)		Interpretation*		
Depth (feet)	Description	Dip (deg.)	Depth (feet)	Description	Clayey rock zone	Joint/ Fault	Clay Bed
16.3	Clay film on joint	15	15.9(?)	Low-angle bedding, etched, with clay (?) (~1/8 inch) N73°W, 15°S			✓?
23.8	Joint	5	23.7- 23.8	Bedding, eroded, with clay (?) (~1/4 inch) N66°W, 15°SW			✓
41.1- 41.4	Clay films on two joints, slickensides	20-30	40.3- 40.5	Moderately steep joint, etched, no visible clay		✓	
44.1	Clay (0.2 inch) on bedding?	0-5	43.6	Subhorizontal bedding, etched to eroded, thin clay (?), irregular			✓?
55.8- 56.2	Sandstone some clay	5	54.9	Subhorizontal, irregular bedding (?), etched to eroded, clay (?)		✓?	?
65.3	Soft clay (1/4 inch) on joint, bedding (?)	5	65.0	Moderately steep joint, etched, slight clay (?) (water in hole, image fuzzy)		✓	

Table 21-2 Evaluation of Clay 'Seams' on Low-Angle Fractures and Bedding, ISFSI Study Area Borings (continued)**Boring 01-D**

Log of Rock Boring (DCPP ISFSI Data Report B)			NORCAL Televiewer Image† (DCPP ISFSI Data Report E)		Interpretation*		
Depth (feet)	Description	Dip (deg.)	Depth (feet)	Description	Clayey rock zone	Joint/ Fault	Clay Bed
26.5- 27.0	Joint, crumbly zone	30	25.9- 26.9	Eroded zone between two moderately steep joints, clayey (?), rock (6.25 inches wide)		✓	
55.0- 55.5	Crushed zone with clay, joint at 55.2	--	53.4- 54.9	Eroded and etched zone (clayey?), rough bedding (?) at base N33°W, 11°N	✓?		

Boring 01-E

Log of Rock Boring (DCPP ISFSI Data Report B)			NORCAL Televiewer Image† (DCPP ISFSI Data Report E)		Interpretation*		
Depth (feet)	Description	Dip (deg.)	Depth (feet)	Description	Clayey rock zone	Joint/ Fault	Clay Bed
12.85	Clay layer (1/8 inch)	10	12.1- 12.7	Vein, joints, etched, clayey (?)		✓	
20.8	Clay gouge (1/16 inch), joint	30	20.4- 20.5	Shallow joint, etched, irregular, with thin clay (?)		✓	
23.0- 25.0	Zone of clay coated joints, polished, with rubble	30	23.1- 24.3	Moderately steep, tight to slightly etched, joints		✓	
71.7	Clay film on joint	30	71.4- 72.1	Steep, tight joint (hole has water, image fuzzy)		✓	
77.4	Clay filled joint	0	77.0- 78.0	No joints evident (hole has water, image fuzzy)		✓	

**Table 21-2 Evaluation of Clay 'Seams' on Low-Angle Fractures and Bedding,
ISFSI Study Area Borings (continued)**

Boring 01-F

Log of Rock Boring (DCPP ISFSI Data Report B)			NORCAL Televiewer Image† (DCPP ISFSI Data Report E)		Interpretation*		
Depth (feet)	Description	Dip (deg.)	Depth (feet)	Description	Clayey rock zone	Joint/ Fault	Clay Bed
5.5	Clay film (<1/16 inch), joint	0	4.7- 6.6	Fractured zone with clay (?)		✓	
6.8	Clay film (<1/16 inch), joint	20	6.6	Partly open joint with thin clay (?), shallow bedding (?) N70°W, 9°SW		✓?	✓?
10.5- 10.8	Sandy, clayey rock zone	--	10.2- 10.5	Partly etched zone	✓		
16.1- 16.3	Fractured clayey zone	--	15.2- 16.4	Weak, etched and eroded rock	✓		
29.2	Clayey crushed rock mixed with harder rock fragments	--	29.0- 30.2	Weak, etched zone	✓		?
35.5- 38.0	Clayey fractured zone, altered	--	35.0- 38.0	Soft, partly etched, locally fractured rock	✓		
43.8- 44.4	Clayey fractured zone, altered	0-10 80-90	43.7- 45.3	Fractured rock with tight, subhorizontal joint and steep, partly open joints, some clay (?)	✓	✓	
46.6- 46.8	Clayey fracture zone, altered, bounded by joints	0	46.0- 47.0	Steep, eroded joints and fractured rock with clay		✓	
57.5- 57.7	Clayey zone along possible bedding	5-15	57.9	Subhorizontal, tight lamination, slight clay (?) (<1/16 inch)		✓?	✓?
58.6	Clay films on joint with slickensides, possible bedding	20	57.0- 59.0	Tight joints and subhorizontal laminations, possible clay (<1/16 inch)		✓	?
58.6- 58.8	Clayey lens in rock and clay films with slickensides, joint	10	58.7- 58.9	Moderately dipping joint, etched, with clay (?) (<1/16 inch)	✓	✓	
94.3- 94.4	Clayey, silty crushed rock with clay bed (1/4-1/2 inch thick)	0-10	93.2	Subhorizontal joint along bedding, etched, with 1/4 inch clay (?), etched EW, 14°S			✓
98.0- 98.4	Broken zone with clayey- silty matrix	70	98.0- 99.0	Fractured zone with apparent softer rock pockets, eroded (clay ?)	✓		

**Table 21-2 Evaluation of Clay 'Seams' on Low-Angle Fractures and Bedding,
ISFSI Study Area Borings (continued)**

Boring 01-F (continued)

Log of Rock Boring (DCPP ISFSI Data Report B)			NORCAL Televiewer Image† (DCPP ISFSI Data Report E)		Interpretation*		
Depth (feet)	Description	Dip (deg.)	Depth (feet)	Description	Clayey rock zone	Joint/ Fault	Clay Bed
103.8	Thin silt/clay coating on joint	20	103.0-104.4	Fractured zone with steep joints		✓	
104.4	Clay on joint	30	103.0-104.4	Fractured zone with steep joints		✓	
105.5	Clay seam (?) (<~1/2 inch) in broken zone (clay in crushed zone)	65-80	105.0-106.0	Tight rock with few steep fractures, laminations, no clay seam evident	✓	✓?	
107.3	Trace clay on joint	20	106.5-108.0	Solid, unfractured rock, no clay or joints evident		?	
111.3	Trace clay on joint	20	111.1-111.4	Moderately steep joint, irregular, partial thin clay (?)		✓	
111.9	Clay (<1/32 inch) on joint	0	111.5-112.5	Moderately steep, hairline fracture in otherwise solid unfractured rock		?	
117.0	Clay layer (0.4 inch) bedding (?)	8-12	116.4	Subhorizontal bedding, etched, possible thin clay (~1/8 inch) N70°W, 6°-12°SW			✓?
124.8	Joint lined with 1/16 inch clay	30	123.6-124.5	Tight to open, steep joints, no clay evident		✓	
125.9	Joint with trace clay, polished	35	124.5-126.5	Tight, sound rock with few tight to locally open, steep fractures		✓	

**Table 21-2 Evaluation of Clay 'Seams' on Low-Angle Fractures and Bedding,
ISFSI Study Area Borings (continued)**

Boring 01-G

Log of Rock Boring (DCPP ISFSI Data Report B)			NORCAL Televiwer Image† (DCPP ISFSI Data Report E)		Interpretation*		
Depth (feet)	Description	Dip (deg.)	Depth (feet)	Description	Clayey rock zone	Joint/ Fault	Clay Bed
8.6- 9.0	Weak zone with clay, crushed	--	7.6- 8.6	Moderately steep joints, partly broken out, with thin clay (?), massive rock below		✓	
14.3	Clay lined joints	30	14.0- 14.2	Tight, moderately steep joint, no visible clay		✓	
18.7	Clay seam (1/2-3/4 inch) above broken rock zone on bedding (?)	Top, ~0; Base, 0-5	18.5	Subhorizontal, tight bedding laminations possible thin (<1/4 inch clay) (?), N22°W, 13°SW			✓
25.4	Joint with clay coatings (<0.5 inch)	0- ~15	25.0	Subhorizontal bedding, tight with thin clay (?) (<1/8 inch), N78°W, 15°S			✓
29.1	Joint with very thin film	0	28.8	Bedding (?), partly broken out in zone of massive rock N60°W, 12°SW			✓?
50.3	Zone of silty clay	--	49.2- 50.6	Steep, partly open joints and broken rock	?	✓	
56.3	Clayey fracture zone parallel to laminations	0-10	55.8- 57.5	Steep joints and broken rock, localized clay (up to ~1/2 inch) on joint		✓	
67.2	Minor clay/silt laminations	--	67.0- 68.0	Laminated tight rock with steep joint, no visible clay	✓		
75.6	Thin clay film on joints	30-40		Below televiwer log		✓	

Table 21-2 Evaluation of Clay 'Seams' on Low-Angle Fractures and Bedding, ISFSI Study Area Borings (continued)

Boring 01-H

Log of Rock Boring (DCPP ISFSI Data Report B)			NORCAL Televiewer Image† (DCPP ISFSI Data Report E)		Interpretation*		
Depth (feet)	Description	Dip (deg.)	Depth (feet)	Description	Clayey rock zone	Joint/ Fault	Clay Bed
10.0	Clay films	30	9.2- 9.4	Moderately dipping joint partly broken out, with some clay (?)		✓	
39.4	Two very thin clay layers between fracture blocks	10	39.4	Subhorizontal bedding, slightly etched, with thin clay (?), N30°W, 15°SW			✓
40.3	Joint with thin clay coating	13	39.6- 41.0	Massive, laminated rock		✓?	
50.5	Clay "clast" (1/4-3/4 inch), bedding parallel	30	49.7- 51.6	Massive rock, no clay evident, thin, slightly etched beds at 50.3 and 50.4	✓		
59.9	Clay layer (1/8 inch thick)	--	59.1- 59.8	Subhorizontal softer rock zone, etched contact, vague	✓		✓?
67.2	Clay layer (1/8 inch thick)	30	66.7- 66.9	Moderately dipping joint, slightly etched, with thin clay (?) (<1/16 inch)		✓	
67.4	Clay layer (1/8 inch thick)	30	66.7- 66.9	Moderately dipping joint with thin clay (?) (<1/16 inch)		✓	
72.8	Clay on joint (1/16 inch thick)	30	72.2	Irregular, thin clay (?) layer in massive rock		✓?	✓?
82.3	Clay seam (3/4 inch thick)	0	81.4	Subhorizontal bedding laminations, tight, no clay evident, N45°W, 12°SW			?
89.6	Sandstone (1/16 inch clay bed twisted by drilling)	0	88.8	Bedding, textured change, N67°W, 11°SW			✓
94.5	Dark gray clay layer (1/4 inch thick)	10-30	93.6	Subhorizontal bedding, eroded with clay (?) (~1/4 inch), N38°W, 21°SW			✓

Table 21-2 Evaluation of Clay 'Seams' on Low-Angle Fractures and Bedding, ISFSI Study Area Borings (continued)**Boring 01-I**

Log of Rock Boring (DCPP ISFSI Data Report B)			NORCAL Televiewer Image† (DCPP ISFSI Data Report E)		Interpretation*		
Depth (feet)	Description	Dip (deg.)	Depth (feet)	Description	Clayey rock zone	Joint/ Fault	Clay Bed
15.6	Clay on joint (0.2-0.4 inch)	10	15.0- 16.0	Broken zone, clay (?) along joints		✓	
18.9	Clay on joint (1/16 inch)	0	17.8- 20.0	Broken out zone along steep joints, clay (?)		✓	
20.2	Silty/clayey crushed rock zone (not clay bed)	10-20	20.4- 21.0	Broken, jointed zone		✓	
33.9	Clay film (1/16 inch) on bedding, joint (?)	10	34.9	Subhorizontal lamination, tight to partly eroded bedding, N39°E, 6°NW			✓
39.0- 40.0	Crushed zone with silt, clay films	--	37.9- 40.1	Fractured zone, steep joints, partly broken out		✓	
43.1	Clay on joint (1/4 inch)	20	43.4- 43.6	Thin clay, eroded and etched along bedding (?), N55°E, 18°NW			✓
45.6	Clay bed (0.8 inch)	10-15	46.2	Well imaged thin clay, etched, bedding parallel, N54°E, 14°NW			✓
48.1	Clay seam (0.4 inch) on joint associated with CaCO ₃ vein	10-20	48.8	Subhorizontal joint/clay seam, etched, with clay (1/4-1/2 inch), N50°E, 13°NW			✓
57.2	Sandy crushed zone	--	57.6- 57.9	Subhorizontal, planar opening along eroded soft rock zone (1/2 to 1 inch); thin clay (?) along base, bedding, N25°E, 8°-15°NW			✓
61.0- 61.4	Crushed rock zone with some clay, not bedding	--	60.0- 62.5	Steep joints with clay (?)		✓	
62.7- 63.1	Crushed rock zone with silt and clay, not bedding	--	63.3- 63.9	Moderately steep, smooth joints with crushed and weak rock mixed with clay (?) in lower part (~2 inch thick)		✓	

**Table 21-2 Evaluation of Clay 'Seams' on Low-Angle Fractures and Bedding,
ISFSI Study Area Borings (continued)**

Boring 01-I (continued)

Log of Rock Boring (DCPP ISFSI Data Report B)			NORCAL Televiwer Image† (DCPP ISFSI Data Report E)		Interpretation*		
Depth (feet)	Description	Dip (deg.)	Depth (feet)	Description	Clayey rock zone	Joint/ Fault	Clay Bed
68.6- 69.2	Clay zone with crushed altered rock (not bedding)	--	68.3- 70.2	Moderately steep to steep joints bounding 1 foot-thick, weak rock, deeply eroded with possible clay		✓	
70.8- 71.1	Crushed zone with clay	--	70.5- 70.8	Moderately steep fracture, partly open, with clay (?)		✓	
85.8	Trace clay on joint	20	85.4- 85.6	Moderately steep, open joint, possible thin clay washed out?		✓	
90.1	Clay (0.1-0.2 inch) on joint	20	89.2- 90.7	Massive unjointed rock with laminations		✓	
93.4- 93.9	Three joints with trace clay	30	93.4- 94.6	Steep joints, with thin clay (?), partly eroded and bounded by massive unjointed rock with color laminations		✓	
100.2- 100.6	Trace clay on two joints	20	98.0- 100.8	Fractured rock with steep open joints, discontinuous		✓	
106.6	Clayey/silty/sand seam (~3/4 inch), bedding	10-12	106.4	Subhorizontal clayey seam (1 to 2 inches thick), eroded and etched along bedding N19°W, 12°-14°W			✓
108.9	Broken clay along joints	18-20	108.0- 116.2	Broken rock zone with steep joints, clay (?)		✓	
110.0	Sandy clay (0.4 inch) at bottom of run, possible slough	--	108.0- 116.2	Broken rock zone with steep joints, clay (?)		✓	
123.0	Joint with 0.2 inch clay	20	121.1- 124.1	Broken rock zone, subhorizontal fabric, possible thin clay (?) laminations		✓	
123.8- 124.1	Clayey sandstone bed above coarse, 1.2 inch-thick sandstone bed	10-20	124.1	Irregular bedding contact between broken rock and soft, granular rock, eroded, N46°W, 16°NE	✓		

Table 21-2 Evaluation of Clay 'Seams' on Low-Angle Fractures and Bedding, ISFSI Study Area Borings (continued)

Boring 01-I (continued)

Log of Rock Boring (DCPP ISFSI Data Report B)			NORCAL Televiwer Image† (DCPP ISFSI Data Report E)		Interpretation*		
Depth (feet)	Description	Dip (deg.)	Depth (feet)	Description	Clayey rock zone	Joint/ Fault	Clay Bed
127.6- 127.8	Crushed clayey zone (2.4 inches)	20-35	126.5- 129.2	Steep joints and broken rock, partly open, with clayey (?) zone at 127.8	✓	✓	
130.3	Stiff clay seam (1/4-1/2 inch) along bedding	10		Bedding with clay (?) slightly etched N12°E, 3°S			✓
131.0	Joint with clay	20	131.6	Bedding with thin clay, subhorizontal, N81°E, 8°S			✓?
146.3	Clay (1/8 inch) on joint (or drilling clay?)	20	145.2- 148.7	Open, steep joint, eroded, possible washed-out soft rock or clay zone		✓?	
151.4- 151.9	Crushed silty/clayey zone, part slough?	--	149.5- 151.2	Fractured rock, partly open and etched	✓		
156.1	Shaley seam (1/4 inch) with slickensides along bedding contact	15-18	156.5- 156.8	Softer rock zone, eroded and etched, subhorizontal, possible clay at base of zone, bedding N65°E, 12°-18°NW			✓?
167.4- 167.8	Zone with multiple clay seams (1/8-1/4 inch) along bedding	10	167.0	Thin clay (?), etched along bedding			✓
171.0- 171.2	Crushed zone with silty clay in joint (1/8 inch), possible slough at bottom	10	170.0- 172.0	Clear laminations and steep, partly open joints with clay N20°E, 12°NW		✓	
185.0- 185.3	Two clay beds (0.8 inch; 0.4 inch) with crushed zone between	10-20	185.7- 186.1	Subhorizontal clay bed (4.8 inches-thick), etched N47°E, 12°-14°NW			✓
188.5	Clay film (1/16 inch) on joint	10	188.0- 189.0	Solid rock with color laminations, slightly etched, N3°W, 7°E			✓?

**Table 21-2 Evaluation of Clay 'Seams' on Low-Angle Fractures and Bedding,
ISFSI Study Area Borings (continued)**

Boring 01-I (continued)

Log of Rock Boring (DCPP ISFSI Data Report B)			NORCAL Televiewer Image† (DCPP ISFSI Data Report E)		Interpretation*		
Depth (feet)	Description	Dip (deg.)	Depth (feet)	Description	Clayey rock zone	Joint/ Fault	Clay Bed
197.0	Clay films on joint	0	196.0- 198.0	Massive rock with color laminations, slight etching at 197.1, N20°E, 12°NW			✓?
210.2	Crushed clayey, sandy zone at top of crushed zone	--	209.0- 211.0	Broad color laminations and near-vertical joint with clay (?)	✓	✓	
215.8- 216.0	Crushed zone with clay seam, slickensides	--	215.9- 216.4	Irregular, subhorizontal bedding with brown clay (1 inch), eroded and etched, bottom contact N4°E, 29°W			✓
223.1	Clay film on joint	0	221.1- 223.8	Massive rock with weak color laminations, moderately dipping, tight joint at 223.8			✓?
230.7	Irregular clay seam/bed (?) (0.4 inch)	5-15	230.2- 231.0 230.9	Steep joint with clay (?) Top of light color band, etched, clay (?)		✓	✓?
236.3	Stiff clay seam (0.4 inch) on bedding	15	236.8	Subhorizontal clay (1/4-1/2 inch) along laminations, etched and squeezing into hole N17°W, 13°SW			✓
245.1	Clay on joint (0.4 inch)	0	244.8- 246.2	Massive rock with a steep, tight to slightly open joint		✓	
289.9- 290.1	Clay seam/bed (0.2-0.4 inch)	10-15	290.4	Subhorizontal clay bed (1/4-1/2 inch) along laminations, etched N62°E, 18°NW			✓

Note: Clay on fractures steeper than 30 degrees are not included because bedding has dips less than 20 degrees in the site area.

† Bedding attitudes from Table 21-1

* Interpretation Categories

Bold type highlights clay bed or possible clay bed shown on cross sections

- ✓ Significant clay bed (> 1/4 inch thick, follows bedding; thickness in most cases taken from measurements on core)
- ✓ Clay along bedding, joint or fault
- ✓? Probable clay along bedding, joint or fault
- ? Possible clay along bedding, joint or fault

Table 21-3 Thickness Measurements of Clay Beds in Borings and Trenches

Location	Boring Depth (feet)	Trench Station (meters)	Thickness (inches) ^a		Notes on Thickness ^b	Subunit ^c
			minimum	maximum		
98BA-1	93.7	na	0.06	0.06	1, 2	Tof _{b-2}
98BA-1	142.8	na	0.06	0.06	1, 2	Tof _{b-2}
98BA-1	165.3	na	0.06	0.06	1, 2	Tof _{b-2}
98BA-1	170.7	na	0.06	0.06	1, 2	Tof _{b-2}
98BA-1	175.8	na	0.25	1.20	1	Tof _{b-2}
98BA-1	194.2	na	0.06	0.06	1, 2	Tof _{b-2}
98BA-1	203.3	na	0.06	0.06	1, 2	Tof _{b-2}
98BA-2	5.9	na	0.06	0.12	3	Tof _{b-2}
98BA-2	53.4	na	0.06	0.12	3	Tof _{b-2}
98BA-2	59.6	na	0.06	0.12	3	Tof _{b-2}
98BA-2	63.6	na	0.06	0.12	3	Tof _{b-2}
98BA-2	67.3	na	0.06	0.12	3	Tof _{b-2}
98BA-2	128.5	na	0.06	0.06	1, 2	Tof _{b-2}
00BA-1	23.0-23.2	na	0.06	0.12	3	Tof _{b-1}
00BA-1	55.6 to 56.3	na	8.40	8.40	1	Tof _{b-1}
00BA-1	79.5	na	0.12	0.12	1	Tof _{b-1}
00BA-1	105.4	na	0.25	0.25	1	Tof _{b-1}
00BA-1	106.5	na	0.12	0.25		Tof _{b-1}
00BA-1	140.0 to 141.0	na	0.06	0.06	1, 2	Tof _{b-1}
00BA-2	29.8-30.0	na	0.12	0.25	3	Tof _{b-1}
00BA-3	26.5	na	0.06	0.06	1, 2	Tof _{b-2}
01-A	37.7-37.8	na	0.06	0.06	1, 2	Tof _{b-2}
01-A	42.1	na	0.06	0.12	3	Tof _{b-2}
01-A	54.9	na	0.50	1.00		Tof _{b-2}
01-A	55.8	na	0.06	0.12	3	Tof _{b-2}
01-A	58.8	na	0.25	0.50		Tof _{b-2}
01-C	16.3	na	0.06	0.06	1, 2	Tof _{b-2}
01-C	23.8	na	0.25	0.25	1	Tof _{b-2}
01-C	44.1	na	0.06	0.20	3	Tof _{b-2}
01-F	6.8	na	0.06	0.06	1, 2	Tof _{b-1}
01-F	57.5-57.7	na	0.06	0.06	1, 2	Tof _{b-2}
01-F	94.3 to 94.4	na	0.25	0.50		Tof _{b-2}
01-F	117	na	0.12	0.40		Tof _{b-1} and Tof _{b-1a}
01-G	18.7	na	0.12	0.25	6	Tof _{b-1}
01-G	25.4	na	0.12	0.12	6	Tof _{b-1}
01-G	29.1	na	0.06	0.06	1, 2	Tof _{b-1}

Table 21-3 Thickness Measurements of Clay Beds in Borings and Trenches

(continued)

Location	Boring Depth (feet)	Trench Station (meters)	Thickness (inches) ^a		Notes on Thickness ^b	Subunit ^c
			minimum	maximum		
01-H	39.4	na	0.06	0.06	1, 2	Tof _{b-2}
01-H	59.9	na	0.12	0.12	1	Tof _{b-2}
01-H	72.8	na	0.06	0.06	1	Tof _{b-2}
01-H	89.6	na	0.06	0.06	1	Tof _{b-2}
01-H	94.5	na	0.25	0.25	1	Tof _{b-2}
01-I	33.9	na	0.06	0.06	1	Tof _{b-1}
01-I	43.1	na	0.25	0.25	1	Tof _{b-1}
01-I	45.6	na	0.06	0.80	3	Tof _{b-1}
01-I	48.1	na	0.25	0.50		Tof _{b-1}
01-I	57.2	na	0.06	0.12	3	Tof _{b-1}
01-I	106.6	na	1.00	2.00	6	Tof _{b-1}
01-I	130.3	na	0.25	0.50		Tof _{b-1}
01-I	131	na	0.06	0.12	3	Tof _{b-1}
01-I	156.1	na	0.25	0.25	1	Tof _{b-1}
01-I	167.4-167.8	na	0.12	0.25		Tof _{b-1}
01-I	185	na	0.40	0.40	1	Tof _{b-1}
01-I	185.3	na	0.80	0.80	1	Tof _{b-1}
01-I	188.5	na	0.06	0.06	1	Tof _{b-1}
01-I	197.0	na	0.06	0.06	1, 2	Tof _{b-1}
01-I	215.8 to 216.0	na	1.00	1.00	1	Tof _{b-1}
01-I	223.1	na	0.06	0.06	1, 2	Tof _{b-1}
01-I	230.7	na	0.40	0.40	1	Tof _{b-1}
01-I	236.3	na	0.25	0.50		Tof _{b-1}
01-I	289.9 to 290.1	na	0.25	0.50		Tof _{b-1}
T-11A	na	3.0 to 7.5	0.06	0.12	5	Tof _{b-1} and Tof _{b-1a}
T-11A	na	7.5 to 11.0	0.20	0.80	4	Tof _{b-1} and Tof _{b-1a}
T-11B	na	0.5 to 5.4	0.20	0.60	5	Tof _{b-1} and Tof _{b-1a}
T-11C	na	-1 to 2.3	0.20	0.60	4	Tof _{b-1} and Tof _{b-1a}
T-11D	na	0 to 8.5	0.20	0.80	4	Tof _{b-1} and Tof _{b-1a}
T-12	na	4.5 to 11.0	0.06	0.25	5	Tof _{b-1} and Tof _{b-1a}
T-14A	na	0 to 8.5	1.00	4.00	5	Tof _{b-1}
T-14A	na	8.5 to 22.0	0.25	2.00	5	Tof _{b-1}
T-14B	na	0.00 to 4.00	2.00	4.00	7	Tof _{b-1}
T-15	na	6.0 to 19.0	2.00	4.00	4	Tof _{b-1}
T-18A	na	1.0 to 4.5	0.06	0.25	4	Tof _{b-1}
T-19	na	11.8 to 17	0.25	0.25	4	Tof _{b-1}

Table 21-3 Thickness Measurements of Clay Beds in Borings and Trenches
(continued)

STATISTICS ON CLAY BED THICKNESS

Measurements from boreholes and trenches

	<u>minimum</u>	<u>maximum</u>
number of thickness measurements =	72	72 measurements
minimum thickness =	0.06	0.06 inches
maximum thickness =	8.40	8.40 inches
median thickness =	0.09	0.23 inches
mean thickness =	0.35	0.59 inches
1 standard deviation =	1.03	1.25 inches

Trench Data

Cumulative length of clay beds exposed in trenches (feet) (minimum because clay beds extend beyond end of trench) ≤ 1/4 inch thick	= 64.64 feet (28%)
> 1/4 inch thick	= 169.96 feet (72%)
Total	234.60 feet (100%)

Boring Data

Number of clay beds encountered in borings	≤ 1/4 inch thick	= 44 (73%)
	> 1/4 inch thick	= 16 (27%)
	Total	60 (100%)

Footnotes: ^a measurements taken from trench exposures and borings; thicknesses may not represent the true ranges for individual beds

^b To_{f_{b-1}} = dolomite subunit, To_{f_{b-1a}} = friable dolomite subunit, To_{f_{b-2}} = sandstone subunit

^c Notes on thickness

1. Only a single measurement taken; this value used in both minimum and maximum columns
2. Field description of film as "very thin"; assumed thickness of 0.06 (1/16) inch
3. Field description of "thin" given range of 0.06 to 0.12 inches
4. Thickness range recorded in trenches reflects two discrete measurements made along clay bed.
5. Thickness range is estimated from notes on trench logs
6. Thickness estimates using televiewer information only (boring log not used).
7. Thickness measured from photographs.

Table 21-4. Friable Rock Zones in ISFSI Study Area Borings.

Boring	Depth Interval of friable rock (feet)	Test Sample I.D.	Elevation Interval (feet)	Friable Zone Interval Thickness (ft)
98BA-1	Elevation at ground surface		372.0	
	90.0-96.0		282.0-276.0	6.0
	118-133.5		254.0-238.5	15.5
	138.7-140.0		233.3-232.0	1.3
	142.8-145.2		229.2-226.8	2.4
	167.3-172.3		204.7-199.7	5.0
	182.3-200.0		189.7-172.0	17.7
	206.0-206.8		166.0-165.2	0.8
Total Borehole Depth =	250.0		Total Friable Zone Interval Footage =	48.7 % Friable = 19.5
98BA-2	Elevation at ground surface		322.0	
	5.0-15.0		317.0-307.0	10.0
	46.5-48.5		275.5-273.5	2.0
	56.6-60.0		265.4-262.0	3.4
	65.0-68.0		257.0-254.0	3.0
	70.0-89.0		252.0-233.0	19.0
	96.0-97.0		226.0-225.0	1.0
	103.5-107.2		218.5-214.8	3.7
	146.0-150.0		176.0-172.0	4
Total Borehole Depth =	165.0		Total Friable Zone Interval Footage =	46.1 % Friable = 27.9
98BA-3	Elevation at ground surface		322.0	
	171.6-175.0		150.4-147.0	3.4
	205.0-212.0		117.0-110.0	7
Total Borehole Depth =	220.0		Total Friable Zone Interval Footage =	10.4 % Friable = 4.7
00BA-1	Elevation at ground surface		450.0	
	29.0-34.0		421.0-416.0	5
Total Borehole Depth =	150.0		Total Friable Zone Interval Footage =	5.0 % Friable = 3.3
00BA-2	Elevation at ground surface		363.0	
	0.0-32.0		363.0-331.0	32.0
	38.2-40.6		324.8-322.4	2.4
	42.0-47.5		321.0-315.5	5.5
Total Borehole Depth =	55.0		Total Friable Zone Interval Footage =	39.9 % Friable = 72.5

Table 21-4 Friable rock zones in ISFSI Study Area borings. (continued)

Boring	Depth Interval of friable rock (feet)	Test Sample I.D.	Elevation Interval (feet)	Friable Zone Interval Thickness (ft)	
00BA-3	Elevation at ground surface		306.0		
	4.0-5.6		302.0-300.4	1.6	
	11.1-12.8		294.9-293.2	1.7	
	21.6-24.0		284.4-282.0	2.4	
Total Borehole Depth =	30.0		Total Friable Zone Interval Footage =	5.7	% Friable = 19.0
01CTF-A	Elevation at ground surface		306.1		
	6.3-10.6		299.8-295.5	4.3	
	18.0-24.7		288.1-281.4	6.7	
	34.4-35.8		271.7-270.3	1.4	
	37.7-39.5		268.4-266.6	1.8	
	48.5-58.6		257.6-247.5	10.1	
Total Borehole Depth =	58.6		Total Friable Zone Interval Footage =	24.3	% Friable = 41.5
01-A	Elevation at ground surface		305.7		
	5.4-6.5		300.3-299.2	1.1	
	26.2-28.4		279.5-277.3	2.2	
	33.4-37.0		272.3-268.7	3.6	
	46.2-48.8		259.5-256.9	2.6	
	58.8 - 59.0		364.5 - 364.7	0.2	
	70.0-71.6		235.7-234.1	1.6	
Total Borehole Depth =	71.8		Total Friable Zone Interval Footage =	11.3	% Friable = 15.7
01-B	Elevation at ground surface		318.9		
	38.0-39.8		280.9-279.1	1.8	
	54.5-57.0		264.4-261.9	2.5	
Total Borehole Depth =	72.0		Total Friable Zone Interval Footage =	4.3	% Friable = 6.0
01-C	Elevation at ground surface		323.0		
	7.0-14.0		316.0-309.0	7.0	
	40.4-42.0		282.6-281.0	1.6	
Total Borehole Depth =	67.0		Total Friable Zone Interval Footage =	8.6	% Friable = 12.8

Table 21-4. Friable rock zones in ISFSI Study Area borings. (continued)

Boring	Depth Interval of friable rock (feet)	Test Sample I.D.	Elevation Interval (feet)	Friable Zone Interval Thickness (ft)	
01-D	Elevation at ground surface		325.2		
	22.0-37.6		303.2-287.6	15.6	
	67.0-68.5		258.2-256.7	1.5	
Total Borehole			Total Friable Zone		
Depth =	68.5		Interval Footage =	17.1	% Friable = 25.0
01-E	Elevation at ground surface		337.6		
	4.7-14.0		331.3-323.6	9.3	
	39.2-43.0		298.4-294.6	3.8	
	68.4-80.7		269.2-256.9	12.3	
Total Borehole			Total Friable Zone		
Depth =	81.0		Interval Footage =	25.4	% Friable = 31.4
01-F	Elevation at ground surface		390.6		
	33.0-33.9		357.6-356.7	0.9	
	37.0-38.0		353.4-352.6	0.8	
	43.8-45.0		346.8-345.6	1.2	
	46.6-47.4		344.0-343.2	0.8	
	57.6-60.0		333.0-330.6	2.4	
	103.0-106.0		287.6-284.6	3.0	
	117.0-121.8		273.6-268.8	4.8	
	123.0-124.2		267.6-266.4	1.2	
	130.0-130.5		260.6-260.1	0.5	
Total Borehole			Total Friable Zone		
Depth =	130.5		Interval Footage =	15.6	% Friable = 12.0
01-G	Elevation at ground surface		316.8		
	11.0-12.4		305.8-304.4	1.4	
	19.2-20.4		297.6-296.4	1.2	
	24.2-25.6		292.6-291.2	1.4	
	66.0-76.0		250.8-240.8	10	
Total Borehole			Total Friable Zone		
Depth =	76.0		Interval Footage =	14.0	% Friable = 18.4

Table 21-4. Friable rock zones in ISFSI Study Area borings. (continued)

Boring	Depth Interval of friable rock (feet)	Test Sample I.D.	Elevation Interval (feet)	Friable Zone Interval Thickness (ft)		
01-H	Elevation at ground surface		346.6			
	12.0-12.6		334.6-334.0	0.6		
	23.7-24.0		322.9-322.6	0.3		
	29.4-32.0		317.2-314.6	2.6		
	55.5-58.6		291.1-288.0	3.1		
	61.0-61.2		285.6-285.4	0.2		
	81.0-83.0		265.6-263.6	2.0		
	89.2-98.2		257.4-248.4	9.0		
Total Borehole			Total Friable Zone			
Depth =	101.0		Interval Footage =	17.8	% Friable =	17.6
01-I	Elevation at ground surface		566.9			
	33.6-39.8		533.3-527.1	6.2		
	61.0-61.4		505.9-505.5	0.4		
	62.7-63.0		504.2-503.9	0.3		
	68.5-69.1		498.4-497.8	0.6		
	109.0-115.8		457.9-451.1	6.8		
	155.6-156.6		411.3-410.3	1.0		
	252.4-252.8		314.5-314.1	0.4		
Total Borehole			Total Friable Zone			
Depth =	321.0		Interval Footage =	15.7	% Friable =	4.9

Table 21-5 Discontinuity Data for Minor Faults¹

Trench/Field Number	Trench Location	Fault Strike	Fault Dip	Fault Striation Rake	Slickensides (s) or mullions (m)	Person and Date
T-1	St. 23	170	85 S	50 S	m	JLB 6/9/00
T-1	St. 24	297	72 S	5-10 W	s	CMB 6/9/00
T-2A	St 0.4	279	70 S	8 E	m	JLB 6/11/00
T-2A	St. 15	286	75 NE	20 W	s	JLB 6/11/00
T-2C	St. 3.6	281	70 N	68 E	s	JNB/CMB 6/20/00
T-2C	St. 1.2	264	84 S	15 W	s	JNB/CMB 6/20/00
T-2C	St. 0	280	70 S	0	s	JNB/CMB 6/20/00
T-2C	St. 0	295	80 S	0	s	JNB/CMB 6/20/00
T-3	St. 7.5	295	55-75 S	18 SE	m	WDP 7/10/00
T-5	St. 18	70	85 N	2 E	s	WDP 8/2/00
T-7	St. 3.6	265	65 N	15 E	s	JLB 6/12/00
T-11A	St. 6	304	81 S	43 E	s	RDK 8/8/00
T-11A	St. 2.4	282	87 N	Subhor.	s	RDK 8/8/00
T-11C	St. 3.5	85	73 S	Subhor.	s	JNB 6/19/00
T-12	St. 4	291	75 N	10 E	s	JNB 6/20/00
T-12	St. 4	291	75 N	8 E	m	JNB 6/20/00
T-12	St. 4.7	300	56 S	10 E	s	JNB 6/20/00
T-12	St. 14	292	60 S	10 W	s	JNB 6/20/00
T-13	St. 6.5	301	44 S	10 W	s	JNB 6/20/00
T-14B	St. 1.0	95	81 N	0	m	JLB 8/7/00
T-14B	St. 1.5	101	86 S	Subhor.	m	JLB 8/7/00
T-14B	St. 2.0	104	88 N	Subhor.	m	JLB 8/7/00
T-15	St. 18.5	297	83 N	Subhor.	s	JNB 6/20/00
T-17A	St. 41	265	84 N	65 W	s	JLB 8/2/00
T-17A	St. 39	296	80 N	47 W	s	JLB 8/2/00
T-17A	St. 45.5	254	65 N	Subhor.	s	JLB 8/2/00
T-17A	St. 11	90	85 S	Subhor.	s	JLB 8/2/00
T-18B	St. 7.5	300	86-90 S	Subhor.-45	m	JLB 8/23/00
T-20A	St. 26	298	63 S	16 SE	s	JLB 11/30/00
T-20B	St. 3.2	273	61 S	16 W	s	JLB 12/6/00
T-21	St. 20.5	286	80 N	Subhor.	s	JLB 4/16/01 WRL 4/28/01
Field 1	Diablo Canyon Rd. cut across from Raw Water Reservoirs and along projection of ISFSI site faults.	305	75 N	Subhor.	m+s	WRL

Table 21-5 Discontinuity Data for Minor Faults¹ (continued)

Trench/Field Number	Trench Location	Fault Strike	Fault Dip	Fault Striation Rake	Slickensides (s) or mullions (m)	Person and Date
Field 2	Diablo Canyon Rd. cut across from Raw Water Reservoirs and along projection of ISFSI site faults. Confirmed with JLB-17-1 station GPS 023 N 35° 51.264' W 120° 51.264'.	305	75 N	10 E	m+s	WRL/JLB/WDP 5/17/01
JLB-17-2	GPS 024 N35°12.927' W120°51.234'. North wall of Diablo Canyon.	296	80 N	10 E	m (?)	WRL/JLB/WDP

¹ Fault is any discontinuity along which displacement of rock has occurred.

Table 21-6 Selected Fractures (Joints, Faults and Shears) Observed in Borings and Trenches.

Boring ⁽¹⁾	ID ⁽²⁾	Dip(3)	Dip Direction(4)	Depth ⁽⁵⁾ of Fracture
00BA-1	1	65.8	206	146.872
	2	56.2	219	146.613
	3	57.3	218	145.523
	4	63.5	68	137.049
	5	63.6	67	136.372
	6	72.4	62	136.243
	7	46.0	61	133.425
	8	73.0	229	132.268
	9	57.2	219	131.512
	10	69.2	54	130.582
	11	55.8	224	130.211
	12	67.5	229	129.655
	13	68.7	221	129.307
	14	63.5	303	128.736
	15	57.0	56	128.311
	16	60.4	73	126.856
	17	32.9	27	119.599
	18	69.6	265	117.687
	19	72.6	66	117.523
	20	63.7	84	110.720
	21	41.7	245	108.077
	22	17.9	253	106.846
	23	17.1	248	106.357
	24	12.2	257	105.331
	25	29.6	344	104.677
	26	41.8	90	104.074
	27	65.6	226	102.022
	28	78.1	203	95.511
	29	77.5	190	94.048
	30	72.1	214	92.707
	31	47.6	190	92.399
	32	62.2	230	91.544
	33	46.3	37	91.195
	34	68.0	67	90.227

Boring ⁽¹⁾	ID ⁽²⁾	Dip(3)	Dip Direction(4)	Depth ⁽⁵⁾ of Fracture
00BA-1 continued	35	36.5	86	86.763
	36	68.0	253	86.297
	37	36.2	235	83.310
	38	38.1	221	83.292
	39	63.7	229	80.387
	40	61.7	252	79.791
	41	72.0	201	78.688
	42	60.9	205	76.367
	43	52.9	201	75.547
	44	61.0	213	75.241
	45	33.9	221	73.429
	46	77.6	186	72.946
	47	38.2	40	72.034
	48	42.7	50	71.330
	49	68.5	233	71.055
	50	61.1	353	69.457
	51	68.6	261	62.156
	52	61.6	40	60.866
	53	44.7	202	59.012
	54	63.6	353	54.100
	55	64.6	218	52.725
	56	31.4	192	52.470
	57	65.7	360	51.869
	58	79.2	196	49.721
	59	70.9	4	48.368
	60	70.7	233	47.689
	61	59.0	238	47.077
	62	24.4	16	45.703
	63	73.7	215	25.729
	64	75.3	242	23.770
	65	49.6	232	23.152
	66	37.3	196	18.001
	67	65.5	214	13.289

Table 21-6. Selected Fractures (Joints, Faults and Shears) Observed in Borings and Trenches (continued).

Boring ⁽¹⁾	ID ⁽²⁾	Dip(3)	Dip Direction(4)	Depth ⁽⁵⁾ of Fracture
00BA-2	1	40.5	205	53.453
	2	18.6	267	50.147
	3	74.1	223	48.521
	4	48.9	237	40.597
	5	67.7	205	39.467
	6	66.8	214	39.208
	7	41.9	232	39.113
	8	40.5	240	38.731
	9	44.2	282	35.604
	10	48.1	272	34.321
	11	72.0	101	27.219
	12	71.0	120	26.263
	13	64.0	224	9.438

Boring ⁽¹⁾	ID ⁽²⁾	Dip(3)	Dip Direction(4)	Depth ⁽⁵⁾ of Fracture
01CTF-A	1	51.3	205	45.134
	2	55.1	250	44.431
	3	69.6	212	34.263
	4	55.1	216	31.310
	5	35.7	151	19.592

Boring ⁽¹⁾	ID ⁽²⁾	Dip(3)	Dip Direction(4)	Depth ⁽⁵⁾ of Fracture
01-A	1	70.5	264	69.083
	2	61.2	240	68.545
	3	76.6	235	68.240
	4	64.8	265	57.922
	5	49.8	199	57.577
	6	37.5	257	56.422
	7	35.7	358	53.227
	8	69.3	184	52.954
	9	67.6	249	51.988
	10	64.5	248	51.772
	11	29.4	182	51.682
	12	58.1	194	51.196
	13	34.4	55	50.081
	14	48.3	39	44.392
	15	35.1	225	42.265
	16	31.8	251	41.065
	17	24.3	243	40.711
	18	73.5	93	39.856
	19	35.8	229	37.372
	20	23.7	284	36.913
	21	26.6	224	36.724
	22	34.7	240	34.384
	23	78.8	192	33.245
	24	67.9	192	32.682
	25	76.3	150	31.869
	26	71.5	243	30.474
	27	56.5	223	23.229
	28	77.4	54	21.080
	29	67.2	231	19.973
	30	81.5	30	16.441
	31	31.3	171	15.275
	32	36.3	330	8.838
	33	77.2	50	7.758
	34	42.2	188	6.300

Table 21-6. Selected Fractures (Joints, Faults and Shears) Observed in Borings and Trenches (continued).

Boring ⁽¹⁾	ID ⁽²⁾	Dip(3)	Dip Direction(4)	Depth(5) of Fracture
01-B	1	71.5	215	
	2	41.6	245	66.291
	3	69.0	250	65.902
	4	59.6	237	64.885
	5	36.5	194	47.241
	6	62.1	214	37.695
	7	60.8	266	33.099
	8	28.5	277	27.706
	9	83.0	257	26.796
	10	41.5	259	26.506
	11	39.4	163	22.992
	12	75.6	243	21.277
	13	27.8	180	20.117
	14	25.6	326	18.984
	15	28.7	273	16.330
	16	65.8	229	11.573

Boring ⁽¹⁾	ID ⁽²⁾	Dip(3)	Dip Direction(4)	Depth ⁽⁵⁾ of Fracture
01-C	1	28.6	229	65.059
	2	26.6	251	64.267
	3	63.1	246	62.051
	4	54.7	222	61.360
	5	42.8	195	57.847
	6	49.1	285	57.648
	7	64.4	76	57.448
	8	68.1	237	51.833
	9	67.2	39	50.875
	10	69.8	47	49.852
	11	30.7	194	49.044
	12	48.4	239	47.992
	13	32.6	167	45.804
	14	35.5	201	43.648
	15	37.7	203	40.429
	16	57.0	186	37.897
	17	15.5	206	37.393
	18	42.9	229	34.720
	19	41.2	176	31.155
	20	27.8	235	30.823
	21	52.9	345	30.601
	22	33.7	206	30.313
	23	72.9	236	29.238
	24	49.9	239	29.013
	25	40.9	250	28.693
	26	45.1	176	27.019
	27	64.8	232	26.428
	28	34.9	206	25.726
	29	58.6	226	24.910
	30	29.1	326	24.787
	31	40.2	224	22.735
	32	78.2	219	21.430
	33	59.7	249	19.690
	34	38.3	178	14.635
	35	50.0	184	13.636
	36	51.3	214	12.883
	37	60.2	187	12.247
	38	75.5	209	11.445

Table 21-6. Selected Fractures (Joints, Faults and Shears) Observed in Borings and Trenches (continued).

Boring ⁽¹⁾	ID ⁽²⁾	Dip(3)	Dip Direction(4)	Depth ⁽⁵⁾ of Fracture
01-D	1	34.1	251	58.192
	2	44.3	192	50.247
	3	65.5	265	49.672
	4	33.6	191	47.825
	5	66.9	278	42.957
	6	61.8	275	42.454
	7	62.9	254	42.040
	8	51.6	108	40.118
	9	30.4	282	36.591
	10	26.2	303	36.454
	11	62.7	266	36.174
	12	42.8	204	34.882
	13	60.7	77	34.449
	14	30.9	328	33.706
	15	44.1	299	33.413
	16	19.1	346	32.307
	17	32.5	304	28.878
	18	42.4	332	26.744
	19	44.2	297	26.046
	20	34.5	200	24.130
	21	48.1	183	23.318
	22	37.7	229	17.242
	23	86.9	95	13.485
	24	77.6	241	8.355
	25	64.5	273	7.020

Boring ⁽¹⁾	ID ⁽²⁾	Dip(3)	Dip Direction(4)	Depth ⁽⁵⁾ of Fracture
01-E	1	51.8	210	79.228
	2	64.7	208	78.505
	3	72.1	210	75.400
	4	79.4	281	66.396
	5	75.2	253	59.959
	6	76.9	215	57.898
	7	67.6	229	54.626
	8	69.2	220	53.573
	9	85.4	232	51.698
	10	81.1	22	36.199
	11	63.8	267	35.461
	12	68.3	278	29.089
	13	45.0	236	25.673
	14	66.5	2	15.680
	15	72.7	342	13.177
	16	67.1	203	9.579

Table 21-6. Selected Fractures (Joints, Faults and Shears) Observed in Borings and Trenches (continued).

Boring ⁽¹⁾	ID ⁽²⁾	Dip(3)	Dip Direction(4)	Depth ⁽⁵⁾ of Fracture
01-F	2	42.6	224	120.021
	3	79.2	45	87.824
	4	61.3	197	82.255
	5	57.9	213	82.036
	6	60.5	215	81.472
	7	62.7	228	81.159
	8	66.0	231	80.287
	9	48.0	238	71.965
	10	66.4	218	69.880
	11	66.8	190	69.665
	12	72.1	194	68.299
	13	65.5	223	64.732
	14	70.3	17	63.379
	15	53.9	178	61.017
	16	38.9	317	58.766
	17	29.0	200	53.569
	18	65.9	2	51.178
	19	40.0	182	50.897
	20	43.6	194	49.677
	21	71.8	230	46.728
	22	31.5	185	43.719
	23	32.2	188	41.198
	24	34.3	193	26.194
	25	53.6	211	4.924

Boring ⁽¹⁾	ID ⁽²⁾	Dip(3)	Dip Direction(4)	Depth ⁽⁵⁾ of Fracture
01-G	1	78.5	212	71.790
	2	61.6	272	70.765
	3	46.1	227	65.647
	4	68.2	210	63.781
	5	70.6	64	61.594
	6	69.4	237	50.116
	7	67.3	244	49.801
	8	67.4	249	49.303
	9	78.5	281	31.327
	10	58.5	297	26.302
	11	31.3	243	14.083
	12	72.1	286	11.392
	13	63.2	265	7.867

Boring ⁽¹⁾	ID ⁽²⁾	Dip(3)	Dip Direction(4)	Depth ⁽⁵⁾ of Fracture
01-H	1	42.3	289	91.717
	2	69.0	306	91.210
	3	75.9	259	82.788
	4	69.8	249	77.589
	5	69.6	242	75.574
	6	33.7	259	66.793
	7	34.5	253	66.625
	8	55.2	42	28.355
	9	51.0	275	24.063
	10	58.4	264	22.203
	11	35.1	230	16.238
	12	72.3	119	14.676
	13	79.4	256	11.530
	14	33.9	235	9.324
	15	25.5	231	7.332
	16	34.4	244	7.207
	17	56.2	253	6.520
	18	37.5	223	5.819
	19	52.8	6	4.867
	20	35.3	247	4.466
	21	41.4	227	4.297

Table 21-6. Selected Fractures (Joints, Faults and Shears) Observed in Borings and Trenches(continued).

Boring ⁽¹⁾	ID ⁽²⁾	Dip(3)	Dip Direction(4)	Depth ⁽⁵⁾ of Fracture
01-I	1	60.3	68	267.961
	2	76.1	20	245.512
	3	60.4	244	236.269
	4	81.0	73	234.018
	5	67.2	251	232.393
	6	65.7	308	230.599
	7	58.9	109	229.744
	8	68.6	198	205.711
	9	73.0	244	193.105
	10	61.5	259	187.690
	11	58.4	216	186.571
	12	77.9	240	170.377
	13	45.7	308	154.348
	14	70.8	243	146.380
	15	71.1	251	136.045
	16	60.8	228	134.206
	17	78.8	247	128.566
	18	69.7	225	127.132
	19	44.5	200	125.797
	20	36.6	131	125.125
	21	81.1	226	114.905
	22	81.6	234	103.383
	23	84.7	45	102.430
	24	70.2	44	99.427
	25	59.3	204	94.844
	26	69.2	71	94.040
	27	63.5	219	93.767
	28	63.9	277	91.139
	29	67.0	273	91.100
	30	32.2	248	85.493
Boring ⁽¹⁾	ID ⁽²⁾	Dip(3)	Dip Direction(4)	Depth ⁽⁵⁾ of Fracture
01-I	31	67.5	51	78.887
Continued	32	31.3	212	75.704
	33	51.4	255	75.464
	34	70.5	235	74.900
	35	26.5	334	72.003
	36	41.9	55	70.583
	37	43.4	50	69.833
	38	75.5	30	68.897
	39	33.2	312	68.243
	40	32.0	353	67.022
	41	52.8	242	65.306
	42	34.7	253	63.965
	43	28.7	267	63.620
	44	62.8	232	63.491
	45	86.3	100	62.249
	46	70.3	224	59.336
	47	64.7	279	54.240
	48	81.7	246	52.161
	49	76.3	204	47.551
	50	72.4	44	44.221
	51	71.1	231	43.762
	52	70.2	213	36.817
	53	30.7	231	28.024
	54	73.2	52	19.099
	55	73.2	84	18.667
	56	57.2	238	16.602
	57	56.3	71	11.194
	58	31.1	262	9.688
	59	56.5	46	9.493
	60	63.3	97	7.176

Table 21-6. Selected Fractures (Joints, Faults and Shears) Observed in Borings and Trenches (continued).

Trench ⁽¹⁾	ID ⁽²⁾	Dip(3)	Dip Direction(4)	Type ⁽⁵⁾ of Fracture
T-1	1	56	270	Joint
	2	88	347	Joint
	3	60	200	Joint
	4	84	200	Joint
	5	75	10	Joint
	6	74	5	Joint
	7	84	198	Fault
	8	76	78	Joint
	9	76	78	Joint
	10	78	215	Joint
	11	47	202	Joint
	12	47	202	Joint
	13	47	202	Joint
	14	72	355	Fault
	15	58	190	Joint
	16	82	182	Joint
	17	88	190	Joint
	18	72	175	Fault
	19	82	192	Joint
	20	65	185	Joint
	21	86	192	Joint
	22	86	192	Joint
	23	76	210	Fault
	24	85	195	Fault
	25	85	195	Fault
	26	48	175	Joint
	27	72	296	Joint
	28	83	235	Joint
	29	28	290	Joint
	30	80	205	Joint
	31	80	200	Joint
	32	88	260	Joint

Trench ⁽¹⁾	ID ⁽²⁾	Dip(3)	Dip Direction(4)	Type ⁽⁵⁾ of Fracture
T-1 Continued	33	64	242	Joint
	34	87	285	Joint
	35	70	188	Joint
	36	74	71	Joint
	37	87	204	Joint
	38	54	75	Joint
	39	76	95	Joint
	40	64	255	Joint
	41	72	207	Fault
	42	72	195	Fault
	43	79	203	Fault
	44	70	210	Fault
	45	76	60	Joint
	46	85	220	Joint
	47	78	235	Joint
	48	70	40	Joint
	49	60	175	Joint
	50	65	25	Joint
	51	86	210	Joint
	52	80	8	Joint
	53	88	305	Joint
	54	80	200	Joint
	55	82	15	Joint
	56	86	194	Joint
	57	52	268	Joint
	58	80	252	Joint
	59	85	186	Joint
	60	70	250	Joint
	61	86	210	Joint
	62	74	260	Joint
	63	82	205	Joint
	64	55	265	Joint

Table 21-6. Selected Fractures (Joints, Faults and Shears) Observed in Borings and Trenches (continued).

Trench ⁽¹⁾	ID ⁽²⁾	Dip(3)	Dip Direction(4)	Type ⁽⁵⁾ of Fracture
T-2	1	76	253	Joint
	2	85	187	Joint
	3	71	246	Joint
	4	73	1	Joint
	5	67	251	Joint
	6	86	199	Joint
	7	70	284	Joint
	8	75	24	Joint
	9	71	263	Joint
	10	84	229	Joint
	11	45	297	Joint
	12	86	223	Joint
	13	25	359	Joint
	14	56	277	Joint
	15	70	12	Joint
	16	65	251	Joint
	17	57	15	Joint
	18	64	246	Joint
	19	62	244	Joint
	20	76	290	Joint
	21	70	249	Joint
	22	40	311	Joint
	23	83	350	Joint
	24	89	211	Joint
	25	79	219	Joint
	26	78	65	Joint
	27	69	249	Joint
	28	71	236	Joint
	29	70	273	Joint
	30	84	26	Joint
	31	80	90	Joint
	32	84	215	Joint
	33	64	195	Fault
	34	65	266	Joint
	35	79	204	Joint
	36	75	286	Fault
	37	62	235	Joint
	38	53	323	Joint
	39	83	258	Joint
	40	88	220	Joint
	41	80	223	Joint
	42	86	106	Joint
	43	90	220	Joint
T-2 Continued	44	80	194	Joint
	45	89	114	Joint
	46	76	211	Joint
	47	85	196	Joint
	48	74	122	Joint
	49	86	289	Joint
	50	84	227	Joint
	51	80	100	Joint
	52	84	118	Joint
	53	51	301	Joint
	54	46	268	Joint
	55	81	119	Joint
	56	86	269	Joint
	57	85	200	Joint
	58	59	261	Joint
	59	86	95	Joint
	60	77	201	Joint
	61	84	278	Joint
	62	86	36	Joint
	63	44	198	Joint
	64	87	75	Joint
	65	65	212	Joint
	66	80	113	Joint
	67	74	222	Joint
	68	84	272	Joint
	69	86	216	Joint
	70	83	256	Joint
	71	70	190	Fault
	72	80	205	Fault
	73	89	3	Joint
	74	72	263	Joint
	75	84	174	Fault
	76	81	32	Joint
	77	90	181	Joint
	78	87	176	Fault
	79	60	2	Joint
	80	64	256	Joint
	81	80	11	Fault
	82	55	199	Joint
	83	61	191	Joint
	84	90	35	Joint
	85	61	286	Joint
	86	55	276	Joint

Table 21-6. Selected Fractures (Joints, Faults and Shears) Observed in Borings and Trenches (continued).

Trench ⁽¹⁾	ID ⁽²⁾	Dip(3)	Dip Direction(4)	Type ⁽⁵⁾ of Fracture
T-3	1	71	208	Joint
	2	69	261	Joint
	3	74	226	Fault
	4	85	91	Joint
	5	76	261	Joint
	6	76	320	Joint
	7	73	234	Joint
	8	76	20	Joint
	9	90	190	Joint
	10	67	9	Joint
	11	30	206	Joint
	12	79	309	Joint
	13	65	187	Joint
	14	64	240	Joint
	15	74	208	Fault
	16	60	255	Joint
	17	85	180	Joint
	18	51	248	Fault
	19	66	21	Joint
	20	61	208	Joint
	21	79	218	Joint
	22	90	205	Joint
	23	62	291	Joint
	24	74	201	Joint
	25	90	269	Joint

Table 21-6. Selected Fractures (Joints, Faults and Shears) Observed in Borings and Trenches (continued).

Trench ⁽¹⁾	ID ⁽²⁾	Dip(3)	Dip Direction(4)	Type ⁽⁵⁾ of Fracture
T-4	1	88	275	Joint
	2	85	5	Joint
	3	77	258	Joint of crushed zone
	4	75	248	Joint
	5	88	105	Joint
	6	60	11	Joint
	7	89	85	Joint
	8	58	186	Joint
	9	60	5	Joint
	10	86	94	Joint
	11	42	340	Joint
	12	65	100	Joint
	13	86	105	Joint
	14	88	106	Joint
	15	30	185	Joint
	16	56	158	Joint
	17	86	275	Joint
	18	74	220	Joint
	19	74	95	Joint
	20	50	352	Joint
	21	35	332	Joint
	22	66	240	Joint
	23	42	347	Joint
	24	62	250	Joint
	25	70	200	Joint
	26	82	355	Fault

Trench ⁽¹⁾	ID ⁽²⁾	Dip(3)	Dip Direction(4)	Type ⁽⁵⁾ of Fracture
T-4	27	82	125	Joint
Continued	28	88	330	Joint
	29	80	115	Joint
	30	12	275	Joint
	31	48	278	Joint
	32	68	335	Joint
	33	70	342	Joint
	34	82	5	Joint
	35	52	260	Joint
	36	80	164	Joint
	37	65	238	Joint
	38	75	215	Joint
	39	80	190	Joint
	40	45	220	Joint
	41	68	330	Joint
	42	68	272	Joint
	43	82	185	Joint
	44	80	60	Joint
	45	88	200	Joint of crushed
	46	58	280	Joint
	47	72	275	Joint
	48	8	250	Joint
	49	89	305	Joint
	50	70	275	Joint
	51	76	340	Joint
	52	62	260	Joint

Table 21-6. Selected Fractures (Joints, Faults and Shears) Observed in Borings and Trenches (continued).

Trench ⁽¹⁾	ID ⁽²⁾	Dip(3)	Dip Direction(4)	Type ⁽⁵⁾ of Fracture
T-5	1	90	277	Joint
	2	90	307	Joint
	3	87	301	Joint
	4	90	283	Joint
	5	50	217	Joint
	6	83	198	Joint
	7	70	121	Joint
	8	90	201	Joint
	9	70	70	Joint
	10	85	330	Fault
	11	70	70	bric of crushed zone
	12	76	76	Joint
	13	77	105	Joint
	14	64	291	Joint
	15	90	42	bric of crushed zone
	16	87	294	Joint
	17	57	131	Joint
	18	55	265	Joint
	19	75	344	Joint
	20	50	254	Joint
	21	70	144	Joint
	22	65	249	Joint
	23	83	146	Joint
	24	84	55	Joint
	25	78	165	Joint

Trench ⁽¹⁾	ID ⁽²⁾	Dip(3)	Dip Direction(4)	Type ⁽⁵⁾ of Fracture
T-5	26	63	250	Fault
Continued	27	86	252	Joint
	28	74	345	Joint
	29	25	242	Joint
	30	75	264	Joint
	31	63	271	Joint
	32	78	249	Joint
	33	77	209	Joint
	34	70	270	Joint
	35	86	261	Joint
	36	76	204	Joint
	37	51	280	Joint
	38	70	252	Joint
	39	74	18	Joint
	40	75	258	Joint
	41	90	339	Fault
	42	85	340	bric of crushed
	43	79	206	Joint
	44	78	71	Joint
	45	83	185	Joint
	46	84	289	Joint
	47	57	226	Joint
	48	61	243	Joint
	49	75	241	Joint

Table 21-6. Selected Fractures (Joints, Faults and Shears) Observed in Borings and Trenches(continued).

Trench ⁽¹⁾	ID ⁽²⁾	Dip(3)	Dip Direction(4)	Type ⁽⁵⁾ of Fracture
T-6	1	70	0	Joint
	2	40	215	Joint
	3	48	10	Joint
	4	90	220	Joint
	5	78	70	Joint
	6	89	82	Joint
	7	71	92	Joint
	8	82	265	Joint
	9	68	25	Fault
	10	88	105	Joint
	11	82	52	Joint
	12	88	95	Joint
	13	90	310	Joint
	14	62	15	Joint
	15	15	240	Joint
	16	70	6	Joint
	17	88	85	Joint
	18	22	225	Joint
	19	80	255	Joint
	20	84	345	Joint
	21	18	230	Joint
	22	74	75	Joint
	23	72	238	Joint
	24	76	4	Joint

Trench ⁽¹⁾	ID ⁽²⁾	Dip(3)	Dip Direction(4)	Type ⁽⁵⁾ of Fracture
T-6	25	86	190	Joint
Continued	26	78	70	Joint
	27	82	200	Fault
	28	89	265	Joint
	29	78	255	Joint
	30	22	235	Joint
	31	89	180	Joint
	32	85	270	Joint
	33	85	145	Joint
	34	82	70	Joint
	35	80	255	Joint
	36	90	145	Joint
	37	86	46	Joint
	38	78	292	Joint
	39	76	333	Joint
	40	80	290	Joint
	41	78	185	Joint
	42	84	185	Joint
	43	74	245	Joint
	44	78	260	Joint
	45	86	215	Joint
	46	76	65	Joint
	47	75	250	Joint
	48	75	10	Joint

Table 21-6. Selected Fractures (Joints, Faults and Shears) Observed in Borings and Trenches (continued).

Trench ⁽¹⁾	ID ⁽²⁾	Dip(3)	Dip Direction(4)	Type ⁽⁵⁾ of Fracture
T-11	1	79	122	Joint
	2	63	346	Joint
	3	80	317	Joint
	4	81	15	Joint
	5	65	349	Joint
	6	78	41	Joint
	7	65	314	Joint
	8	70	238	Joint
	9	70	1	Joint
	10	85	285	Joint
	11	84	295	Joint
	12	75	198	Joint
	13	50	355	Joint
	14	55	260	Joint
	15	86	180	Joint
	16	87	255	Joint
	17	85	10	Joint
	18	70	281	Joint
	19	35	314	Joint
	20	90	249	Joint
	21	82	264	Joint
	22	65	260	Joint
	23	85	171	Joint
	24	71	208	Joint
	25	89	242	Joint
	26	90	255	Joint
	27	64	0	Joint
	28	68	70	Joint
	29	72	221	Joint
	30	84	61	Joint
	31	80	164	Joint
	32	76	267	Fault
	33	81	66	Joint
	34	79	6	Joint
	35	79	229	Joint
	36	77	193	Joint

Trench ⁽¹⁾	ID ⁽²⁾	Dip(3)	Dip Direction(4)	Type ⁽⁵⁾ of Fracture
T-12	1	49	274	Joint
	2	83	236	Joint
	3	79	20	Fault
	4	77	180	Joint
	5	79	197	Joint
	6	85	1	Joint
	7	77	231	Joint
	8	55	258	Joint
	9	64	175	Joint
	10	73	226	Joint
	11	88	228	Joint
	12	45	213	Joint
	13	90	25	Joint
	14	67	221	Joint
	15	60	158	Fault
	16	80	350	Fault

Trench ⁽¹⁾	ID ⁽²⁾	Dip(3)	Dip Direction(4)	Type ⁽⁵⁾ of Fracture
T-13	1	81	208	Joint
	2	90	195	Joint
	3	66	248	Joint
	4	89	244	Joint
	5	87	202	Joint
	6	82	248	Joint
	7	55	210	Fault
	8	43	209	Fault
	9	81	340	Fault
	10	79	265	Joint
	11	23	205	Joint
	12	81	85	Joint
	13	47	46	Joint
	14	61	200	Joint
	15	14	200	Joint
	16	80	186	Joint
	17	69	9	Joint
	18	76	256	Joint
	19	51	254	Joint
	20	82	24	Joint
	21	83	195	Joint
	22	60	233	Joint
	23	86	15	Joint

Table 21-6. Selected Fractures (Joints, Faults and Shears) Observed in Borings and Trenches (continued).

Trench ⁽¹⁾	ID ⁽²⁾	Dip(3)	Dip Direction(4)	Type ⁽⁵⁾ of Fracture
T-14	1	87	11	Joint
	2	49	266	Joint
	3	83	2	Joint
	4	74	195	Joint
	5	68	99	Joint
	6	48	154	Joint
	7	90	226	Joint
	8	30	1	Joint
	9	68	245	Joint
	10	86	183	Joint
	11	74	273	Joint
	12	59	4	Joint
	13	52	184	Joint
	14	50	185	Joint
	15	78	165	Joint
	16	71	264	Joint
	17	76	178	Joint
	18	85	279	Joint
	19	87	299	Joint
	20	83	250	Joint
	21	84	0	Joint
	22	86	279	Joint
	23	80	352	Joint
	24	85	322	Joint
	25	90	2	Joint
	26	79	6	Joint
	27	88	185	Joint
	28	90	270	Joint
	29	52	356	Joint
	30	75	162	Joint
	31	90	13	Joint
	32	84	330	Joint
	33	85	22	Joint
	34	80	266	Joint
	35	61	176	Joint
	36	90	279	Joint

Trench ⁽¹⁾	ID ⁽²⁾	Dip(3)	Dip Direction(4)	Type ⁽⁵⁾ of Fracture
T-14	37	84	333	Joint
Continued	38	85	81	Joint
	39	80	28	Joint
	40	86	196	Joint
	41	81	174	Joint
	42	85	115	Joint
	43	69	3	Joint
	44	81	96	Joint
	45	90	220	Joint

Trench ⁽¹⁾	ID ⁽²⁾	Dip(3)	Dip Direction(4)	Type ⁽⁵⁾ of Fracture
T-15	1	77	229	Joint
	2	66	209	Joint
	3	83	69	Joint
	4	85	72	Joint
	5	90	66	Joint
	6	86	70	Joint
	7	90	32	Joint
	8	90	64	Joint
	9	87	71	Joint
	10	85	246	Joint
	11	30	140	Joint
	12	83	44	Joint
	13	69	185	Joint
	14	83	248	Joint
	15	80	81	Joint
	16	62	39	Joint
	17	81	238	Joint
	18	65	312	Joint
	19	60	56	Joint
	20	76	255	Joint
	21	72	254	Joint
	22	78	222	Joint
	23	84	25	Joint
	24	87	21	Joint
	25	90	250	Joint
	26	87	240	Joint
	27	90	272	Joint
	28	87	285	Fault

Table 21-6. Selected Fractures (Joints, Faults and Shears) Observed in Borings and Trenches (continued).

Trench ⁽¹⁾	ID ⁽²⁾	Dip(3)	Dip Direction(4)	Type ⁽⁵⁾ of Fracture
T-17	1	70	270	joint
	2	86	290	joint
	3	50	190	joint
	4	85	250	joint
	5	46	235	joint
	6	75	285	joint
	7	68	286	joint
	8	50	205	joint
	9	84	235	shear zone
	10	66	228	joint
	11	30	320	joint
	12	82	90	joint
	13	80	250	joint
	14	78	75	joint
	15	88	270	joint
	16	82	268	joint
	17	72	82	joint
	18	87	280	joint
	19	78	345	joint
	20	86	90	joint
	21	88	266	joint
	22	56	135	joint
	23	47	138	joint
	24	75	65	fault
	25	58	75	joint
	26	72	190	joint
	27	65	205	joint
	28	85	260	joint
	29	90	230	joint
	30	90	250	joint
	31	84	230	joint
	32	85	252	joint
	33	70	345	joint
	34	84	60	joint
	35	86	205	joint
	36	34	325	joint
	37	64	75	joint/ shear

Trench ⁽¹⁾	ID ⁽²⁾	Dip(3)	Dip Direction(4)	Type ⁽⁵⁾ of Fracture
T-17	38	81	80	joint/ shear
Continued	39	72	75	joint
	40	10	313	joint/ shear
	41	86	305	joint
	42	74	15	joint
	43	68	92	joint
	44	85	180	fault
	45	74	190	fault
	46	90	182	fault
	47	72	65	joint
	48	76	170	joint
	49	58	276	joint
	50	68	200	joint
	51	68	220	fault
	52	60	255	joint
	53	50	22	joint
	54	68	210	joint
	55	65	342	fault
	56	88	68	joint
	57	38	302	joint
	58	74	230	fault
	59	64	272	joint
	60	56	356	joint
	61	69	243	joint
	62	87	210	joint
	63	72	68	joint
	64	86	184	joint
	65	86	232	joint
	66	56	282	joint
	67	72	356	joint
	68	70	172	fault
	69	68	355	joint/ fault
	70	78	30	fault
	71	82	40	joint
	72	75	15	joint
	73	86	275	joint
	74	76	15	joint

Table 21-6. Selected Fractures (Joints, Faults and Shears) Observed in Borings and Trenches (continued).

Trench ⁽¹⁾	ID ⁽²⁾	Dip(3)	Dip Direction(4)	Type ⁽⁵⁾ of Fracture
T-17	75	85	60	joint
Continued	76	88	85	joint
	77	45	345	joint
	78	41	315	joint
	79	90	235	joint
	80	56	245	joint
	81	65	205	fault
	82	65	185	joint
	83	60	236	joint
	84	69	350	joint
	85	38	182	joint
	86	74	204	joint
	87	64	335	joint
	88	64	232	joint
	89	66	245	joint
	90	77	200	joint
	91	82	15	joint
	92	63	320	joint
	93	82	182	joint
	94	64	191	joint
	95	87	270	joint
	96	88	244	joint
	97	27	272	joint
	98	12	217	joint
	99	74	78	joint
	100	74	49	joint
	101	90	271	joint
	102	4	221	joint
	103	88	269	joint
	104	21	220	joint
	105	74	196	joint
	106	89	70	joint
	107	88	120	joint
	108	88	254	joint
	109	88	207	joint
	110	68	33	joint
	111	82	120	joint
	112	11	195	joint
	113	81	185	joint
	114	84	250	joint

Table 21-6. Selected Fractures (Joints, Faults and Shears) Observed in Borings and Trenches (continued).

Trench ⁽¹⁾	ID ⁽²⁾	Dip(3)	Dip Direction(4)	Type ⁽⁵⁾ of Fracture
T-18	1	76	165	joint
	2	47	245	joint
	3	80	240	joint
	4	88	148	joint
	5	70	237	joint
	6	26	235	joint
	7	87	300	joint
	8	73	228	joint
	9	25	230	joint
	10	71	232	joint
	11	30	218	joint
	12	21	225	joint
	13	89	231	joint
	14	39	247	joint
	15	38	230	joint
	16	32	227	joint
	17	84	215	joint
	18	87	210	joint
	19	78	105	joint
	20	80	192	joint
	21	72	98	joint
	22	84	270	joint
	23	84	325	joint
	24	80	268	joint
	25	25	234	joint
	26	87	210	joint
	27	82	275	joint
	28	72	320	joint
	29	76	40	shear zone
	30	78	245	joint
	31	88	88	joint
	32	79	257	joint
	33	87	100	joint
	34	88	95	joint
	35	82	280	shear zone
	36	80	250	joint
	37	62	265	joint
	38	82	250	joint
	39	72	273	joint
	40	80	5	joint
	41	88	262	joint

Trench ⁽¹⁾	ID ⁽²⁾	Dip(3)	Dip Direction(4)	Type ⁽⁵⁾ of Fracture
T-18	42	75	5	joint
Continued	43	76	298	joint
	44	88	46	joint
	45	57	250	joint
	46	79	250	joint
	47	86	215	joint
	48	28	250	joint
	49	88	279	joint
	50	84	240	joint
	51	69	292	joint
	52	70	205	joint
	53	68	285	joint
	54	87	210	joint
	55	72	287	joint
	56	67	257	joint
	57	80	205	shear zone
	58	38	325	joint
	59	78	80	joint
	60	76	10	joint
	61	80	110	joint
	62	83	5	fault
	63	88	16	fault
	64	60	282	joint

Trench	ID	Dip(3)	Dip Direction(4)	Type ⁽⁵⁾ of Fracture
T-19	1	38	319	Fault
	2	71	42	Joint
	3	85	32	Joint
	4	84	225	Joint
	5	74	224	Joint
	6	74	332	Joint
	7	76	22	Joint
	8	79	355	Joint
	9	90	344	Joint
	10	88	224	Joint
	11	85	169	Joint
	12	68	75	Joint
	13	88	162	Joint
	14	86	226	Joint
	15	86	160	Joint

Table 21-6. Selected Fractures (Joints, Faults and Shears) Observed in Borings and Trenches (continued).

Trench ⁽¹⁾	ID ⁽²⁾	Dip(3)	Dip Direction(4)	Type ⁽⁵⁾ of Fracture
T-20	1	63	208	Fault
	2	75	11	Fault
	3	68	242	Joint
	4	53	316	Joint
	5	72	189	Joint
	6	69	264	Joint
	7	83	47	Joint
	8	84	261	Joint
	9	82	29	Joint
	10	77	265	Joint
	12	59	215	Fault
	13	70	270	Joint
	14	70	48	Joint
	15	62	293	Joint
	16	61	220	Joint
	17	80	291	Joint
	18	56	286	Joint
	19	82	205	Joint
	20	74	231	Joint
	21	60	351	Fault
	22	76	176	Fault
	23	68	185	Fault
	24	80	10	Joint
	25	85	290	Joint

Trench ⁽¹⁾	ID ⁽²⁾	Dip(3)	Dip Direction(4)	Type ⁽⁵⁾ of Fracture
T-21	1	51	324	Joint
	2	85	353	Joint
	3	25	28	Joint
	4	44	42	Joint
	5	56	7	Joint
	6	77	68	Joint
	7	71	4	Joint
	8	40	331	Joint
	9	48	332	Joint
	10	20	344	Joint
	11	80	40	Joint
	12	53	320	Joint
	13	77	188	Joint
	14	83	314	Joint
	15	64	3	Fault

Notes: (1) Boring or trench where discontinuities, excluding known bedding, were made. In borings, NORCAL from the televiewer images and reviewed by WLA geologists (DCPP ISFSI SAR Section 2.6 Topical Report Appendix E). In trenches, discontinuities were directly observed and measured by field geologists (DCPP ISFSI SAR Section 2.6 Topical Report Appendix D).

- (2) Within each subsurface exploration (boring or trench), a unique number was assigned to each discontinuities were numbered sequentially beginning with the deepest (reverse stratigraphic order). In trenches, discontinuities were numbered sequentially from one end of excavation to the other.
- (3) In borings Dips shown to 0.1 of a degree originated from NORCAL interpretation of televiewer logs (Appendix E). In trenches, Dips were measured by field geologists (DCPP ISFSI SAR Section 2.6 Topical Report Appendix D).
- (4) Dip direction in azimuth degrees.
- (5) Depth (in feet) of discontinuity encountered in borings from NORCAL televiewer logs (ISFSI SAR type of discontinuity (fault, joint, or crushed zone) classified in trenches (DCPP ISFSI SAR Topical Report Appendix D).